

**Role of fibroblast growth factors in pulmonary
parenchymal and vascular remodeling**

**Inauguraldissertation
zur Erlangung des Grades eines Doktors der Medizin
des Fachbereichs Medizin
der Justus-Liebig-Universität Gießen**

**vorgelegt von
Felix Schwind
aus Fulda**

Gießen 2022

Aus dem Zentrum für Innere Medizin
Exzellenz-Cluster Cardio-Pulmonary System
des Fachbereichs Medizin

Gutachter: Prof. Dr. Schermuly

Gutachter: Prof. Dr. Bellusci

Tag der Disputation: 19.06.2023

List of contents

1	Introduction	1
1.1	Anatomy and physiology of the cardiopulmonary system	1
1.2	Pulmonary Hypertension	5
1.2.1	Idiopathic pulmonary arterial hypertension	6
1.2.2	Vascular remodeling	7
1.2.3	Pathogenesis	9
1.2.4	Diagnosis	12
1.2.5	Treatment	13
1.3	Idiopathic pulmonary fibrosis (IPF)	14
1.3.1	Remodeling	15
1.3.2	Pathogenesis	16
1.3.3	Treatment	18
1.4	Fibroblast-Growth Factors (FGF)	19
1.4.1	FGFR2-Signaling	22
1.4.2	FGF7 and FGF10	22
1.5	Hypothesis and aims	24
2	Materials and Methods	26
2.1	Reagents and Kits	26
2.1.1	Immunohistochemistry and structural staining	26
2.1.2	Immunofluorescent staining	28
2.2	Consumables	28
2.3	Devices and Equipment	29
2.4	Methods	30
2.4.1	Tissue origin	30
2.4.2	Tissue preparation	30
2.4.3	Immunohistochemical staining	30
2.4.4	Structural staining	32
2.4.5	Microscopy and semi-automated quantification	35
2.4.6	Statistical evaluation	37
2.4.7	Immunofluorescence staining	37
3	Results	39
3.1	Common features of remodeled lung tissue in IPF and IPAH patients	40
3.2	FGF7 is upregulated in human IPF lungs	41

3.3	Upwards trend in FGF7 expression in IPAH samples.....	42
3.4	Elevated FGF10 expression in IPF samples.....	43
3.5	Elevated FGF10 expression in IPAH samples.....	43
3.6	Elevated FGFR2 expression in IPF samples.....	44
3.7	Elevated FGFR2 expression in IPAH samples.....	44
3.8	Ubiquitous FGFR1 expression in Donor, IPF and IPAH samples.....	45
3.9	Conclusion.....	46
3.10	Identification and quantification of LipidTOX-positive cells in the human lung.....	49
4	Discussion.....	51
4.1	Overall findings.....	51
4.2	Fibroblast-growth factors in PAH.....	51
4.3	Fibroblast-growth factors in IPF.....	53
4.4	Interpretation of the expression patterns.....	54
4.5	Lipofibroblasts in the context of IPF.....	55
4.6	Methodological challenges and limitations.....	59
5	Summary.....	61
5.1	Zusammenfassung.....	63
6	Literature.....	67
7	Appendix.....	89
7.1	Abbreviations.....	89
7.2	List of figures.....	94
7.3	List of tables.....	95
8	Publication index.....	96
9	Acknowledgements.....	97
10	Declaration.....	98
11	Curriculum Vitae.....	99

1 Introduction

1.1 Anatomy and physiology of the cardiopulmonary system

The human lung lies embedded within the thoracic cavity and represents the central organ of the respiratory tract. Primary task is the removal of carbon dioxide (CO₂) and oxygenation of oxygen-deprived blood, entering from the systemic circulation through the right heart. Its structural anatomy is dedicated to gas exchange by provision of a large surface area (150-200 m²) combined with a minimal diffusion path (0,2-1 μm). Coordinated interaction between *perfusion*, *ventilation* and *diffusion* enables a passive gas exchange along the partial pressure gradients of the alveolar–capillary barrier (1, 2):

Ventilation

When at rest, inspiration is mainly achieved through contraction of the diaphragm and the resulting expansion of lung volume. Consequentially, intrapulmonary pressure is lowered below ambient atmospheric pressure, causing an inwardly directed airflow (2). As air passes the upper respiratory tract (nose, mouth, pharynx and larynx) it enters the trachea, which marks the beginning of the lower respiratory tract and furcates into the left and right main bronchus. Division proceeds further into three right and two left lobar bronchi, followed by segmental-, conducting- and terminal bronchi. Respiratory bronchioles mark the end of the anatomic dead space and beginning of the respiratory zone, which extends throughout alveolar ducts into alveolar sacs, containing a multitude of alveoli enclosed by capillaries (3). While inspiration is an active process, expiration is mainly based on passive retraction forces, exerted by stromal elastic fibers and surface tension within the alveoli (1, 2, 4). With an approximate total of 3×10^8 alveoli, the left and right lobe feature respective volumes of 1400 cm³ and 1500 cm³ at respiratory rest position. Minute ventilation amounts to an average of 7 l/min but can be increased up to 120 l/min under severe physical exertion and with the aid of auxiliary respiratory musculature (average adult male) (2). Regulation is accomplished through respiratory centers located within the medulla oblongata of the brainstem. A variety of chemo- and mechanoreceptors provide information via reflex arcs, with increased arterial partial pressure of CO₂ (PaCO₂) being the strongest respiratory stimulus under physiological conditions (1, 2).

Perfusion

Deoxygenated blood reaches the pulmonary circulation through the right ventricle and

pulmonary valve, following the course of the pulmonary trunk into the left and right pulmonary artery. These arteries function as “public vessels” and branch out along the bronchial tree towards the location of gas exchange in the capillary beds of the alveolar sac. Henceforth arterialized blood then flows in venules and veins which ultimately conflate into four major pulmonary veins before entering the left atrium (3). Bronchial “private vessels” are either branches from the thoracic aorta or intercostal arteries, which supply nutritive, oxygenated blood to the lungs connective tissue and bronchi, but not the alveoli. They belong to the systemic circulation and, therefore, are part of a “high pressure system”. Interestingly, a certain proportion of the then deoxygenated blood from the lung’s private vessels is lead into pulmonary veins, thereby diluting the arterialized blood before it reaches the left atrium (3).

The pulmonary circulation is a “low pressure system” that features low vascular resistance and a mean pulmonary arterial pressure (mPAP) in the range of 14.0 ± 3.3 mmHg at rest, with slight variance depending on factors like age and posture (5). Pulmonary vascular resistance (PVR) in healthy adults averages at 74 ± 30 dyn·s·cm⁻⁵ and increases significantly with age (5). A key regulatory mechanism is the hypoxic pulmonary vasoconstriction (HPV) or Euler-Liljestrand mechanism. It restricts blood flow towards the capillary beds of alveoli with low oxygen partial pressure and intensifies the perfusion of well-ventilated areas with high oxygen partial pressure. Benefit is an optimized ventilation/perfusion match under physiological conditions, however, pathologies accompanied by chronic hypoxia might lead to the adverse effects of chronic pulmonary vasoconstriction, increased vascular pressure and remodeling (6). While at rest only 50 % of alveolar capillaries are perfused, increasing vascular pressures upon exercise enable a pressure-dependent “recruitment” of further capillaries, thereby effectively decreasing PVR (2). In addition, “capillary distention” and enlargement of the capillary cross-sectional area decreases not only resistance, but also the flow rate for an improved diffusion (1).

Pulmonary capillary wedge pressure (PCWP) allows for an indirect estimation of left atrial pressure and left ventricular end diastolic pressure (LVEDP) during right heart catheterization (RHC). Measured behind the temporarily occluded branch of a pulmonary artery, it normally does not exceed 15 mmHg in healthy individuals and provides valuable, yet debatable information regarding the distinction between pulmonary- or left heart-associated causes for pulmonary hypertension (PH) (7). Due to their nature as part of a “low pressure system”, pulmonary arteries feature thinner walls and only sparse

muscularization, when compared to their systemic counterparts (1). After all, this might at least partially explain their vulnerability to increased pressures as they occur in a variety of pulmonary, cardiac and systemic disorders.

Diffusion

Gas exchange across the blood-air-barrier is driven by passive diffusion and relies on differences in partial pressures between the alveolar space and circumfluent blood within the surrounding capillaries (2). Diffusing capacity (D_L) is a parameter used to quantify the rate at which a certain amount of gas is transferred across the alveolar-capillary membrane per partial pressure difference. Deriving from Fick's laws of diffusion, it is mostly determined by surface area, membrane thickness and solubility of a particular gas (1). It thus becomes clear, that the large surface area and the thin blood-air-barrier both directly contribute to an optimized diffusion (1). Conversely, the loss of lung surface area or thickening of the alveolar-capillary membrane, as common in fibrotic lungs, hinders gas exchange and is reflected in a decreased D_L (1). Carbon monoxide (CO) possesses an affinity for hemoglobin 250 times that of oxygen (O_2). As a result, the diffusing capacity for carbon monoxide (D_{LCO}) is far less influenced by perfusion and contact time than that of O_2 or CO_2 , thereby making D_{LCO} most suitable for the isolated assessment of the diffusion in a clinical setting (1, 2).

Selected cells of the alveolar landscape

The alveolar epithelium is comprised of alveolar epithelial cells type (AEC) I and II, throughout connected via tight junctions. AECI cover >95 % of the alveolar surface and compose the blood-air-barrier, together with the capillary endothelium and their interjacent, fused basal-laminas (8, 9). Characterized by surfactant protein C (SPC) expression and distinctive lamellar bodies, AECII produce, store and secrete surfactant, essential for decreasing surface tension and facilitation of various immunological responses including opsonization (9, 10). Furthermore, about 20 % of AECII function as alveolar epithelial progenitors (AEP) and present a distinct group within the heterogeneous AECII population (11, 8, 12). The number of AEP remains fairly constant throughout homeostasis, but is able to increase upon lung injury. In this instance, AEP are thought to undergo transdifferentiation into AECI in order to replace damaged epithelial cells (11).

The highly diverse fibroblasts are the predominant cell type of the interstitial space, involved in synthesizing and maintaining the extracellular matrix (ECM), as well as deeply enrooted within the lungs mechanisms to cope with injury (13). Many of their cellular actions require prior activation through growth factors, physical stress and interaction with the nearby epithelium (14). Intriguingly, the integrity of the alveolar epithelium seems to pose a precondition for functional epithelial-mesenchymal crosstalk and its disruption can be associated with adverse responses in fibroblasts, such as the reinforcement of pro-fibrotic phenotypes, proliferation and excessive accumulation of ECM (15). Distinction of the various fibroblast subgroups presents a challenge, since most established markers lack specificity. At the time of our experiments, identification therefore demanded an overall, careful assessment of location, staining and expression profile (16). In more recent years, emerging single cell data sets have improved the differentiability and gave rise to databases of transcriptomic signatures and additional markers, however, there is still a high degree of overlap between the respective transcriptomes (17).

Myofibroblasts (MYF) are a subgroup of fibroblasts and display additional, contractile properties by means of α -smooth muscle actin (α -SMA) expression. During physiological wound healing they are capable of contracting their matrix and were thought to enter apoptosis or dedifferentiation, once healing is completed (18, 19). In the pathophysiological context of pulmonary fibrosis, activated MYF exert many of the alterations which ultimately form the aspect of remodeled tissue (20). Through their accumulation and deposition of collagen, MYF play an essential role in the corruption of the lungs structural integrity during remodeling (19, 21). More recently, these cells and their origins have become the focus of attention and were identified as possible targets for pharmacological intervention (19, 22).

Lipofibroblasts (LFB) store neutral-lipids in the shape of cytosolic droplets and are commonly located in the vicinity of AECII. They are identifiable by their expression of adipose differentiation related protein (ADRP) and differ from other lipid-containing alveolar cells, such as AECII and macrophages, through storage of neutral- instead of phospholipids (23). Up until half a decade ago, the existence of LFBs in the human lung was highly controversial (24, 25) and primarily documented in rodents, where they are not only involved in the transfer of lipids and regulation of surfactant synthesis, but also demonstrate overall protective properties against oxidant lung injury (16). Furthermore, LFBs seem to reside in an epithelial stem cell niche and facilitate developmental

processes including alveolar septation (26, 27). Part of the reported work in this doctoral dissertation is dedicated to the human alveolar LFB and presents evidence for its existence in the human lung. These results ultimately contributed to a study that demonstrated the plasticity of the fibroblast phenotype and significantly advanced our understanding of the underlying mechanisms during fibrosis formation (19). Our group hereby revealed, that fibroblast subpopulations likely inherent the ability to switch between phenotypes and acquire either more lipofibroblast- or myofibroblast-like characteristics in the context of idiopathic pulmonary fibrosis (IPF) (19). This is reflected in the additional observation, that LFBs and MYFs share a common, fibroblast growth factor 10 (FGF10) expressing progenitor during embryonic development, contributing to both, adipogenic and myogenic lineages (28).

1.2 Pulmonary Hypertension

Pulmonary hypertension (PH) is a severe medical condition that is usually accompanied by a shortened life expectancy and overall reduced quality of life. Due to a marked heterogeneity in the pathogenesis and pathology of this disease, five groups have been defined by the World Symposium on Pulmonary Hypertension (WSPH) (Table1).

Commonly characterized by increased pressure in the pulmonary vascular system, the established hemodynamic definition previously relied on the elevated mPAP of >25 mmHg measured by right heart catheterization (RHC) at rest. Historically, exercise mPAP has also been used to define PH, however deemed as impractical during the 4th WSPH in 2008 and again in 2018 due to concerns regarding physiological changes with age and undetermined reference ranges (29).

Groups 1, 3, 4 and partly 5 can be described as pre-capillary PH, meaning the site of vascular alteration and pathological loss of cross-sectional area is located in pulmonary arteries and arterioles. Post-capillary PH in contrast, is reflected by increased PCWP and rooted either in reduced left heart function or systemic diseases affecting the pulmonary-venous system. During the most recent, 6th WSPH, an update of the current definition has been proposed. Changes consist primarily of a lowered threshold for an abnormal mPAP down to >20 mmHg and the emphasized importance of including pulmonary vascular resistance (PVR) ≥ 3 WU, in order to incorporate cardiac output into the definition of pre-capillary PH (29, 30)

1.2.1 Idiopathic pulmonary arterial hypertension

Pulmonary arterial hypertension (PAH) forms Group 1 and includes several pre-capillary variants of PH, which differ in etiology and epidemiology, yet share common vascular alterations and defects. Several registries are currently active worldwide, collecting data regarding the incidence and prevalence of PAH, which interestingly revealed a steady increase for both parameters over the past years (31).

Table 1 Updated classification of pulmonary hypertension as published by Simonneau et al. 2019 (29)

<p>1 PAH</p> <ul style="list-style-type: none">1.1 Idiopathic PAH1.2 Heritable PAH1.3 Drug- and toxin-induced PAH1.4 PAH associated with:<ul style="list-style-type: none">1.4.1 Connective tissue disease1.4.2 HIV infection1.4.3 Portal hypertension1.4.4 Congenital heart disease1.4.5 Schistosomiasis1.5 PAH long-term responders to calcium channel blockers1.6 PAH with overt features of venous/capillaries (PVOD/PCH) involvement1.7 Persistent PH of the newborn syndrome <p>2 PH due to left heart disease</p> <ul style="list-style-type: none">2.1 PH due to heart failure with preserved LVEF2.2 PH due to heart failure with reduced LVEF2.3 Valvular heart disease2.4 Congenital/acquired cardiovascular conditions leading to post-capillary PH <p>3 PH due to lung diseases and/or hypoxia</p> <ul style="list-style-type: none">3.1 Obstructive lung disease3.2 Restrictive lung disease3.3 Other lung disease with mixed restrictive/obstructive pattern3.4 Hypoxia without lung disease3.5 Developmental lung disorders <p>4 PH due to pulmonary artery obstructions</p> <ul style="list-style-type: none">4.1 Chronic thromboembolic PH4.2 Other pulmonary artery obstructions <p>5 PH with unclear and/or multifactorial mechanisms</p> <ul style="list-style-type: none">5.1 Haematological disorders5.2 Systemic and metabolic disorders5.3 Others5.4 Complex congenital heart disease <p>PAH: pulmonary arterial hypertension; PVOD: pulmonary veno-occlusive disease; PCH: pulmonary capillary haemangiomatosis; LVEF: left ventricular ejection fraction</p>

In 2016, Hoepfer MM et al. published a review of multiple previous publications, including, but not limited to data from the French and Spanish national registry, which lead to estimates for incidence and prevalence ranging from 1.1 to 7.6 per million adults per year, and 6.6–26.0 per million adults, respectively (32). In this instance no distinction between idiopathic, heritable, drug and toxin induced PH was made. Prevalence seems to be stronger among the female sex and younger age groups. More recent studies however suggest, that the average age at the time of diagnosis lies around 50 years and therefore later, than previously presumed (31, 33). Consistently, throughout data from several registries, including the REVEAL Registry and multiple national registries, Idiopathic pulmonary arterial hypertension (IPAH) has been the most prevalent among Group 1. Percentages range from 30 % up to 93 % of all PAH cases, with 50-60 % being the most common ratio (31, 32). The cause of IPAH is unknown to this date and no certain risk factors have been identified. Key characteristics are excessive vasoconstriction and vascular remodeling affecting all vessel layers, which result in loss of cross-sectional area and consecutive right heart strain (34, 35).

1.2.2 Vascular remodeling

The term pulmonary vascular remodeling is used to describe structural alterations of pulmonary vessels which include thickened vascular walls through excessive muscularization and neo-muscularization, consecutive narrowing of the lumen and increased pulmonary vascular resistance. In addition to vasoconstriction, other aspects such as cell autonomous growth and lack of apoptosis are presumably the result of, but also contribute further to increased pulmonary vascular pressures (36). As mentioned above, in contrast to other forms of PH, remodeling in IPAH affects all three vascular layers.

Intimal remodeling is driven by endothelial injury and endothelial-cell (EC) proliferation, accompanied by fibrosis and invasion of fibroblast-like cells (34, 37, 36). Intima thickening comprises “neointima” formation and the phenomenon of “occlusive neointimal lesions”, the latter of which is considered almost pathognomonic for PAH. The neointima is a newly emerging layer of alpha-smooth-muscle actin (α SMA) positive cells and matrix in between the endothelium and the membrana elastica interna, which thereby obstructs the lumen and hinders gas exchange due to an increased diffusion path (38). Occlusive neointimal lesions such as plexiform lesions consist of rogue endothelial, smooth muscle cells and myofibroblasts, which compose disorganized blood vessels,

channels and matrix deposits. The result is a significant loss of overall cross-sectional area and thus increased pulmonary vascular resistance (38, 39).

Medial remodeling can be regarded as a salient feature of PH and comprises the hypertrophy and primarily the proliferation of resident α SMA⁺ cells (38, 37, 40). Intriguingly, intima plus media fractional thickness, meaning their summated thicknesses relative to the overall diameter of the vessel seem to positively correlate with disease severity, displaying a 3-fold increase in severe cases of PAH. Media fractional thickness on its own also exhibits a direct correlation with both the mPAP and PVR (37, 36).

The adventitia has been characterized as “sensor tissue” and “control hub” for the vessel walls response to a variety of stimuli, such as injury, hypoxia, shear- or hormonal stresses. These influences lead to an “activation” that involves cell proliferation, expression of extracellular matrix (ECM) proteins and cytokine/chemokine/growth factor secretion (41). In this context fibroblasts are of particular interest, as they are the predominant adventitial cell type and thought to largely exert the responses outlined above – as well documented for hypoxic conditions (41–43). Upon stimulation, certain subpopulations of adventitial fibroblast are believed to transdifferentiate into myofibroblasts and traverse towards media and intima – thereby directly contributing to vascular remodeling (41). In this scenario, additional, potential sources for activated myofibroblasts are potentially found in bone marrow–derived circulating cells (I.E. fibrocytes) and endothelial-mesenchymal transition (EndMT), although not supported by recent studies (44, 45, 40). A common denominator in vascular remodeling and one underlying factor is chronic vascular inflammation, which seems to be initiated and maintained in the adventitia. Leukocytes initially invade in response to various stimuli (hypertension, hypoxia I.A.), while triggered adventitial fibroblasts then subsequently express a multitude of chemokines/cytokines and their receptors, thereby perpetuating inflammation, which then proceeds from the adventitia towards the vascular center. (46, 47). Findings regarding the extent of adventitial remodeling are inconsistent, lastly due to a certain degree of arbitrariness, when distinguishing adventitia from surrounding tissue. Stacher et al. for instance, reported no statistically significant differences in adventitia fractional thickness between PAH lungs versus control lungs (37). Other reports state, that adventitial remodeling in fact precedes media and intima remodeling with an increase in thickness and cell count, before changes in other vascular layers become noticeable (41, 48).

1.2.3 Pathogenesis

For both predominant features of PAH - vasoconstriction and vascular remodeling - a multitude of underlying pathomechanisms have been suggested and are under current investigation (Fig1):

There is a general excess of vasoconstrictors in patients with PAH, namely endothelin 1 and thromboxane, while vasodilators such as prostacyclin and nitric oxide are found in lower quantities, compared to controls (34, 49, 50). Heightened serotonin levels and 5-HT_{2B} receptor expression in pulmonary arteries appear to amplify hypoxia-induced pulmonary hypertension in the mouse model and have been linked to PAH in humans (51). Furthermore, pharmaceutically enhanced concentrations of serotonin, induced by amphetamine-like anorectic agents, can lead to drug- and toxin-induced PAH (52). Serotonin hereby not only mediates vasoconstriction, but also functions as a paracrine growth-factor inducing proliferative effects in vascular SMC via 5-HT receptors (53, 34). Additionally, Ito et al. demonstrated that serotonin promotes Interleukin-6 (IL-6) synthesis in human vascular SMC and thereby likely facilitates inflammatory processes in the vascular tissue (54). Impaired function of voltage-gated K⁺ channels and consecutive opening of Ca²⁺ channels in SMC have been observed in IPAH, thus generating muscle contraction and additional proliferative effects (55).

Mechanical strain, hypoxia and inflammation seem to elevate concentrations of vascular endothelial growth factor (VEGF), platelet-derived growth factor (PDGF), fibroblast growth factors (FGF) and transforming growth factor- β 1 (TGF- β 1). Interestingly, levels of these growth factors were found to be increased significantly in patients with PAH (34, 56–58), where they induce proliferation, migration and resistance to apoptosis within certain populations of endothelial cells (EC) and pulmonary smooth muscle cells (59). Ranchoux et al identified EndMT as a source of conglomerating smooth-muscle cells, particularly in occlusive neointimal lesions: in this case, certain EC are believed to develop α SMA-positivity, acquire a migratory phenotype and extend into subendothelial space. Intriguingly, TGF- β induced EndMT has been linked to reduced bone morphogenic type 2 receptor (BMP2) expression and appears to be attenuated by stimulation of BMP2 signaling, conversely (60). Appositely, 80% of familial PAH and 20% of IPAH cases are attributed to mutations involving BMP2, a transmembrane serine/threonine receptor kinase of the TGF- β superfamily that is known to play a role in extracellular matrix secretion, cell proliferation, -migration and -differentiation (38, 34, 61). Nevertheless, BMP2 mutations display low penetrance, which implies the need for

an additional trigger in the development of PAH. Inflammation likely presents such a trigger and possibly functions as a catalyst for the manifestation. After all, the presence of inflammatory mediators in the context of PAH has been well described, with multiple inflammatory cytokines and increased numbers of macrophages/monocytes, dendritic cells and T cells found in the walls of PAH vessels (62, 38, 47).

Apelin (APLN) is a peptide which acts through the apelin receptor, widely expressed in the pulmonary endothelium. Kim et al. were able to demonstrate, that apelin-signaling interacts with fibroblast growth factor 2 (FGF2) and is downregulated in endothelial cells of IPAH-patients (63, 64). Decreased apelin-expression, in turn, is associated with increased expression of FGF2 and fibroblast growth factor receptor 1 (FGFR1) – both of which facilitate the proliferation of pulmonary smooth muscle cells, at least partially through endothelin-1 (64, 63, 65)

Peroxisome proliferator-activated receptors γ (PPAR- γ) serve as transcription-factors and are expressed in various cell types throughout the organism, particularly in vascular SMCs and ECs. Their significance in upholding vascular pulmonary homeostasis is underlined by PPAR- γ -knockout mice, which develop spontaneous PH (34, 66). Intriguingly, PPAR- γ expression was significantly downregulated in plexiform lesions of patients with PAH, leading Ameshima et al. to reason, that loss of PPAR- γ expression might be a characteristic trait of the “proliferating, apoptosis-resistant endothelial cell phenotype” (67). Conversely, stimulated PPAR- γ signaling displays anti-proliferative, pro-apoptotic properties and is involved in BMP-2 mediated inhibition of pulmonary arterial SMC proliferation (68). Reduced levels of endothelin 1 and attenuation of serotonin induced SMC proliferation have also been attributed to stimulated PPAR- γ signaling, making it a potential pharmaceutical target (69, 70, 34).

- Vasoconstriction**
- endothelin 1 and thromboxane ↑ (49)
 - prostacyclin and nitric oxide ↓ (50)
 - serotonin levels ↑ (51)
 - opened Ca²⁺ channels in SMC (55)
- Vascular remodeling**
- serotonin levels ↑ (53)
 - increased levels of fibroblast growth factors FGF1 and FGF2 ↑ (150, 189)
 - increased levels of VEGF, PDGF and TGF-β1 ↑ (56)
 - PPAR_γ expression ↓ (66)
- Stimuli**
- Mechanical strain (58)
 - Hypoxia
 - Infections
 - Drugs (52)
 - BMPR2 mutations and other genetic factors (61)
- Intima:**
- Endothelial injury, proliferation, migration and resistance to apoptosis within populations of endothelial cells (36, 37)
 - EndMT, although controversial (60)
 - Neointimaformation, Occlusive neointimal lesions (38)
 - Luminal obstruction
 - Hypercoagulation
- Media:**
- Hyperplasia und hypertrophy of resident αSMA+ cells (37, 40)
 - Proliferation, migration and resistance to apoptosis within populations of vascular smooth muscle cells (36, 39)
 - excessive muscularization and neo-muscularization
 - vasoconstriction
- Adventitia:**
- Invasion of inflammatory cells (46, 47)
 - Triggered adventitial fibroblasts subsequently expressing a multitude of chemokines/cytokines (41)
 - Adventitial fibroblast potentially transdifferentiating into myofibroblasts and traversing towards media/intima (41)
 - Inflammation proceeding from the adventitia towards the vascular center (46, 47)

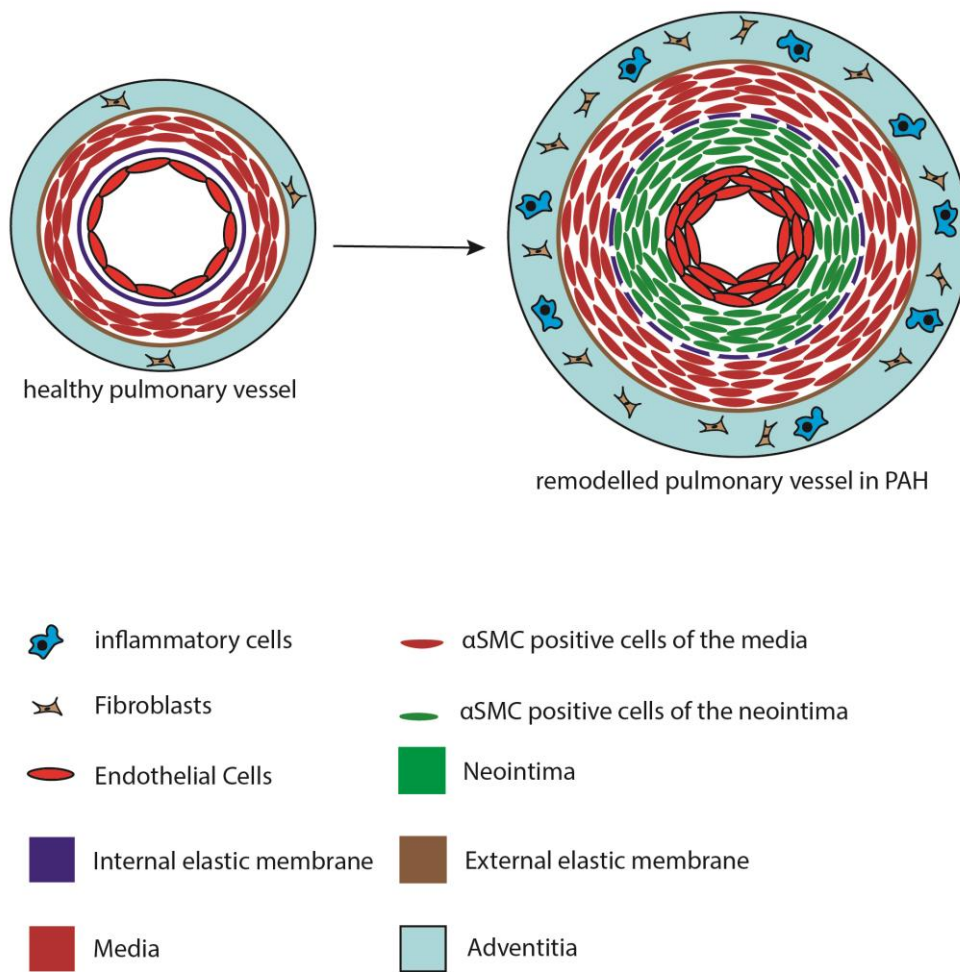


Fig.1 Synopsis of the various pathophysiological principles leading to the phenomenon of vascular remodeling in pulmonary arterial hypertension - self-created illustration based on publications by Schermuly, Ghofrani et al. 2011 (34)

1.2.4 Diagnosis

Initial symptoms are mild and rather unspecific, thereby hampering early diagnosis and treatment. Exertional dyspnea, tachycardia and fatigue are among the most frequent early signs, however, are also common to a variety of other medical conditions. In later stages of the disease, imminent right heart failure manifests in the form of dyspnea at rest, hypoxemia and drastically reduced quality of life (71). In case of suspected PAH, initial assessment via transthoracic echocardiography (TTE) allows for ruling out left-heart disease and provides a non-invasive and cost-effective estimation of systolic pulmonary artery pressure (sPAP). Tricuspid regurgitation velocity (TRV), right atrial pressure (RAP) and right atrial size (RA) are also taken into account, as the echocardiographically determined sPAP entails certain inaccuracies and is commonly overestimated. Consequentially, peak TRV is now seen as a more reliable echocardiographic surrogate parameter for PH. Further diagnostics should include a blood gas analysis, high-resolution computed tomography (HRCT) and ventilation / perfusion lung scan in order to differentiate from chronic thromboembolic pulmonary hypertension (CTEPH) and parenchymal lung disease (72, 73). When overall findings suggest an intermediate to high probability for PH, RHC is the gold standard. The updated definition hereby requires a mean pulmonary arterial pressure (mPAP) of above 20 mmHg, a pulmonary vascular resistance (PVR) ≥ 3 WU and PAWP ≤ 15 mmHg. Once PAH has been diagnosed, infectious or rheumatoid causes have to be considered and further investigated (73).

Subjective severity can be assessed using the symptom-oriented “World Health Organization (WHO) functional class system” and “six-minute walk test” (6-MWT), while further risk stratification involves additional, more objective parameters: Plasma levels of N-terminal pro-B-type natriuretic peptide (NTproBNP), a cardiac biomarker released by the myocardium upon increased volume load, are a viable indicator for progressing heart failure. Additional parameters include echocardiographic determined RA and pericardial effusion, among others. According to the 2015 European Society of Cardiology (ESC)/European Respiratory Society (ERS) guidelines, patients are to be categorized into low, intermediate and high-risk groups, with 1-year mortality rates ranging from $<5\%$, $5\text{-}10\%$ up to $>10\%$, respectively. Any clinical signs of heart failure (cyanosis, edema, orthopnea I.A.) are inevitably associated with high risk, as right heart failure is the most common cause of death among patients with PAH (74, 75). Congruously, changes in risk category either due to amelioration or disease progression have proven to be accurate predictors of long term survival (74).

1.2.5 Treatment

Current strategies aim for disease stabilization within a certain, preferably lower risk group. Despite multinational efforts and recent advancements, PAH still remains an incurable and fatal disease. General symptomatic treatment involves diuretics to reduce right heart overload and long-term oxygen therapy to compensate for hypoxemia (arterial pO₂ <60 mmHg). Complementary rehabilitation and physiotherapy can help further to retain cardiac function and quality of life (75, 76). Anticoagulation has been recommended in the past, but is now restricted to patients with CTEPH or specific comorbidities. Upon diagnosis, patients should be referred to competence centers and evaluated for possible long-term response to calcium channel blockers. In the course of right heart catheterization vasoreactivity is tested, as “responders” (mPAP decreases by ≥ 10 mmHg to < 40 mmHg without a decrease in CO) demonstrate vastly improved outcomes under monotherapy with calcium channel blockers (< 5 % of all patients with PAH) (75, 76). For specific pharmacological treatment of “non-responders”, five substance classes targeting three different pathways are currently available, usually administered in combinations of two or more substances depending on disease severity: Endothelin receptor antagonists (ERAs) act on ET_A and ET_B receptors, repressing Endothelin 1 mediated vasoconstriction and associated proliferative effects on pulmonary SMC. Selective ET_A-blockage might be desirable, as vasoconstrictive effects are primarily mediated through ET_A receptors. Representative substances are Bosentan and Ambrisentan (30, 76).

Phosphodiesterase-5 (PDE5) inhibitors like Tadalafil and Sildenafil prevent rapid degradation of cyclic guanosine monophosphate (cGMP), which acts as a second messenger for nitric oxide (NO) and thereby exerts vasodilatative effects. Soluble guanylate cyclase (sGC) stimulators like Riociguat act on the same pathway (30, 75, 76). Prostacyclin analogues (Epoprostenol) and Prostacyclin-IP-receptor-agonists (Selexipag) display strong vasodilatative and anti-inflammatory properties via heightened levels of intracellular cyclic adenosine monophosphate (cAMP) (30, 75, 76).

For patients with low to intermediate risk, guidelines allow for a combination of an ERA with a PDE5- inhibitor or sGC stimulator. A triple combination of a PDE5 inhibitor or sGC stimulator with an ERA and prostacyclin analogue is reserved for patients with high risk or not responding to dual therapy (30, 76). Ultimately, a lung transplantation remains the final option for patients not improving under pharmacotherapy.

1.3 Idiopathic pulmonary fibrosis (IPF)

IPF is part of a broad spectrum of interstitial lung diseases (Table 2) which share progressive scarring of lung tissue as their prominent feature. Among the subgroup of idiopathic interstitial pneumonias (IIPs), IPF is the most prevalent representative. Due to the unknown origin and progressive nature of this disease, mortality is high - with a median survival of 2-3 years upon diagnosis. Estimated incidences range between 2.8-19 per 100000 in North America and Europe, while recent reports suggest a significant incline in the past decade. Peak age of onset is at 60-70 years and the male sex is more frequently affected (77–81).

Table 2 Classification of Interstitial lung disease (ILD) as published by Vincent Cottin, Athol U. Wells et al. in the European Respiratory Review Dec 2018 (82)

1. *Interstitial lung disease (ILD)*

1.1 *Idiopathic interstitial pneumonias (IIP)*

- 1.1.1 Idiopathic pulmonary fibrosis (IPF)
- 1.1.2 Idiopathic nonspecific interstitial pneumonia (INSP)
- 1.1.3 Respiratory bronchiolitis–interstitial lung disease
- 1.1.4 Desquamative interstitial pneumonia (DIP)
- 1.1.5 Cryptogenic organizing pneumonia (COP)
- 1.1.6 Acute interstitial pneumonia (AIP)
- 1.1.7 Rare idiopathic interstitial pneumonias
- 1.1.8 Idiopathic lymphoid interstitial pneumonia (LIP)
- 1.1.9 Idiopathic pleuroparenchymal fibroelastosis (PPFE)
- 1.1.10 Unclassifiable idiopathic interstitial pneumonias

1.2 *Autoimmune ILD*

1.3 *Hypersensitivity Pneumonitis*

1.4 *Sarcoidosis*

1.5 *Other ILDs*

Main characteristic is the usual interstitial pneumonia (UIP) with irregular fibrosis of lung parenchyma and excessive ECM deposition, leading to ongoing loss of physiological lung structure, progressive decline in lung function and ultimately to the patients' demise. Diagnosis of IPF is primarily based upon signs of UIP in the high-resolution computed tomography (HRCT) and requires the exclusion of known causes for other ILDs. The positive predictive value for the detection of histological UIP through HRCT is stated at over 90 %, making it the primary diagnostic tool (80, 83). The UIP pattern features honeycombing, subpleural traction bronchiectasis, reticulate consolidations and ground-glass opacity (among others). In case of absent honeycombing but otherwise fully established picture, current guidelines recommend use of the term “probable UIP”, as it

is still highly likely. While in some cases a cryo- or surgical lung biopsy can be necessary, most of the time radiological findings in combination with typical clinical constellations are sufficient for the diagnosis to be made (77, 80). This is particularly favorable, as biopsies are associated with certain complications, especially among elderly, comorbid patients.

Initial clinical manifestations are unspecific and range from dyspnea and persistent coughing to chronic fatigue. At this point, patients are often misdiagnosed with chronic obstructive pulmonary disease (COPD), not least because of a high prevalence of ex-smokers among patients with IPF (84, 85). Sclerosiphonia, a distinct crackling rattle during auscultation, is relatively specific to fibrosis as it originates from distended fibrotic lung tissue. In later stages clubbed fingers attributed to chronic hypoxia complete the clinical picture (71). Typically, functional diagnostics reveal diffusion as one of the first parameters to be affected. Deposits of collagen increase the distance between lung capillaries and the alveolar space, thereby lengthening the diffusion path and hindering gas exchange. This is reflected by an early decrease in DLCO, before changes in other parameters like forced vital capacity (FVC) and total lung capacity (TLC) become apparent. In the course of the disease, further collagen deposition will lead to reduced compliance, impaired ventilation and the constellation of a restrictive ventilatory defect. Prognosis can be estimated using the Gender-Age-Physiology (GAP) scoring system, which incorporates DLCO and FVC in addition to age and gender. Patients are categorized into stages I, II and III, with 1-year mortality rates of 6%, 16% and 39%, respectively (71, 86, 87).

A variety of risk factors have been identified, foremost inhalation exposure to cigarette smoke and potentially noxious allergens like asbestos, metal-, mineral- and sawdust (88). Intriguingly, the time between end of exposure and manifestation of IPF averages at 21 years. Furthermore, there is strong evidence for individual genetic predispositions. Mutations in surfactant proteins (A and C), telomere-related genes and most prominently the MUC5AC gene promoter have been well described in the context of familial pulmonary fibrosis (FIF) and sporadic idiopathic interstitial pneumonias (80, 87, 89).

1.3.1 Remodeling

UIP is the histopathological correlate of IPF and characterized by patchy areas of fibrosis scattered among seemingly healthy lung parenchyma (80). Fibrotic zones feature dense

deposits of collagen and smooth muscle, which tend to cause local retractions thereby inducing cystic airway enlargement and the radiological phenomenon of honeycombing (90, 91). Additional features include hyperplasia of AEC type II cells and the proliferation of airway basal cells into alveolar spaces which create the aspect of bronchiolisation (92). During the early stages, these alterations are usually restricted to the subpleural and basal regions of the lung (80). Fibroblastic foci are a common feature of fully developed UIP and are often located in areas, where fibrotic tissue borders on less afflicted regions. These foci consist of clusters of fibroblasts and myofibroblasts, which show a tendency to arrange parallel to the alveolar surface and represent the active site of fibrosis (90, 91, 21). The peripheral regions of the secondary pulmonary lobules are affected the most, while fibrosis tends to lessen towards the center. This characteristic attribute of initial UIP, combined with only mild signs of inflammation, enables a distinction from autoimmune connective tissue disease or extrinsic allergic alveolitis, which feature centrilobular or peribronchiolar fibrosis and pronounced inflammation (90). Parenchymal remodeling and hypoxic vasoconstriction lead to an overall loss of cross-sectional area, thus impaired perfusion and a consecutive increase in PVR are to be expected (93). Consequentially, in between 8% to 85% of all patients suffering from IPF also meet the diagnostic criteria for PH (94, 95). However, in 10% of those cases the increase in PVR is seen as disproportionately high in comparison to the actual extent of structural alterations caused by IPF (93, 96). Seeger et al. even argue that any increase of PAP above 25 mmHg may be considered out of proportion, as >80% of the lungs parenchyma ought to be lost for such an increase to be proportionate (93). A potential cause might be an independent, underlying vascular remodeling process, connecting the pathologies of IPF and PH (93, 97). This idea is supported by evidence for the shared upregulation of mediators like PDGF, fibroblast growth factors (FGFs), TGF- β and endothelin-1 (97).

1.3.2 Pathogenesis

Historically, IPF has been interpreted primarily as an inflammatory condition, hence immunosuppressive therapy was implemented into previous treatment regimes, with adverse results (98, 99). Nowadays, IPF and the adherent fibrotic occurrences are seen as an aberrant repair process, which likely results from repeated micro-injury of the alveolar epithelium combined with an individual's genetic susceptibility (98). Several genetic variations associated with IPF lead either to impaired surfactant synthesis, reduced lung defense (100) or loss of cellular barrier function (98, 101, 102). In addition, epigenetic

alterations through aging (98, 103) and inhalative toxins (104) create an environment, which renders the alveolar epithelium fragile and susceptible to dysfunctional fibrotic responses upon injury (105). Thus altered AEC2 are impaired in their ability to regenerate damaged AEC1 and feature a variety of activated pro-fibrotic pathways, namely the unfolded protein response (UPR), among others. UPR, in turn, activates intracellular apoptotic pathways and elevates levels of profibrotic signal mediators such as TGF- β 1, PDGF, VEGF and certain FGFs (90).

TGF- β 1 is positioned in the epicenter of this distorted epithelial-mesenchymal crosstalk and thought to mediate many of the processes that might ultimately contribute to pulmonary remodeling: differentiation of fibroblasts to myofibroblasts, debatably epithelial-to-mesenchymal transformation (EMT) and uncontrolled collagen deposition - partially through an upregulation of FGF2, FGFR1 and FGFR2 (90, 106–108). Furthermore, TGF- β 1 seems to inhibit the expression of SP-A, SP-B and SP-C (except SP-D), which likely results in alveolar atelectasis and ultimately the loss of alveoli (109). Intriguingly, TGF- β fulfills a comparable role in the pathophysiology of PAH, thereby implicating a possible link between the pathologies of IPF and PAH – as demonstrated by beneficial effects of tyrosine kinase inhibitors in animal models in the context of both entities (110, 111).

As previously mentioned, MYFs are α -SMA positive, contractile cells characterized by their ability to synthesize ECM components. They play an essential role in physiological tissue repair, wound healing and fibrosis formation (112). While activated myofibroblasts are universally accepted as the primary executive mesenchymal cell type in fibrotic lung remodeling, their source and recruitment however remains a controversial topic: CD45-positive fibrocytes are circulating mesenchymal progenitor cells, which represent one possible source via transdifferentiation (113). Pulmonary epithelial cells are another potential precursor, however, conflicting findings depict epithelial-to-mesenchymal transdifferentiation in this context as less likely (114). Unlike in the pathogenesis of PAH, pre-existing SMC seem not to contribute to the pool of activated MFB, either (19). On the other hand, LFBs have demonstrated their ability to differentiate into activated MYFs in a TGF- β 1 dependent manner (115). Additionally, it has previously been established in animal models, that injury through hypoxia or other pulmonary traumata disrupts and alters the epithelial-mesenchymal crosstalk between LFB and AEC2 (via parathyroid hormone-related protein-signaling [PTHrP] and PPAR γ). In response to these interruptions, LFBs then acquire a myogenic phenotype

and lose their ability to uphold homeostasis (116). Our group confirmed a TGF- β 1-dependent lipogenic-to-myogenic switch in fibroblasts during fibrosis formation in the bleomycin-mouse-model. Furthermore, we were able to show, that PPAR- γ signaling is involved in the reversal of this process during fibrosis resolution. Hyperactive TGF- β 1-signaling hereby seems to surmount PPAR γ -expression, while PPAR-agonists were able to counteract this process (19).

1.3.3 Treatment

A previously widely applied immunosuppressive combination of prednisone, azathioprine, and N-acetylcysteine has been proven as detrimental and associated with an increased risk of death (99). These findings are coherent with a paradigm shift away from understanding IPF primarily as an inflammatory condition. Somewhat recently, a new group of “anti-fibrotic agents” have taken over current treatment regimens and have been implemented into most comprehensive guidelines (117, 118). Logically consistent with pathophysiological considerations, tyrosine kinase inhibitors are among the most significant representatives. Imatinib, primarily a PDGF-receptor α/β - and c-Abl – inhibitor, failed to demonstrate significant advantages in placebo-controlled trials (119). Nintedanib, however, with its broader inhibition including FGFR1-3, PDGFR α/β and VEGFR1-3, mitigated TGF- β associated fibroblast-to-myofibroblast transdifferentiation and collagen deposition in vitro (106, 111, 120). Furthermore, it decelerated disease progression significantly in clinical settings, using FVC stabilization as a surrogate parameter (121, 122). The other relevant anti-fibrotic substance is pirfenidone, which suppresses translation of TGF- β as well as other pro-inflammatory and pro-fibrotic cytokines such as Interleukin 6, tumor necrosis factor (TNF)- α and PDGF in animal models (123–125). The hereby resulting effects entail inhibition of fibroblast proliferation, -migration and -transdifferentiation into myofibroblasts. Additionally, a reduction in ECM deposition and myofibroblast mediated collagen contraction have been observed (126–128). Results in clinical settings are not as clear, but overall benefits in seem to outweigh frequent adverse effects (129, 130). Nintedanib and Pirfenidone both represent valuable treatment options, even though the latter of which has only been approved for mild to moderate cases of IPF. Both drugs are restricted solely to IPF and no other form of ILD, therefore an accurate diagnosis is of utmost importance (117).

1.4 Fibroblast-Growth Factors (FGF)

Signaling via fibroblast growth factors is involved in a variety of pathways in the human organism. They serve as maintainers of the homeostatic balance in the adult organism and restorers of parenchymal integrity upon injury (131), as well as mediators of embryonic organogenesis (132). These evolutionary related polypeptides are comprised of 150-300 amino acids and form a family of 22 members (Fig.2) (133, 134). *FGF1* to *FGF23* have been identified in humans, with the exception of *Fgf15*, which is the ortholog of human *FGF19* and limited to mice. FGFs act in an intracrine, paracrine or endocrine manner, either independently or via cell-surface-bound tyrosine kinase receptors (FGFRs). Based on their function and sequence similarities, FGFs can be categorized into 5 paracrine, one endocrine and one intracrine subfamily (133, 134). Intracrine FGFs, FGF11 to 14, function exclusively in the intracellular environment and primarily regulate the electrical excitability of neurons through voltage gated sodium channels (134, 135).

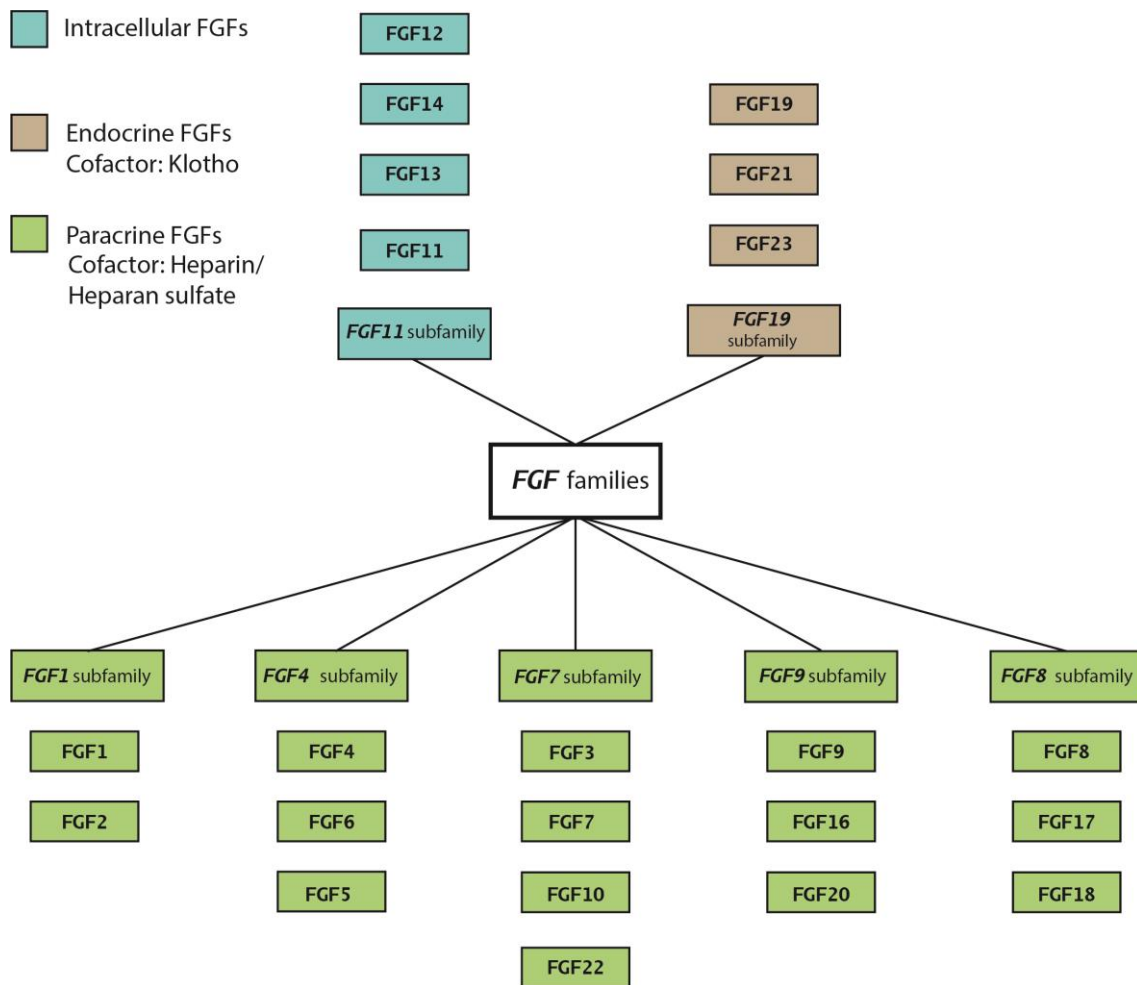


Fig.2 FGFs categorized according to their phylogenetic gene family, cofactors and mode of action – paracrine (canonical), endocrine and intracellular. Self-created illustration based on publications by Ornitz, Itoh et al. 2015 (136)

These four intracrine FGFs are perceived as evolutionary ancestors in the FGF-family, thus demonstrated by phylogenetic and gene-location analysis (133). Paracrine FGFs, FGF1-10, 16, 17, 18, 20 and 22 bind to the extracellular domain of their corresponding FGFR in the presence of a heparan sulfate proteoglycan (HSGP) cofactor. In contrast, FGF15/FGF19, FGF21 and FGF23 display a reduced HSGP-binding affinity and the need for Klotho family cofactors (136), which enables them to diffuse beyond paracrine vicinity and function as endocrine growth factors (133, 137).

There are 4 distinct signaling FGFRs, each of which feature certain FGF-FGFR binding specificities, which are determined by differences in their extracellular domains, cofactors, diverging expression patterns and sequence differences of their ligands (136). FGFRs are receptor tyrosine kinases, composed of approximately 800 amino acids and featuring three extracellular immunoglobulin-like domains (I, II, III) in addition to a transmembrane domain and two intracellular tyrosine kinase domains (Fig.3). The immunoglobulin-like domain III exists in two splice variants – IIIb and IIIc - so that FGFR1-FGFR3 each feature an IIIb and IIIc isoform, which differ in their binding specificity (136). FGF/FGFR-binding in the presence of the appropriate cofactor forms a ternary complex, which then induces transphosphorylation and results in further activation of several, classical downstream pathways – namely the MAPK/ERK pathway, phosphoinositide 3-kinase–Akt pathway, PLC gamma pathway and STAT dependent signaling (138–140). FGF signaling is generally regulated through aforementioned FGF-FGFR binding specificities, as well as through varying spatial and temporal expression patterns of FGFs, FGFRs and their respective co-factors (141–143).

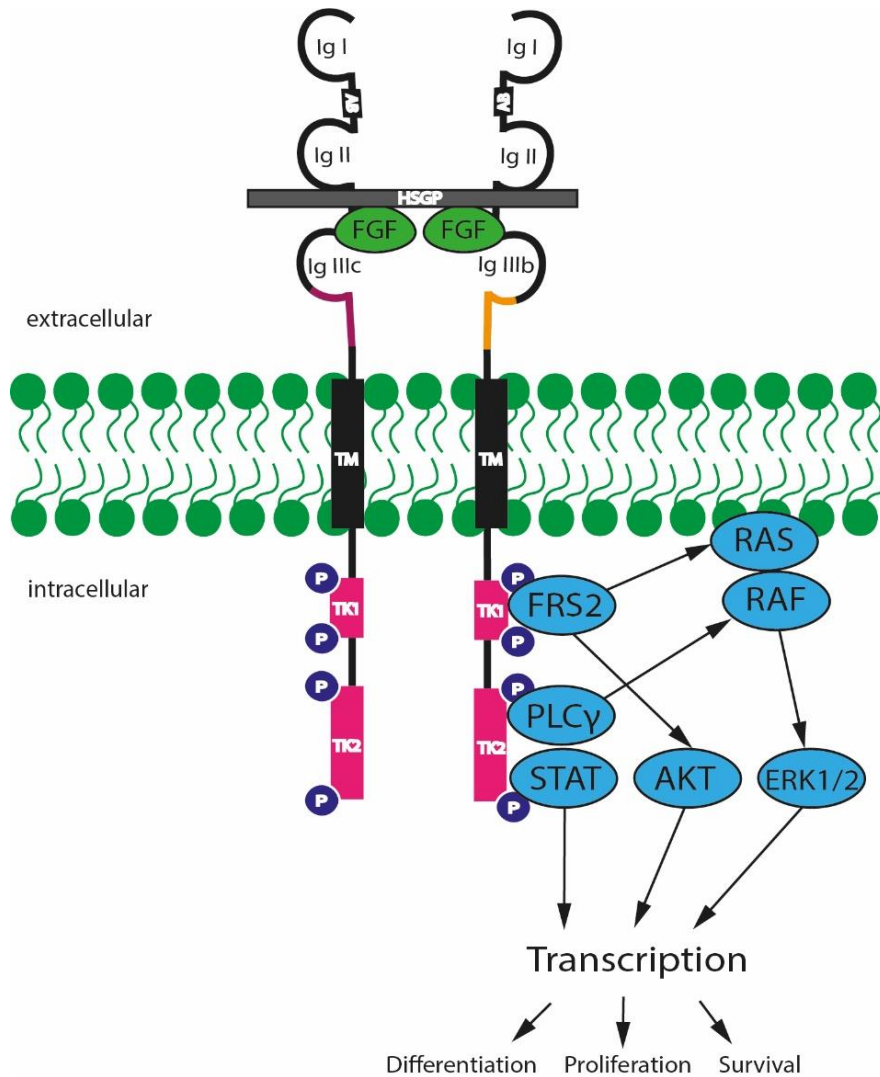


Fig.3 Schematic illustration of the FGF-FGFR structure and simplified overview of downstream pathways – FGFs bind to the extracellular domain and form a ternary complex with FGFR and heparan sulfate proteoglycan (HSGP). This induces the subsequent receptor dimerization and tyrosine phosphorylation of the intracellular domain, which in turn activates downstream pathways depending on the surrounding cellular context (136, 144). Fibroblast growth factor receptor substrate 2 (FRS2) is a signal transducing adaptor protein that, once phosphorylated by the activated FGFR, mediates the activation of the MAPK/ERK (ERK1/2) and phosphoinositide 3-kinase–Akt (AKT) pathway. The PLC gamma pathway (PLC γ) and “signal transducer and activator of transcription” (STAT) signaling are initiated independently from FRS2 (144, 141). These classical pathways are implicated in differentiation, proliferation, cell growth, survival and migration (144, 141, 145); Immunoglobulin-like domains (Ig), Acid-Box (AB), transmembrane domain (TM), intracellular tyrosine kinase domain (TK), phosphoryl group (P), Ras small G-Proteins (RAS), RAF serine/threonine-protein kinase (RAF); Self-created illustration based on publications by Ornitz et al., Touat et al. and Xie et al. (136, 141, 144)

1.4.1 FGFR2-Signaling

During physiological conditions FGF1, 2, 7, 9, 10, 18 and most FGFRs are expressed abundantly in lungs of adult mice, making them a subject worth investigating in the context of pulmonary pathologies (146, 147).

Fibroblast growth factor receptor 2 (FGFR2) takes the center stage in regards to FGF-signaling and its involvement in the pathogenesis of hyperproliferative, nonmalignant pulmonary diseases. However, both isoforms, FGFR2 IIIb and FGFR2 IIIc, differ in their site of action, their binding preferences and impact on pulmonary remodeling. Predominantly mesenchymal FGFR2 IIIc is commonly favored by FGF-ligands expressed in the epithelium and seems to exert pro-fibrotic and hyperproliferative effects (136, 146, 148). Hence, selective inhibition led to attenuation of fibrosis (146, 108) and prevented TGF- β 1-mediated alpha-actin-2 (ACTA2)-expression in the mouse model of bleomycin-induced fibrosis (146, 149). FGF2, as one of the most prolific FGFR2 IIIc ligands, was shown to promote endothelial-cell survival and excessive proliferation, both characteristic features in PAH (146, 150). These effects also extend onto pulmonary smooth muscle cells and were, as to be expected, antagonizable through inhibition of FGF-signaling, e.g. via tyrosine kinase inhibitors (146, 65, 151, 152). Interestingly, FGF1 and FGF9, which also act through FGFR2IIIc, display opposing, anti-fibrotic characteristics by inhibiting or even reverting TGF- β 1-mediated EMT. Nevertheless, in summation the pro-fibrotic effects of FGFR2IIIc-signaling seem to prevail (146, 153, 154).

Contrary to FGFR2IIIc with its adverse role in pulmonary remodeling, mostly epithelial FGFR2IIIb and two major ligands, FGF7 and FGF10, have demonstrated beneficial effects in the form of protective properties against various lung toxins and attenuated fibrosis in animal models (155–159). Their impact on pulmonary parenchymal and vascular remodeling in the context of IPF and IPAH, therefore, is of highest interest and well worth further investigation.

1.4.2 FGF7 and FGF10

Both ligands are part of the FGF7 subfamily and primarily activate the FGFR2 IIIb isoform (136). FGF7 (KGF = Keratinocyte Growth Factor) was first purified in 1989 and defines the subfamily of 4 paracrine-acting members, FGF3, 7, 10 and 22 (160). With its mitogenic effect on keratinocytes it is prominently involved in dermal wound healing (161), but is also known to induce proliferation and differentiation of AEC2 in the normal

adult lung (162). Administration of FGF7 protected against the development of pulmonary hypertension during hyperoxia in the prematurely born rat model (157) and also proved beneficial as pretreatment in animals exposed to bleomycin or hydrochloric acid (155, 156). FGF7-knockout mice demonstrate impaired hair and kidney development (133, 163, 164), but intriguingly, no apparent abnormalities in epidermal growth and healing. Guo et al. therefore suggested a redundancy with an unknown factor (163), which is potentially embodied by FGF10 via their mutual receptor FGFR2 IIIb.

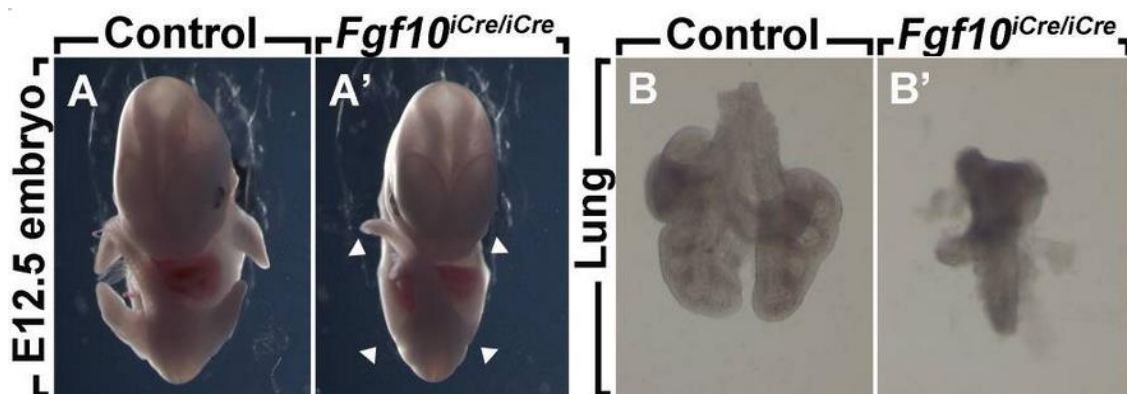


Fig.4 Loss of function of Fgf10 in mice leading to lung and limb agenesis. *Fgf10^{iCre}* is a loss of function allele for *Fgf10* and *Fgf10^{iCre/iCre}* embryos display agenesis of the limbs (A, A') and lung (B, B'), arrowheads illustrate the absence of regular limb formation, *Fgf10^{iCre/+}* embryos were used as controls. Figure adapted from El Agha et al., 2012 (165)

FGF10 is capable of activating the IIIb isoforms of FGFR1 (weaker affinity) and FGFR2 (high affinity) and was first isolated in 1996 by Yamasaki et al. (136, 166, 167). This ligand has been shown to play a vital role in embryonic development, as “*Fgf10*-knockout” mice suffer from defective organ formation, including complete lung agenesis and impaired limb outgrow (Fig.4) (132, 168, 169). “*Fgf10*-hypomorphic” mice with only residuary *Fgf10* expression display a simplified vascular tree and severely limited airway smooth muscle formation (165, 169). Interestingly, postnatal inhibition of FGFR2b-signaling unveiled no significant impact on lung development (170). This led Ramasamy et al. to reason that even though FGF10 might be the sole effective FGFR2IIIb ligand during early embryonic development, other FGFR2IIIb ligands are able to compensate for lost FGF10-signaling during later stages of prenatal development (169, 170).

More recently, certain deletion and nonsense mutations in *FGF10* were found to be associated with a specific COPD phenotype (64, 171). A synoptic interpretation of the various findings, with focus on the respiratory system, highlights FGF10-signaling through FGFR2IIIb as crucial for the development of the pulmonary vascular system and

smooth muscle formation. Overall, both FGF7 and FGF10 seem to facilitate the formation and regeneration of the pulmonary epithelium (64, 169, 172).

1.5 Hypothesis and aims

Even though FGFs and their relevance in repair processes, homeostasis and certain pathologies had been partially elucidated - at the time of our experiments – the involvement of FGF7 and FGF10 in hyperproliferative pulmonary diseases, such as IPF and PAH, had yet to be fully investigated. Both ligands display high affinity to the epithelial FGFR2IIIb isoform (173) and came into sight as particularly promising, given that their overexpression attenuated drug-induced fibrosis in animal models (158) and local administration hampered the development of pulmonary hypertension in a prematurely born rat/hyperoxia model, respectively (157). Intriguingly, established, contemporary treatment regimens for IPF are based on the broad inhibition of receptor tyrosine kinases and likely go in hand with a collateral inhibition of FGFR2IIIb-signaling, thereby also inhibiting any potentially beneficial effects of FGF7 and FGF10 (64). In order to reveal the location and expression patterns of FGFR2 and its ligands in the human context, we opted for an immunohistochemical staining of lung tissue samples and subsequent computer software assisted morphometry. We acquired human tissue specimens from IPF and IPAH patients, which were either derived from explanted lungs during lung transplantation or post mortem, in order to then compare them to samples of presumably healthy donors (controls), provided by a biobank. The author hypothesizes, that FGFR2b signaling is altered in the pathogenesis of IPF/ IPAH and, further, aims to gain insight whether these disturbances in FGF homeostasis are of causative or, indeed, reactive and even regenerative nature. In the further course, this will hopefully shed light on the issue of tyrosine kinase inhibitors and their potential adverse effects on FGF-signaling in the context of pulmonary parenchymal and vascular remodeling.

As mentioned before (compare 1.3.2.), alveolar lipofibroblasts were identified as potential contributors to the group of activated myofibroblasts in the bleomycin mouse model of pulmonary fibrosis (19). Studies from our group suggest a high level of plasticity in fibroblast phenotypes, in which lipofibroblasts are able to undergo a transdifferentiation into myofibroblasts during fibrosis formation. Conversely, the existence of a reversed process in animal models has been proposed, in which a subpopulation of activated myofibroblasts regresses into a lipofibroblast-like state during

fibrosis resolution (19). Findings by our group indicate, that the shift towards the myogenic phenotype might be TGF- β dependent, while PPAR γ -signaling seems to promote the reversal (19). This is particularly fascinating, as TGF- β is a known mediator of several adverse effects in the pathogenesis of both, IPF and IPAH (compare 1.2.3. and 1.3.2.). In contrast, stimulated PPAR γ -signaling is regarded as beneficial in the context of PAH (68), whereas loss of PPAR γ expression has been associated with the development of PH (66). This not only implies a link in the pathogenesis of PAH and pulmonary fibrosis, possibly IPF, but also leaves PPAR γ agonists in the light as a possible therapeutic approach in both conditions. In order to investigate, whether the mentioned phenotypic shifts are relevant to IPF as the corresponding human condition, first the existence of lipofibroblasts in the human lung has to be confirmed. Their presence in the human lung had been controversial (24, 25), but is well established in rodents (174). I hypothesize, that lipofibroblasts are a common occurrence in the human lung, likely with lower numbers in IPF lungs compared to donor lungs, as an indication for aforementioned shifts towards the myogenic phenotype. In the second half of this study, I therefore utilize a neutral lipid stain (LipidTOX™) and fluorescence microscopic imaging on human tissue samples from IPF patients and donors. Following an exploration of their spatial distribution and relative position to AECII using an additional immunofluorescent labeling of SPC, I then aim to quantify the number of lipofibroblasts in both specimen groups.

2 Materials and Methods

2.1 Reagents and Kits

2.1.1 Immunohistochemistry and structural staining

Acetic acid (CH ₃ CO ₂ H)	<i>Carl Roth GmbH & Co. KG, Karlsruhe, Germany</i>
Alanine Blue Stain Sol.	<i>Thermo Scientific, Waltham, MA, USA</i>
Albumine bovine Fraction V	<i>SERVA Electrophoresis GmbH, Heidelberg, Germany</i>
Aqua dest. (Milli-Q, Advantage 10)	<i>Millipore MERCK, Darmstadt, Germany</i>
Citrate buffer	<i>Zymed Laboratories Inc., Invitrogen, Carlsbad USA</i>
DAB Substrate Kit, Peroxidase (HRP)	<i>Vector Laboratories Inc. part of Maravai LifeSciences California, USA</i>
Disodiumhydrogen- phosphatedihydrate (Na ₂ HPO ₄ x 2 H ₂ O)	<i>MERCK, Darmstadt, Germany</i>
Eosin-y sol. (alcoholic)	<i>Thermo Scientific, Rockford, IL, USA</i>
Ethanol 70%	<i>SAV Liquid Production GmbH, Flintsbach am Inn, Germany</i>
Ethanol 96%	<i>Otto Fischar GmbH & Co. KG, Saarbrücken, Germany</i>
Ethanol 99,6%	<i>Berkel AHK Alkoholhandel GmbH & Co. KG, Ludwigshafen, Germany</i>
Hämalaun, sauer; nach Meyer	<i>Waldeck GmbH & Co. KG, Münster, Deutschland</i>
Hematoxylin solution	<i>Thermo Scientific, Waltham, MA, USA/ Invitrogen Corporation, Camarillo, CA, USA</i>
Hydrogen Peroxide 30%	<i>EMSURE® MERCK, Darmstadt, Germany</i>
ImmPRESS® HRP Anti- Rabbit (Peroxidase) Detection Kit	<i>Vector Laboratories Inc. part of Maravai LifeSciences California, USA</i>
Methanol 99.8%	<i>Sigma-Aldrich Chemie GmbH, Steinheim, Germany</i>
Methyl Green Counterstain	<i>Vector Laboratories Inc. part of Maravai LifeSciences, California, USA</i>

Mounting medium (Pertex®)	<i>Medite GmbH, Burgdorf, Germany</i>
Normal Horse Serum Blocking Solution, 2.5%	<i>Vector Laboratories Inc. part of Maravai LifeSciences California, USA</i>
NovaRED™ Peroxidase Substrate Kit	<i>Vector Laboratories Inc. part of Maravai LifeSciences California, USA</i>
Orange G	<i>Carl Roth GmbH & Co. KG, Karlsruhe, Germany</i>
Paraffin (Paraplas Plus®)	<i>Sigma-Aldrich Chemie GmbH, Steinheim, Germany</i>
Pertex®	<i>Medite GmbH, Burgdorf, Germany</i>
Phosphomolybdic/ Phosphotungstic Acid Sol.	<i>Thermo Scientific, Waltham, MA, USA</i>
Potassium chloride (KCL)	<i>Carl Roth GmbH & Co. KG, Karlsruhe, Germany</i>
Potassiumdihydrogen- phosphat (KH ₂ PO ₄)	<i>MERCK, Darmstadt, Germany</i>
2 Propanol	<i>Sigma-Aldrich Chemie GmbH, Steinheim, Germany</i>
Proteinase K (40x) (Dako Real™)	<i>DAKO, Hamburg, Germany</i>
Proteinase K Diluent	<i>DAKO, Hamburg, Germany</i>
Säurefuchsin	<i>Fluka Chemie GmbH, Hannover, Germany</i>
Sodium chloride (NaCl)	<i>Sigma-Aldrich Chemie GmbH, Steinheim, Germany</i>
VECTASTAIN® Universal Quick Kit	<i>Vector Laboratories Inc. part of Maravai LifeSciences California, USA</i>
Vector® VIP Substrate Kit (Peroxidase)	<i>Vector Laboratories Inc. part of Maravai LifeSciences California, USA</i>
Weigert's Iron Hematoxylin (Part A)	<i>Thermo Scientific, Waltham, MA, USA</i>
Weigert's Iron Hematoxylin (Part B)	<i>Thermo Scientific, Waltham, MA, USA</i>
Xylol-substitute (Roti®-Histol)	<i>Carl Roth GmbH & Co. KG, Karlsruhe, Germany</i>

2.1.2 Immunofluorescent staining

Invitrogen™ ProLong™ Gold Antifade Mountant with DAPI	<i>Thermo Scientific, Waltham, MA, USA/ Invitrogen Corporation, Camarillo, CA, USA</i>
Normal Goat Serum	<i>Thermo Scientific, Waltham, MA, USA/ Invitrogen Corporation, Camarillo, CA, USA</i>
HCS LipidTOX™ Deep	<i>Thermo Scientific, Waltham, MA, USA/ Invitrogen Corporation, Camarillo, CA, USA</i>
ROTI®Histofix 4 %	<i>Carl Roth GmbH & Co. KG, Karlsruhe, Germany</i>
TBS-Tris buffered saline (pH 7,2)	<i>Zytomed Systems GmbH, Berlin, Deutschland</i>
Tissue-Tek® O.C.T. Compound	<i>Sakura Finetek Europe B.V., Alphen aan den Rijn, the Netherlands</i>
Triton® X 100	<i>Carl Roth GmbH & Co. KG, Karlsruhe, Germany</i>
Tween® 20	<i>AppliChem, Darmstadt</i>

2.2 Consumables

Coverslips 24x36mm	<i>Menzel GmbH & Co. KG, Braunschweig, Germany</i>
Embedding cassettes	<i>Leica Microsystems, Nussloch, Germany</i>
Gloves (Nitra-Tex®)	<i>Ansell Ltd., Tamworth, Staffordshire, UK</i>
Glass slides (25x75x1mm)	<i>R. Langenbrink, Emmendingen, Germany</i>
Microtome blades (Blade type A35)	<i>Feather Safety Razor Co Ltd, Osaka, Jap.</i>
Pipettes	<i>Eppendorf AG, Hamburg, Germany</i>
Superfrost ultra plus slides	<i>Thermo Scientific, Waltham, MA, USA</i>
Tissue-Tek® Cryomold®	<i>Sakura Finetek Europe B.V., Alphen aan den Rijn, the Netherlands</i>

2.3 Devices and Equipment

Microtome (Leica RM 2165)	<i>Leica Microsystems GmbH, Wetzlar, Germany</i>
Computer (Q 550 IW)	<i>Leica Microsystems GmbH, Wetzlar, Germany</i>
Cooling table (Leica EG 1150 C)	<i>Leica Microsystems GmbH, Wetzlar, Germany</i>
Bath for sections (Leica HI 1210)	<i>Leica Microsystems GmbH, Wetzlar, Germany</i>
Flattening table (Leica HI 1220)	<i>Leica Microsystems GmbH, Wetzlar, Germany</i>
Light microscope (Leica DM6000B)	<i>Leica Microsystems GmbH, Wetzlar, Germany</i>
Q Win V3 Software	<i>Leica Microsystems GmbH, Wetzlar, Germany</i>
Embedding machine (Leica EG 1140 H)	<i>Leica Microsystems GmbH, Wetzlar, Germany</i>
Tissue dehydrator (Leica TP 1050)	<i>Leica Microsystems GmbH, Wetzlar, Germany</i>
Cryostat microtome (Leica CM1850)	<i>Leica Microsystems GmbH, Wetzlar, Germany</i>
Fluorescence microscope (Leica DM5500 B)	<i>Leica Microsystems GmbH, Wetzlar, Germany</i>
Adobe Illustrator®	<i>Adobe Inc., San José, California, USA</i>
GraphPad Prism 6	<i>Graphpad Software Inc., California, USA</i>

2.4 Methods

2.4.1 Tissue origin

Human lung tissue samples were acquired through the European IPF registry (eurIPFreg) and local biobank of the “Universities of Giessen and Marburg Lung Center” (UGMLC), a member of the German Center for Lung Research Biobanking Platform. These samples originate from the peripheral regions of explanted lungs and were obtained either during lung transplantation or post mortem - with documented consent from each individual patient or their next of kin. For the purpose of this study, we included randomly selected specimens of 11 IPF and 11 IPAH patients, while control tissue was obtained from non-utilized, assumingly healthy donor lungs (n= 9-10), also provided by the biobank. Among the IPF patients, nine were male and two female, with a mean age of 54.65 years (± 2.94 SE). In the IPAH group, 6 were male and 5 female, mean age was stated at 26.9 years (± 4.9 SE) and available data on pulmonary artery pressures yielded a mean of 74.6 ± 17 mmHg (\pm SE, available for 5 patients only) and a mean cardiac index of 2.2 ± 0.39 l/min/m² (mean \pm SE, data available for 4 patients only). This study and the inherent procedures were approved by the Ethics Committee of Justus-Liebig University School of Medicine (No. 31/93, 111/08, and 58/15).

2.4.2 Tissue preparation

Preparation of the acquired tissue was performed according to internal standards: At first, tissue samples were fixated in 4 % formalin solution, followed by dehydration in progressively higher concentrations of ethanol, ranging from 70 % up to 99.6 %. Any remaining traces of ethanol then were removed using a xylol substitute, before the tissue was embedded in paraffin wax. Once the wax has sufficiently hardened, a microtome was used to cut 3 μ m sections, which were placed into a water bath for effective positioning and transfer onto specimen slides (Fig.5).

2.4.3 Immunohistochemical staining

After 60 min of incubation at 59 °C, several previous steps were partially reversed: In order to remove the paraffin and rehydrate the tissue, a succession of three xylol baths, with durations of 10 min each, were followed by four baths containing decreasing ethanol concentrations (99.6 % - 70 %). The samples then were first drained, then submerged and allowed to rest in distilled water (Aqua dest.) for complete rehydration. The initial process of fixation is likely to mask the epitope of desired antigens due to covalent bonding in-

between adjacent proteins, known as cross-linking. “Heat induced antigen retrieval” is an established method to “re-open” these bonds and restore accessibility for antibodies through heat exposure and specific buffer solutions (175). The rehydrated samples, therefore were pressure cooked in citrate buffer (pH = 6) for a total of 40 min. Further “proteolytic induced antigen retrieval” was achieved using proteinase K and several washing cycles with methanol solution, distilled water and phosphate buffered saline (PBS). PBS (10x concentrated) was prepared to an internal standard:

- 80,0g NaCl
- + 2,0g KCl
- + 11,5g Na₂HPO₄ x 2 H₂O
- + 2,0g KH₂PO₄ in 900ml aqua dest.



Fig.5 Laboratory equipment used in the process of tissue preparation – Leica® tissue processor, paraffin embedding station, microtome and successive reagent baths

Unspecific antigens tend to cause unwanted background staining, therefore a universal blocking reagent (2.5 % Normal Horse Serum) was applied prior to the primary antibody. During the process of finding the most effective antibody for each selected target, a number of different providers were tested and evaluated in various dilutions. Best immunoreactivity and most consistent results were achieved with the following:

Table 3 Selected targets and their corresponding primary antibodies with the utilized dilutions

TARGET	SUPPLIER	DILUTION
FGF7	Antibodies-online ®	1:50
FGF10	Antibodies-online ®	1:30
FGFR1 (FMS-LG)	Thermo Fisher Scientific ®	1:200
FGFR2 (BEK C-17)	Santa Cruz®	1:200

Primary antibodies then were applied in dilution (Table 3), combined with an additional background blocking agent, and incubated at room temperature overnight. For detection, the “labeled Streptavidin–Biotin” (LSAB) method was chosen - Mainly because of the high efficiency and the expertise in the application of this method, that already existed in our laboratory. Following a rinse cycle with PBS, the secondary biotinylated antibody was applied (“VECTASTAIN® Universal Quick Kit”) and allowed to interact for 10 min, to achieve sufficient binding to the primary antibody. After an additional, thorough rinse with PBS, the streptavidin-peroxidase-enzyme complex (“VECTASTAIN® Universal Quick Kit”) was introduced, which would then bind to the secondary antibody and later ensure the conversion of NovaRED™- peroxidase substrate (Vector®). The NovaRED™-substrate was prepared according to the datasheet, incubated for 10 min and then rinsed off under flowing tap water. For the accompanying, structural staining hematoxylin was chosen, as it is easily compatible with most immunohistochemical stains and offers basic insight into tissue morphology, therefore enabling an assessment of the spatial distribution of the immunohistochemical signal. Hematoxylin “ready-to-use” solution was added to the tissue sections und left to incubate for 3 min. After a succession of ethanol, isopropanol and xylol baths, all sections were covered with the mounting medium Pertex® and coverslips.

For each target of our four targets, 11 IPAH-, 11 IPF- and 10 donor-tissue samples were stained. Additionally, positive controls on human kidney-tissue and negative controls using only the secondary antibody were performed. In both cases there was no indication for any significant, nonspecific binding.

2.4.4 Structural staining

To gain a more elaborate understanding of the microscopic anatomy surrounding our four targets, we opted for additional serial sections of remodeled vessels stained with Hematoxylin + Eosin (H&E) and Masson-Goldner-Trichrom. These stains aid in visualizing the extent of tissue remodeling by accentuating collagen and muscle fibers. For a further differentiation of myofibroblasts, endothelial- and smooth muscle cells, a staining of α -smooth muscle actin (α -SMA) and von-Willebrand-Faktor (vWF) was performed.

2.4.4.1 Hematoxylin and Eosin

The initial steps of removing paraffin and rehydrating the tissue sections (as previously described) also generally apply for structural staining. The tissue then was incubated with Mayer's hemalum solution for 20 minutes, which stains basophilic structures, such as nuclei and the rough endoplasmic reticulum, blue (9). Following a thorough rinse with flowing tap water and a one-minute ethanol 96 % bath, eosin-y solution (alcoholic) was applied. Eosin binds to acidophilic (eosinophilic) cell components – namely proteins (e.g. collagens), mitochondria and the smooth endoplasmatic reticulum – and dyes them red (9).

2.4.4.2 Masson-Goldner-Trichromatic

The tissue sections were incubated in Weigert's iron hematoxylin (Part A and B, 1:1) for 10 minutes, subsequent to a succession of three xylol- and four ethanol-baths in descending concentrations. After a thorough rinse in tap water, they were submerged in Ponceau acid fuchsine for five minutes and then dipped in 1 % acetic acid until any excessive dye was sufficiently washed off. In the further course, they were incubated with Phosphomolybdic/ Phosphotungstic acid + Orange G solution for five minutes, until complete decolorization of the connective fibers was achieved. Several rinse cycles in 1 % acetic acid followed, before a counterstaining with Alanine Blue was performed. The sections then were dehydrated, mounted and covered, as previously described.

2.4.4.3 α -Smooth muscle actin and von-Willebrand-Faktor

The initial step required 60 minutes of incubation at 59 °C in a heating cabinet. All usual steps for paraffin removal and tissue rehydration then were also utilized here. As the secondary antibody is horseradish peroxidase (HRP) conjugated, any unblocked endogenous peroxidase would likely have caused non-specific background staining. The tissue sections were therefore submerged in a hydrogen peroxide-methanol solution (100 ml H₂O₂ 30 % and 100 ml CH₃OH 99 %) for 20 minutes to block endogenous peroxidase activity. Antigen retrieval was achieved with PBS and trypsin, the latter of which was left to incubate at 37 °C for 15 min. In between all following steps, wash cycles with PBS were performed: Bovine Serum Albumin 10 % (BSA) was used for the suppression of non-specific binding sites and incubated for 20 minutes. Then, another non-specific block was performed with 2.5 % Normal Horse Serum (VECTASTAIN® Universal Quick HRP Kit) for 10 minutes, before the primary antibody was applied. The

primary antibody (Table 4; α -SMA mouse monoclonal antibody; Sigma, USA) was left to incubate for 30 minutes, diluted at 1:800 (1 μ l of antibody + 799 μ l of BSA 10 %), before the biotinylated, universal pan-specific secondary antibody (VECTASTAIN® Universal Quick HRP Kit) was added and incubated for 10 minutes. Then the peroxidase-streptavidin complex (VECTASTAIN® Universal Quick HRP Kit) was applied, which would bind to the secondary antibody and facilitate the substrate conversion (176). In a final step, the peroxidase substrate (Vector® VIP Substrate Kit, Peroxidase) was added and allowed to incubate until the tissue sections displayed sufficient purple coloration (177).

For the second part of this double staining, the sections were again washed with PBS and incubated with 10 % BSA for 20 minutes. A 20-minute block with 2.5 % Normal Horse Serum followed, after which the serum was cautiously decanted and the primary antibody (vWF, rabbit, polyclonal, Dako, Denmark) added. It was left to incubate for 30 minutes at 37 °C (diluted to 1:800 with 1 % BSA) before being rinsed off by another PBS wash cycle. The secondary antibody (ImmPRESS® Anti-Rabbit IgG Peroxidase Detection Kit) then was applied for 30 minutes at room temperature, after which two more PBS wash cycles were implemented.

Table 4 Primary antibodies and dilutions utilized in the α -SMA/ vWF double staining

TARGET	SUPPLIER	DILUTION
A-SMA (mouse)	Sigma®, USA	1:800
VWF (RABBIT)	Dako®, Denmark	1:800

The chromogen 3,3'-diaminobenzidine (DAB) was chosen as substrate (Vector® DAB Substrate Kit, Peroxidase, 20 sec. of incubation), which resulted in endothelial cells stained brown. Nuclei then were stained green, utilizing a methyl green counterstain (2 min. of incubation at 60 °C). Finally, all sections were dehydrated with successive ethanol, isopropanol and xylol baths, mounted with Pertex® and covered with coverslips (as previously described).



Fig.6 Desktop workstation featuring the Leica DM6000B® motorized microscope with digital interface

2.4.5 Microscopy and semi-automated quantification

In order to keep the evaluation as unbiased and consistent as possible, a semi-automated approach was chosen, using Leica’s Q Win V3® Software. As previously described by our group (178), an operator selects non-overlapping frames on a microscope, which then are analyzed by the software for signal quantity and intensity (Fig.7). In this manner, each tissue section is scanned frame by frame, while an operator manually excludes artefacts and implausible measurements from the analysis. The evaluation of all 128 tissue sections was performed on a single microscope (Fig.6) and by one, single user. This was done to rule out the impact of variances in technique, which are inevitable once two or more examiners are involved.

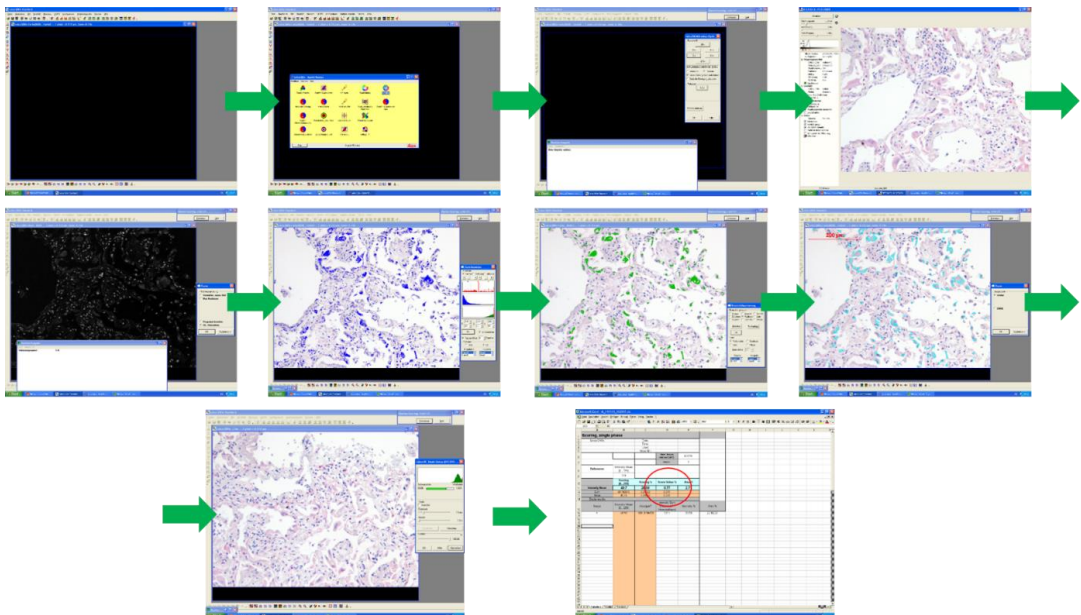


Fig.7 Semi automated workflow – Within each frame the software automatically detects the various color intensities of the red chromogen and compares them to a predetermined intensity maximum (“*intensity mean*”). Artefacts and measuring errors have to be recognized and manually excluded by the operator. Results then are automatically transferred to Microsoft® Excel

To ensure comparability, setup of the aperture diaphragm, exposure and magnification remained the same for all sections. The measurement of each new section started with adjusting white balance levels and locating the point of highest signal intensity (“*Intensity mean*”) (Fig.7). The *intensity mean* is regarded as 100 % intensity and used as reference point for the following measurements. The reaction product of NovaRED® substrate appears in various shades of red (Fig.8), which translate into corresponding signal intensities and correlate with the expression levels of our targets (Fig.7). These intensities (“*scoring*”) are detected by the software and stated as percentages of the previously determined intensity maximum (“*Scoring %*”). Meanwhile, the area of the detected signal is compared to the overall area of the section and specified as “*area %*”.

$$area \% = \frac{overall\ stained\ area \times 100}{overall\ area\ of\ the\ section}$$

For a quantitative and qualitative assessment of the immunoreactivity in different tissue sections, *area %* and *scoring %* are incorporated into the “*score value*”:

$$score\ value = scoring\ \% \times \frac{area\ \%}{100}$$

All values were directly transferred into Microsoft® Excel, but only the *score value* was forwarded to statistical analysis, as it most closely reflects the expression levels of our targets.

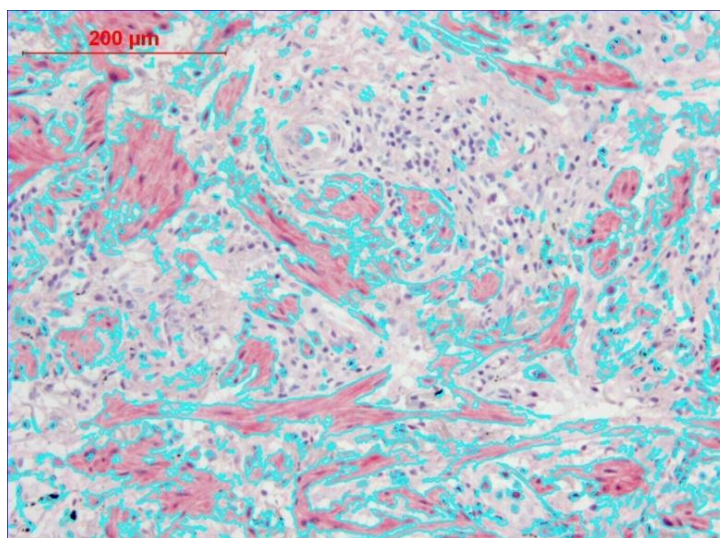


Fig.8 A tissue section of an IPF patient stained for FGF10 – the Q Win V3 Software automatically detects stained areas, as indicated by the turquoise border.

For an additional and more direct comparison of the immunoreactivity in-between fibrotic regions and fibroblastic foci, these regions were also manually selected and assigned a value in the range of “0” up to “6”, depending on the extend of signal (0 = no expression, 6 = maximal profile).

2.4.6 Statistical evaluation

The statistical evaluation was performed using Kruskal-Wallis (for comparing three groups) or Student’s test (for comparing two groups) and considered statistically significant. Data was analyzed using the GraphPad Prism 6 software and displayed as means \pm SE.

2.4.7 Immunofluorescence staining

2.4.7.1 Tissue origin and preparation

For the immunofluorescent staining, lung tissue samples of 8 healthy donors and 8 IPF patients were randomly selected. The origin and acquisition of those tissue specimens have been described above. Initial steps included cryoembedding with the utilization of Tissue-Tek® cryomolds, Tissue-Tek® O.C.T compound embedding medium and dry ice. Cryosections of 9 μ m thickness then were cut at -23 °C using the Leica CM1850 cryostat microtome. Subsequently, these sections were transferred onto Superfrost ultra plus® slides and stored at -80 °C until further processed.

2.4.7.2 Neutral lipid staining

The slides were removed from the -80 °C laboratory freezer and left to defrost at room temperature (approx. 90 minutes). The tissue then was fixated in phosphate buffered 4 % formaldehyde solution (ROTI®Histofix 4 %) for 45 minutes. After a short wash cycle with distilled water, the region around the tissue sections was carefully dried with paper cloth. A circle - functioning as a hydrophobic barrier - was drawn onto each slide and around the tissue, using a PAP pen. Previously diluted LipidTOX™ Red solution (1:50 with PBS) was added onto the tissue and incubated at 4 °C in a high humidity environment overnight. On the next day, the solution was gently washed off with PBS. Finally, all sections were covered with DAPI (4',6-Diamidino-2-Phenylindole, Dihydrochloride), a fluorescent counterstain marking DNA and subsequently nuclei blue.

2.4.7.3 Neutral lipid and Surfactant protein C (Pro SP-C) double staining

The neutral lipid staining with LipidTOX™ Red was performed as described above, up until and including the overnight incubation. Following three wash cycles with TBS-T (Tris-buffered saline with 0,1 % Tween20), a nonspecific block was undertaken with TBS + 3 % BSA + 5 % goat serum + 0,4 % Triton X-100 (permeabilizing reagent), incubated for 60 minutes at room temperature. The primary antibody (Table 5; Pro-SPC) then was applied in a dilution of 1:500 and left to incubate at 4 °C overnight.

Table 5 Primary antibody utilized in the neutral lipid/pro SP-C double staining

TARGET	SUPPLIER	DILUTION
ANTI-N TERMINAL PRO SP-C (RABBIT)	Seven Hills, USA	1:500

Further wash cycles with TBS-T followed, before the secondary antibody “goat anti-rabbit IgG Alexa488” (Alexa Fluor® Invitrogen™ / Thermo Scientific) was diluted at 1:500 and added onto the tissue for the duration of one hour at room temperature. Finally, three more wash cycles with TBS-T (10 minutes each), and one cycle with TBS were performed, after which DAPI and ProLong™ Gold were applied to all sections.

2.4.7.4 Evaluation and statistical analysis

All sections were evaluated under the fluorescence capable microscope Leica® DM5500 B. Settings (magnification: 63X, exposure: 55 ms, intensity: 5) remained largely unchanged throughout the entire evaluation and scoring process. The cells were counted by selecting 10 independent 63X fields per sample, which was performed by a single observer to rule out the impact of any potential differences in technique. Data was analyzed using the GraphPad Prism 6 software and results were presented in number of cells per mm².

3 Results

The following figure (Fig. 9) allows for a direct visual comparison of the different stains and expression patterns in serial sections of human IPF and IPAH lungs. The H&E staining provides an insight into the general structure of the tissue and highlights compacted interstitial space and loss of the lungs' physiological architecture. Masson's trichrome staining accentuates muscle fibers and collagen in respective shades of red and blue, which enables the distinction of remodeled areas with their vast accumulation of collagen and smooth muscle. The α -SMA/ vWF immunostaining allows for a further differentiation into myofibroblasts and smooth muscle cells by labeling the inherent α -SMA in tones of purple. Von-Willebrand-Faktor, on the other hand, is predominantly expressed in endothelial cells and appears as heightened immunoreactivity along the vascular lumen in the form of a brown tones.

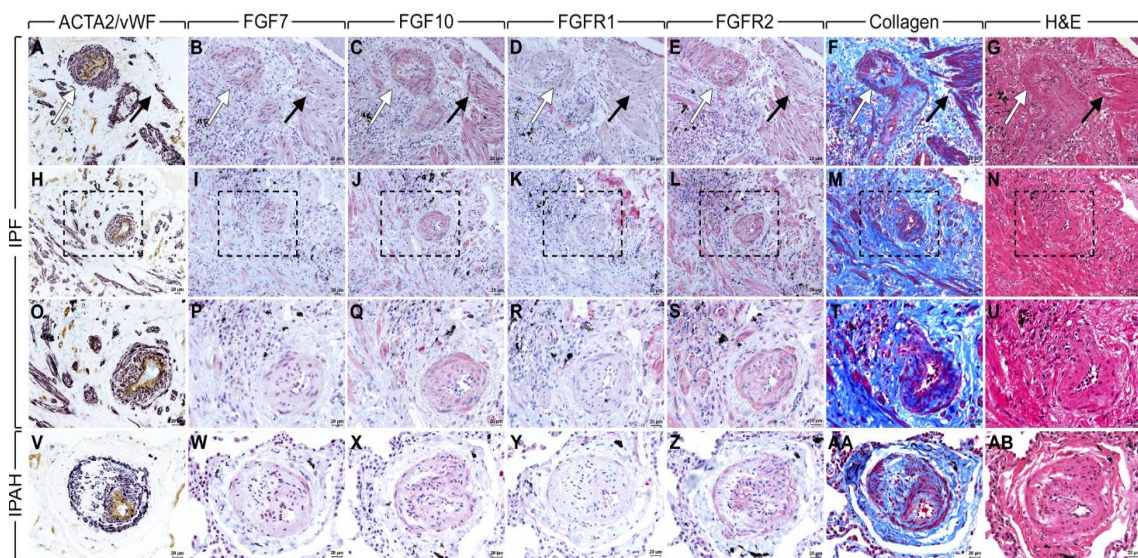


Fig.9 Expression of FGF receptors and ligands in serial sections of human lung tissue in the context of IPF and IPAH –The corresponding tissue sections were treated with ACTA2-, vWF-, FGF7,-10,FGFR1,-R2 antibodies. In addition, Masson's Trichrom- (“Collagen”) and HE-stains (“H&E”) were performed. White arrows indicate vessels, while black arrows indicate remodeled areas (fibrotic regions). **A-E:** In this overview, the heightened signal for FGF7,-FGF10 and FGFR2 in remodeled areas already becomes apparent. **F-G:** structural stains highlighting the compacted interstitial space; The boxes in **H-N** are magnified in **O-U**: the signal for FGF7, -10 and FGFR2 in IPF samples seems concentrated in remodeled areas and the vasculature; **V-AB:** in IPAH, the signal for FGF7, -10 and FGFR2 seems almost restricted to the vasculature, with varying intensities depending on the vascular layer. Scale bars 20 μ m; Pictures taken from own stainings. Figure adapted from El Agha, Schwind et al., *AJP-Lung*, 2018 (64)

3.1 Common features of remodeled lung tissue in IPF and IPAH patients

Each section (Fig.10 and 11) entails a remodeled vessel and surrounding parenchyma with varying degrees of alteration. In IPAH (Fig.10), these vessels typically feature intimal hyperplasia (black arrows), which is largely comprised of hypertrophic and proliferating endothelial cells. In later stages of the disease, said endothelial cells tend to form dysfunctional, aberrant channels, known as plexiform lesions. This phenomenon is one of the hallmarks of IPAH and can be considered pathognomonic (34, 37, 36). The prominent neointima (dotted arrows) is a another characteristic trait and emerges in between the intima and media - more precisely amongst the disintegrated internal elastic membrane and the intima (38, 179). This additional layer is jointly responsible for the obstruction of the vascular lumen and is formed by α SMA-positive cells as well as extracellular matrix. Both are reflected in the respective purple and blue colorations of the α -SMA/ vWF and Masson's Trichrome staining (Fig. 10 A and B). A distinctive, thickened media (black arrowhead) is clearly visible and usually features both, hypertrophy and proliferation of α SMA-positive cells (37). It is distinguishable from the neointima by the pronounced red stain (smooth muscle) of Masson's Trichrome (Fig.10 B). The adventitia (bolt arrows) hosts large amounts of matrix, fibroblasts and immunomodulatory cells, which proliferate upon adventitial activation (48). This activation is thought of as one of the early mechanisms in the pathogenesis of IPAH and is reflected by a visual expansion of the adventitia (Fig.10 B and C).

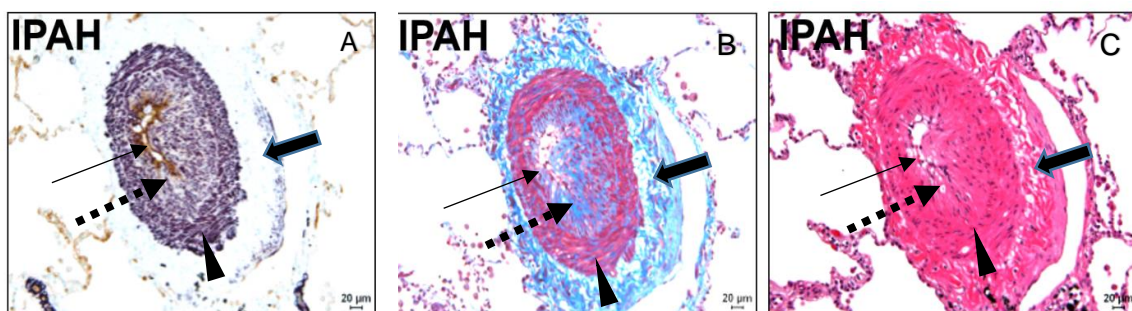


Fig.10 Remodeled pulmonary artery in serial sections of a lung tissue sample from an IPAH patient. Black arrows: intima; dotted arrows; neointima; black arrowheads: media; bolt arrows: adventitia; A: α -SMA/ vWF double staining, B: Masson's Trichrome, C: HE; Scale-bar = 20 μ m

As previously stated, IPF can be characterized as a patchy disease with seemingly spared areas bordering heavily remodeled parenchyma (80). Fibrotic regions generally display an abundance of collagen (Fig. 11 B) leading to thickened alveolar septa and overall compacted parenchyma (Fig. 11 C). Fibroblastic foci represent the sites of active fibrosis

and consist of organized conglomerates of fibroblasts, myofibroblasts and extracellular matrix partially covered in altered alveolar epithelium (180–182). Part of their destructive nature seems to root in their ability to restrict blood flow towards alveoli lateral walls, causing them to collapse and contribute to the aspect of honeycombing (182). The pulmonary vasculature is affected to various degrees. While vessels in severely fibrotic areas seem to be reduced in number and display higher degrees of remodeling, less affected regions seem well vascularized and vessels less impacted (183–185). Affected pulmonary arterioles in IPF stand out by their prominent hypertrophy of the intima (black arrows) and luminal narrowing (Fig.11 A).

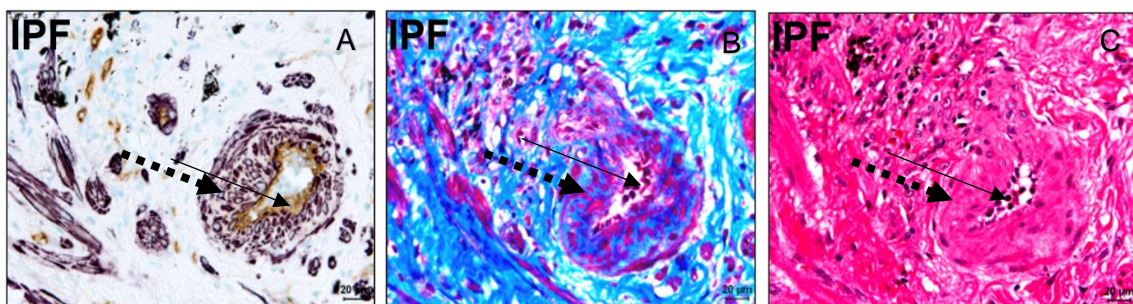


Fig.11 Histopathological features of IPF in serial sections dyed with three different stains – A: α -SMA/ vWF double staining, B: Masson's Trichrome, C: HE; Black arrows: intima; dotted arrows: media; Scale-bar = 20 μ m.

These vessels generally lack a neointima, but feature significant medial thickening (Fig.11 B, dotted arrows) due to smooth muscle proliferation and increased collagen disposition in the arterial walls (186, 187). The adventitia usually is enlarged as fibroblasts proliferate and the deposition of extracellular matrix increases. However, there is no clear line of demarcation between the adventitia and the surrounding fibrotic zone (Fig. 11).

3.2 FGF7 is upregulated in human IPF lungs

The signal for FGF7 was clearly intensified in highly fibrotic regions and vessels of IPF lungs, when compared to lung tissue of donors (Fig.12 a). Interestingly, in sites of early and continuing fibrosis (fibroblastic foci) however, the signal was visibly lighter than in areas of mature fibrosis. Semi-automatic quantification (see methods) of the immunoreactivity revealed a statistically relevant 5.5 ± 1.3 -fold increase in overall FGF7 expression when comparing IPF samples to donors (Fig. 12 b).

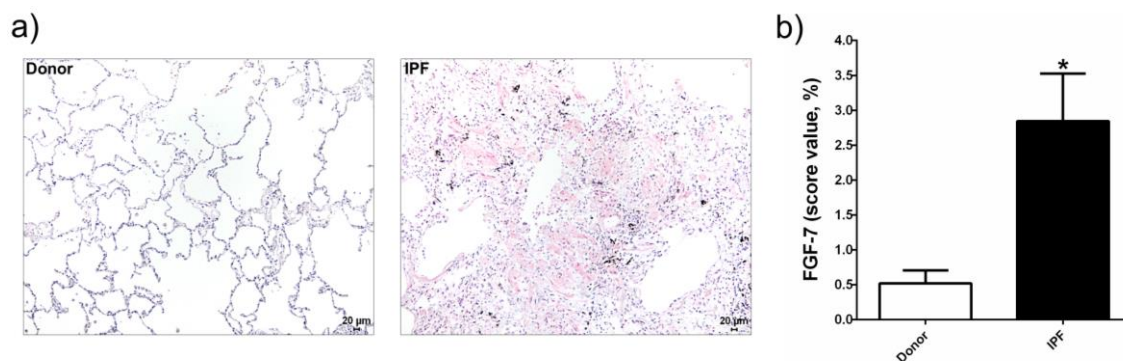


Fig.12 a) Histological sections of donor-tissue and IPF-tissue, stained using hematoxylin and the FGF7 antibody - scale bar 20µm; **a)** The donor tissue exhibits regular alveolar septa with little to no signal present. The compacted IPF lung tissue, in contrast, displays an intense signal in the highly remodeled parenchyma **b)** The quantification does show a statistically relevant increase in FGF7 expression in IPF lungs (n=11) compared to lungs of donors (n=10) bars represent Mean value ± SEM, T-test, *p<0.05

3.3 Upwards trend in FGF7 expression in IPAH samples

For IPAH lungs the results generally exhibited an increased expression of FGF7 - particularly in the hypertrophied media (black arrowhead) and intima (dotted arrow) of remodeled vessels (Fig.13 a). In the neointima (black arrow) of these vessels the signal was visibly traceable, but less intense (Fig.13). In the adventitia only a light staining could be detected occasionally. Overall, semi-automatic quantification under the light microscope did not reveal a statistically relevant increase. However, there was an upwards trend (2.0 ± 0.7 -fold upregulation) in FGF7 expression in IPAH lungs compared to donor lungs.

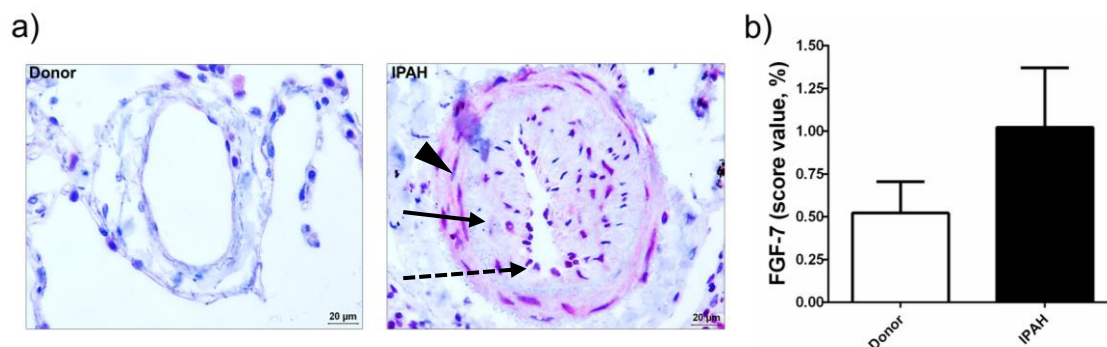


Fig.13 a) FGF7 immunostaining of donor-tissue in comparison to an IPAH-tissue sample. This example of a seemingly healthy vessel with its slim endothelium and media, found in donor lung tissue, shows no visible FGF7 immunoreactivity. The remodeled vessel displays a visibly stronger signal. Scale bar 20µm **b)** Overall, a statistically not significant upregulation of FGF-7 expression in IPAH samples compared to donors was determined.

3.4 Elevated FGF10 expression in IPF samples

The expression patterns for FGF10 and FGF7 displayed high degrees of similarity (Fig.14). In donor samples virtually no signal could be detected, while IPF lungs featured strong immunoreactivity in areas of fully developed fibrosis and remodeled vessels. In fibrotic foci the signal was found to be considerably less intense. Morphometric quantification demonstrated a 6.3-fold increase in FGF10 expression in IPF lungs compared to donor tissue.

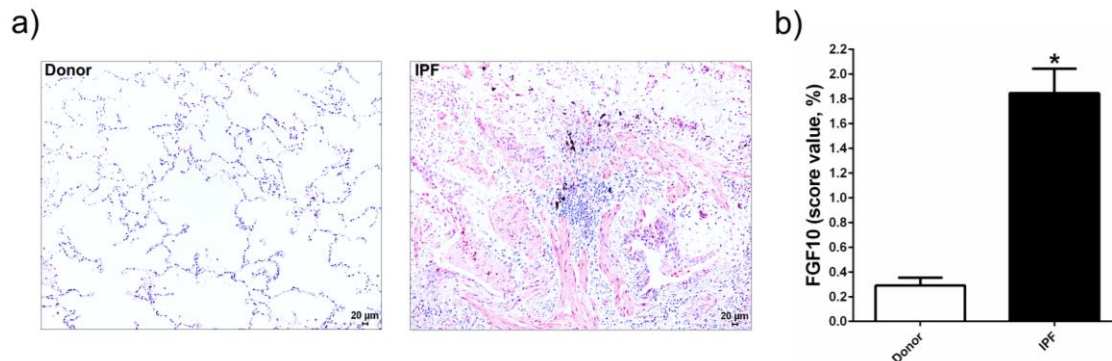


Fig.14 a) FGF-10 immunostaining, donor lung tissue compared to a fibrotic region in a representative IPF sample, scale bar 20µm b) Morphometric quantification revealed a 6.3-fold increase in FGF10 expression in IPF lungs (n=11) compared to lungs of donors (n=10). Bars represent Mean ± SEM, T-test, *p<0.05

3.5 Elevated FGF10 expression in IPAH samples

Again, FGF10 is expressed in a similar manner as FGF7, in both, IPF- and IPAH samples. In IPAH lungs, the remodeled vasculature is the main location of heightened immunoreactivity (Fig.15). The highest intensity is found in the media, followed by the intima and neointima. The adventitia only displays an occasional, light staining.

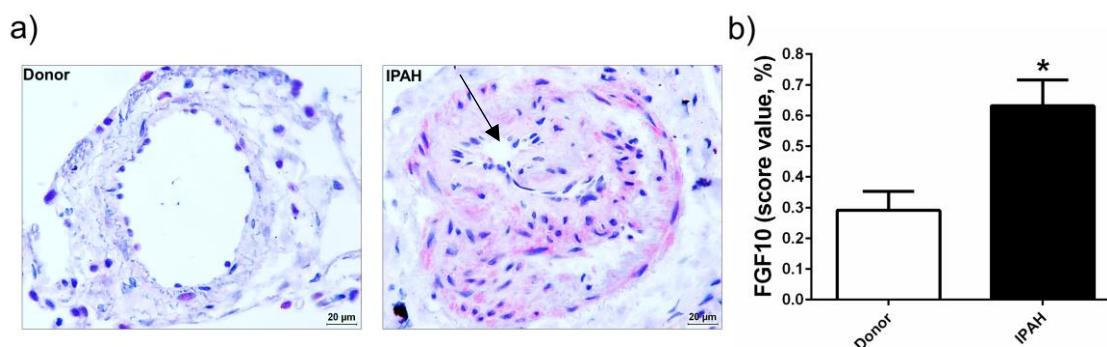


Fig.15 a) FGF10 immunostaining of donor lung tissue compared to a plexiform lesion, typically found in advanced cases of IPAH. The highly remodeled area features some of the representative characteristics of this disease, namely adventitial and medial hypertrophy, neointimal formation and “aberrant channels” (black arrow) in the otherwise obliterated lumen of the vessel (i.e. the plexiform lesion), Scale bar 20µm; b) A statistically relevant 2.2 ± 0.3-fold upregulation of FGF-7 expression in IPAH samples compared to donors could be determined. IPAH lungs (n=11) compared to lungs of donors (n=10). Bars represent Mean ± SEM, T-test, *p<0.05

3.6 Elevated FGFR2 expression in IPF samples

The results for FGFR2 in the context of IPF were familiar (Fig.16). A significant upregulation of FGFR2 expression was observed in areas of dense, fully developed fibrosis and in remodeled vessels, while fibrotic foci displayed a lighter signal. Quantification revealed a statistically relevant 10.9 ± 1.7 -fold increase in FGFR2 expression in IPF lungs (n=11) compared to lungs of donors (n=10).

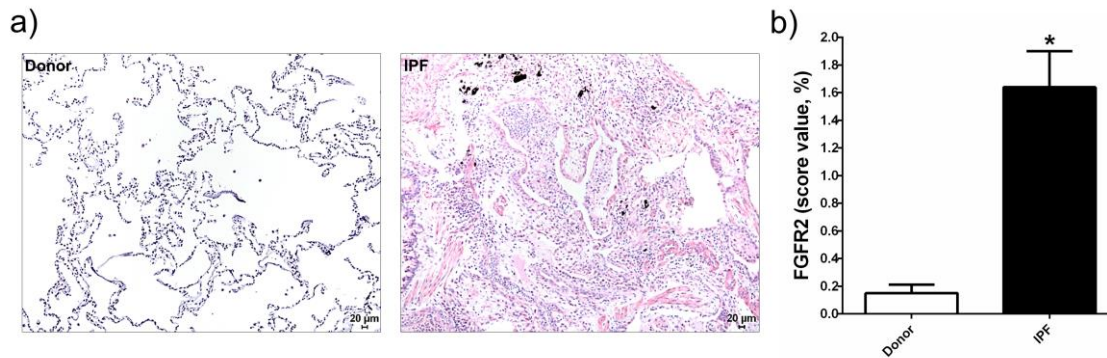


Fig.16 a) FGFR2 immunostaining of donor lung tissue compared to a lung tissue sample of an advanced case of IPF. The pattern of expression shows high similarity to FGF7 and FGF10 - note the intense signal throughout the entire area of mature fibrosis. Scale bar 20µm; Quantification does show a statistically relevant increase in FGFR2 expression in IPF lungs compared to donor tissue. Bars represent Mean value \pm SEM, T-test, *p<0.05

3.7 Elevated FGFR2 expression in IPAH samples

Consistent with previous findings, both, visual and semi-automatic quantification by light microscope confirmed a clear upregulation of FGFR2 in IPAH lungs (Fig.17). The signal seemed mostly confined to all layers of remodeled vessels.

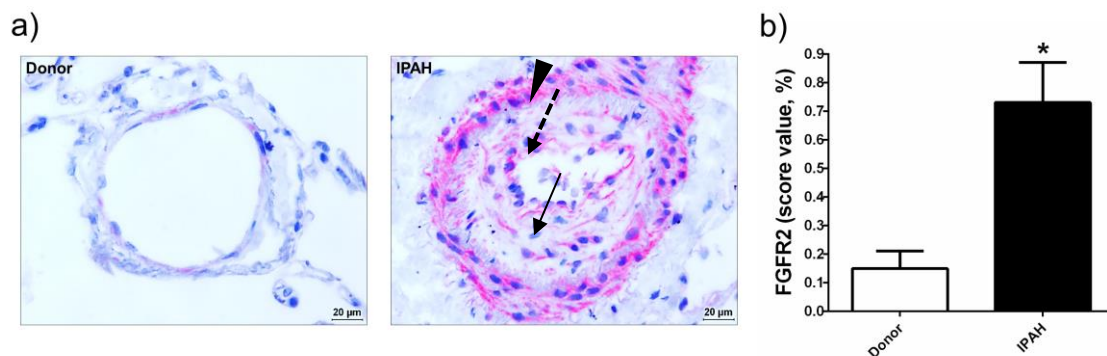


Fig.17 a) FGFR2 immunostaining of donor lung tissue compared to IPAH lung tissue. The effects of vascular remodeling in IPAH are striking in this side-by-side comparison. Note the intense signal in the media (arrowhead), and slightly weaker signal in the intima (dotted arrow) and neointima (narrow arrow). Scale bar 20µm b) By semi-automatic quantification, a statistically relevant 4.9 ± 0.9 -fold upregulation of FGFR2 expression in IPAH samples compared to donors could be determined - IPAH lungs (n=11) compared to lungs of donors (n=10). Bars represent Mean \pm SEM, T-test, *p<0.05

3.8 Ubiquitous FGFR1 expression in Donor, IPF and IPAH samples

In vast contrast to the findings for the other three targets, FGFR1 is expressed in a ubiquitous pattern. This is the case throughout Donor, IPF and IPAH lung tissue samples (Fig.18/19). Visually, as well as by semi-automatic quantification of the immunoreactivity, no significant difference in FGFR1 expression between donor-tissue compared to IPF/IPAH-samples could be detected.

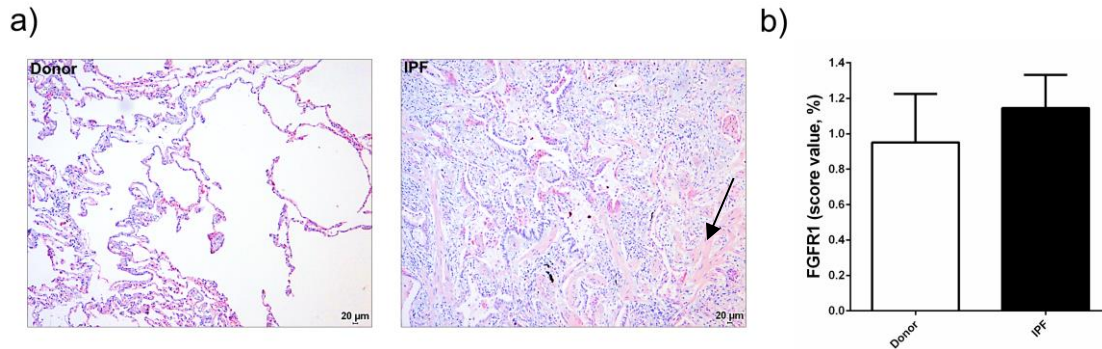


Fig.18 a) FGFR1 immunostaining of donor lung tissue compared to IPF lung tissue FGFR1 is expressed throughout the entire parenchyma and vasculature of both, donor and IPF tissue sections. In IPF samples, there is visible immunoreactivity in all cellular layers of the vasculature and also in dense fibrotic regions (arrow). Scale bar 20µm **b)** Quantification confirmed, that FGFR1 expression is mostly unchanged in IPF, when compared to donors. A statistically not relevant 1.2 ± 2.0 -fold increase could be detected in IPF lungs (n=11) compared to lungs of donors (n=10) bars represent Mean value \pm SEM, T-test, *p<0.05

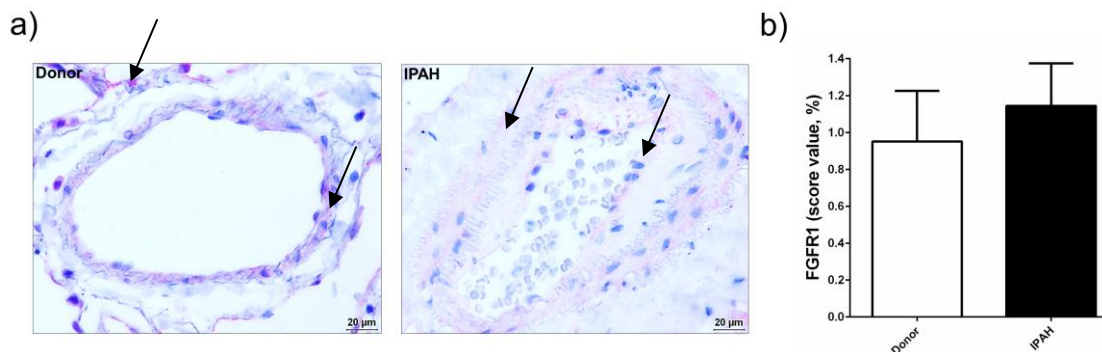


Fig.19 a) FGFR1 immunostaining of a donor lung tissue section compared to remodeled vessel found in an IPAH sample – FGFR1 is expressed in a ubiquitous pattern (arrows), in both, donor and IPAH samples. Visually, as well as by semi-automatic quantification, no statistically relevant difference could be demonstrated. Scale bar 20µm **b)** A not relevant 1.2 ± 2.0 -fold increase was detected in IPAH lungs (n=11) compared to lungs of donors (n=10) bars represent Mean value \pm SEM, T-test, *p<0.05

3.9 Conclusion

It can be concluded (Fig.20/21), that three of four targets (FGF7, FGF10 and FGFR2) display a high level of similarity in their expression patterns. FGF7, FGF10 and FGFR2 were significantly upregulated in IPF and IPAH, compared to donors. Their signal was concentrated almost exclusively in areas of remodeling - in case of IPF in the remodeled parenchyma, vasculature and, though distinctively attenuated, also in fibrotic foci. In case of IPAH the signal seemed confined to the remodeled vasculature. FGFR1 was found ubiquitously throughout all tissue sections and did not show any specific, regional patterns nor significant changes in the context of IPF or IPAH compared to donor tissue.

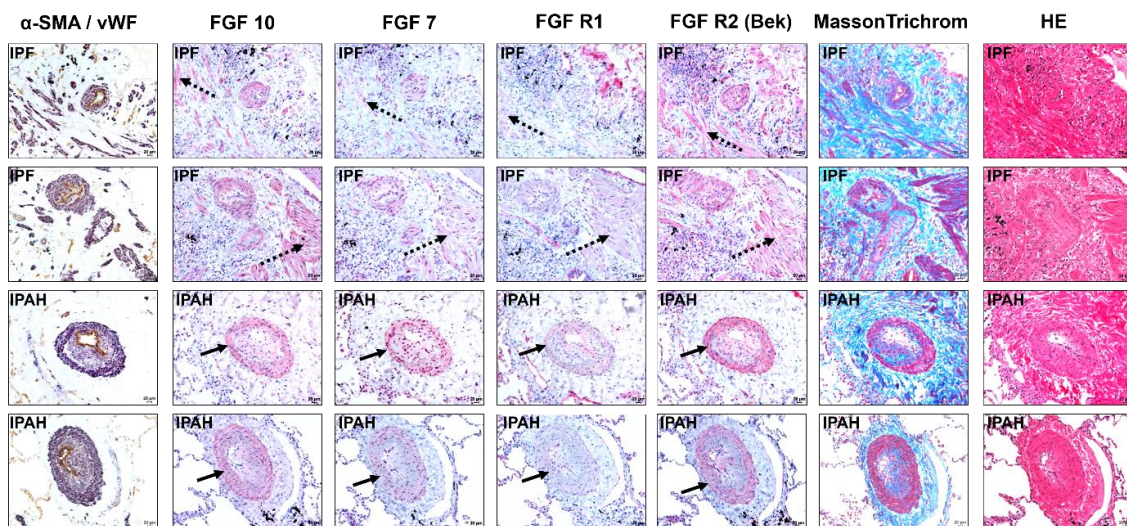


Fig.20 Expression of FGF receptors and ligands in serial sections of human lung tissue in the context of IPF and IPAH – For IPF representative dense, fibrotic regions are marked with dotted arrows and feature a strong signal for FGF7, FGF10 and FGFR2. Remodeled vessels generally display an intensified signal in the media and intima. In IPAH samples, these vessels (black arrows) exhibit a particularly strong signal in plexiform regions with an emphasis in the media, a weaker expression in the intima/neointima and only sporadic signal in the adventitia.

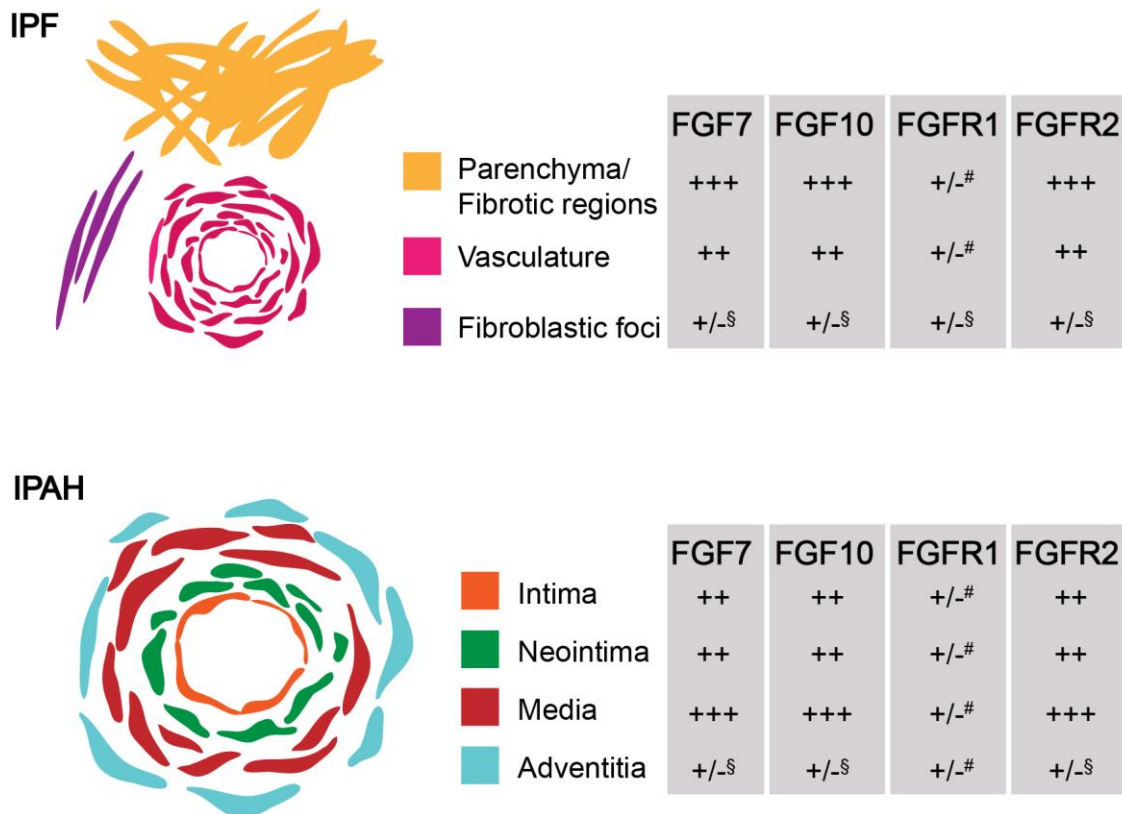


Fig.21 Conclusion of the expression patterns for all four targets in the context of IPF (upper table) and IPAH (lower table). The “+/-[§]” symbol indicates an occasional light staining. The “+/- #” sign indicates no significant difference compared to donor samples. Figure adapted from El Agha, Schwind et al., AJP-Lung, 2018 (64)

In addition to the aforementioned, semi-automated quantification of the overall immunoreactivity, a direct and manual comparison of fibrotic regions and fibroblastic foci in IPF samples was performed. Immunoreactivity in these regions was manually assessed and scored, using values in between “0” and “6” (compare 2.4.5). The results hereby demonstrated consistently higher expression levels of FGF7, FGF10 and FGFR2 in mature fibrotic regions, than in fibroblastic foci (Fig.21; Fig.22 A, B, D).

Based on available data on mPAP values of the corresponding IPAH patients, it was also shown that increased pulmonary FGF10 expression levels correlate inversely with the mPAP measurements (Fig.22 E; $r^2 = 0.83$, $P = 0.02$). In a follow up investigation by our group, a similar inverse correlation was also demonstrated for FGF7 and FGFR2, however, without reaching statistical significance (64).

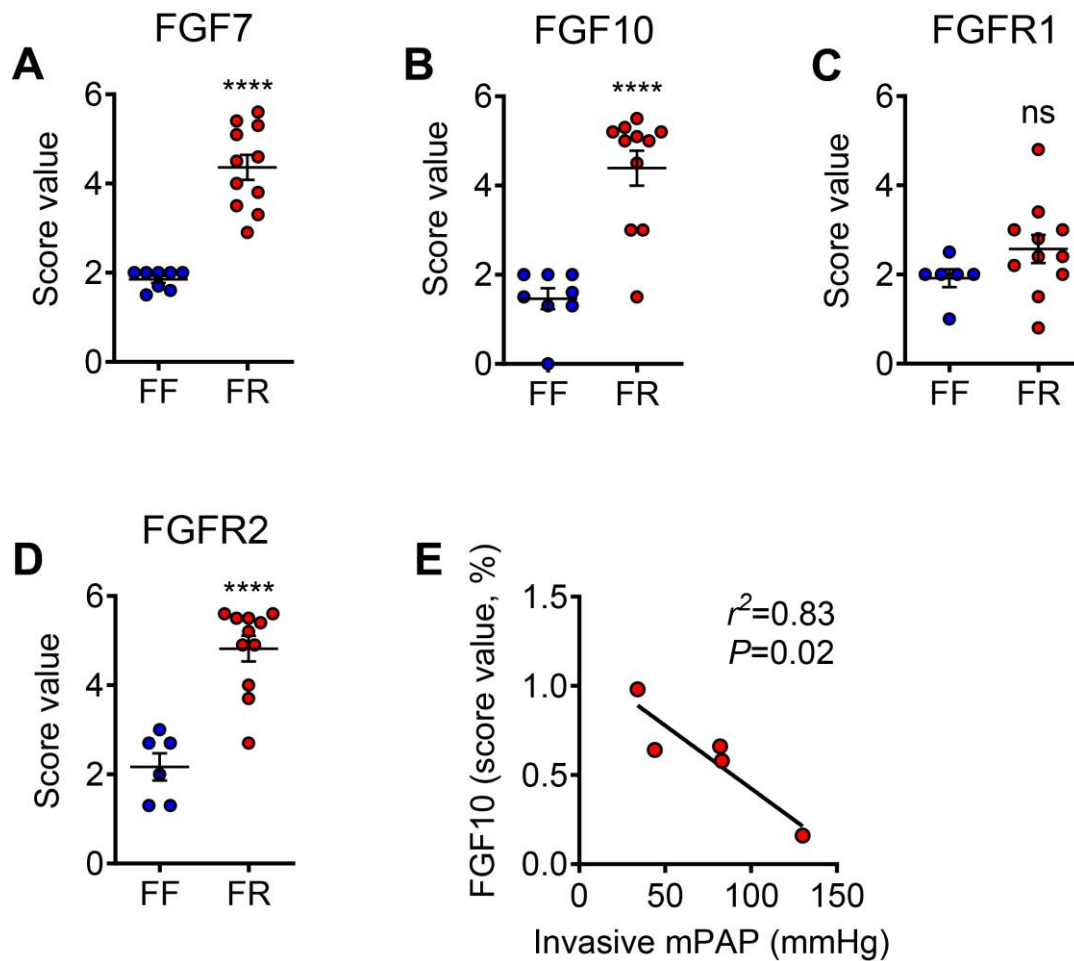


Fig.22 Expression levels in fibrotic regions versus fibroblastic foci; mPAP correlation data; FGF7, FGF10 and FGFR2 displayed significantly higher expression levels in fibrotic regions, when compared to fibroblastic foci (A, B, D); In contrast, FGFR1 showed comparable levels in both, fibrotic regions and fibroblastic foci (C); Note the inverse correlation of invasive mean pulmonary arterial pressure (mPAP) measurements with FGF10 expression levels in IPAH lungs (E). Correlation was calculated using Pearson's correlation coefficient (E); Means were compared using Student's t-test (unpaired, two-tailed) (A, B, C, D). **** $P < 0.0001$. FF = fibroblastic foci; FR = fibrotic regions; ns = not significant.

3.10 Identification and quantification of LipidTOX-positive cells in the human lung

Scattered throughout all cryo-sectioned tissue samples examined, sporadic clusters of droplets in various sizes were observed. These cluster were clearly focused around certain nuclei, which tends to indicate an intracellular location (Fig. 23 A). With its high affinity for neutral lipids, LipidTOX dyed these droplets in bright fluorescent red, while DAPI served as a nuclear-specific dye, highlighting nuclear acids in fluorescent blue (Fig.23, Fig.24). The SPC-staining (fluorescent green) was used to label AECII (Fig.23 B and C) and clearly distinguished them from LipidTOX-positive agglomerates in lungs of human donors (n=8). It further revealed a spatial pattern, in which these neutral-lipid droplets seem to be generally located adjacent to AECII (Fig.23 B and C).

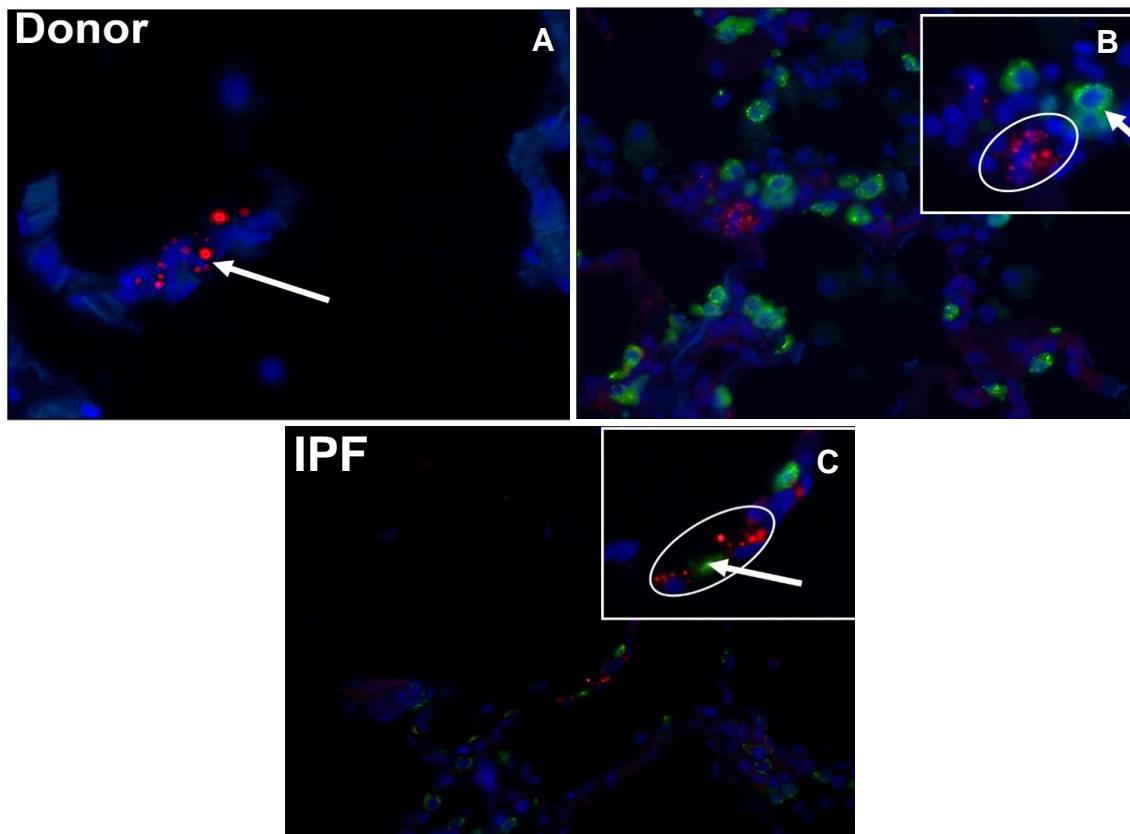


Fig.23: Fluorescent LipidTOX- , DAPI- and SPC-staining of frozen lung tissue sections from human donors and IPF patients – (A) LipidTOX highlighting a cluster of neutral-lipid droplets located around a nucleus [white arrow] in donor lung tissue; (B) AECII [white arrow] in direct proximity of neutral-lipid containing cells [white circle] in donor lung tissue; (C) Signal for SPC [white arrow] in between clusters of neutral-lipid droplets [white circle] in IPF lung tissue. Pictures taken from own stainings. As published by El Agha et al., Cell Stem Cell, 2017 (19)

Similar observations were made for the lungs of IPF patients (Fig.24; n=8). Again, neutral-lipid droplet containing cells commonly resided in the vicinity of AECII (Fig.23 C). Attempts to objectively quantify the lipid-droplet containing cells, however, did not prove to be feasible - mostly due to an unacceptably high level of arbitrariness when determining cellular boundaries (Fig.24).

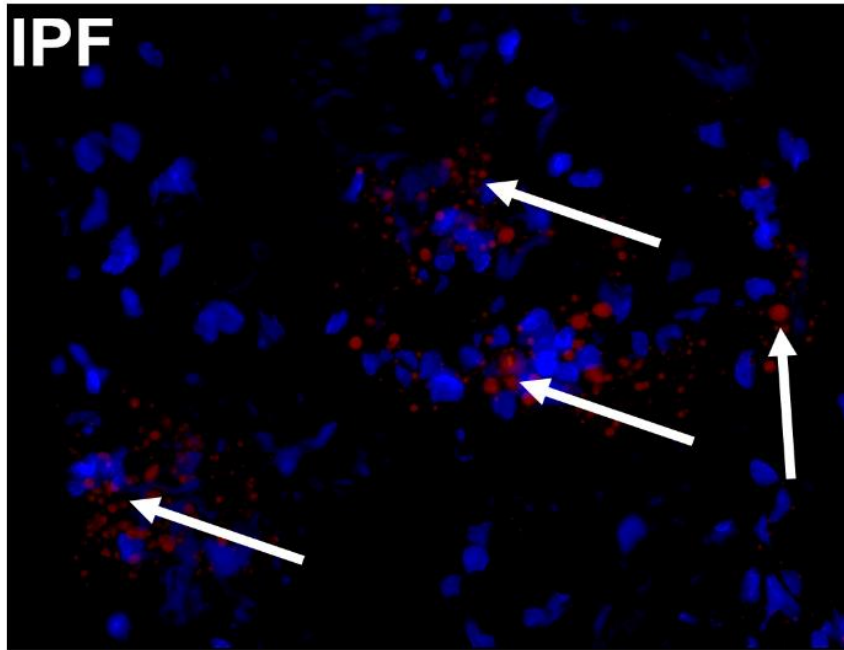


Fig.24: Multiple clusters (white arrows) of neutral-lipid droplets in IPF lung tissue - especially in regions with several lipid-droplet containing cells close together, any attempts to objectively quantify these cells ultimately failed.

4 Discussion

4.1 Overall findings

Results from both the immunohistochemical and immunofluorescence staining conducted in this study, can be concluded as follows:

- FGFR2b signaling is in fact altered in the pathologies of IPF and IPAH. The data suggests an increased expression of FGF7, FGF10 and FGFR2 in regions of matured fibrosis, remodeled vessels and mildly in fibroblastic foci. In IPAH, the signal was almost confined to the remodeled vasculature. FGFR1 expression did not exhibit any relevant alterations in the course of IPAH and IPF compared to donor tissue.
- There is strong evidence for neutral-lipid droplet containing cells in the human lung. Given their specific neutral lipid-content and relative proximity to AECII, these cells are likely to embody human lipofibroblasts.

4.2 Fibroblast-growth factors in PAH

As reviewed by our group (Fig.25), so far contemporary research regarding fibroblast-growth factors and their involvement in PAH has been focused on FGF1 and FGF2 (146): Apoptosis-resistant and highly proliferative endothelial-cells, largely responsible for many of the pathological features in PAH, seem to maintain their detrimental traits by inducing high levels of FGF2, which act via FGFR1 in an autocrine manner (146, 150). This creates an “autocrine loop” that has also been linked to malignant proliferation in certain cancers (150, 188). FGF2 hereby upregulates the anti-apoptotic proteins BCL2/BCL-xL in endothelial cells and promotes proliferation through stimulated extracellular signal-regulated kinases 1/2 (ERK1/2) (150). Jointly with FGF1, FGF2 also facilitates the proliferation of pulmonary arterial smooth-muscle cells and causes vasoconstriction through upregulated Endothelin-1-endothelin-A-receptor signaling – as demonstrated for hypoxia-induced pulmonary hypertension in rats (146, 189). Additionally, FGF2 most likely stimulates the transdifferentiation of pericytes into a smooth-muscle-like phenotype (151). Disrupted Apelin-signaling in pulmonary artery endothelial cells leading to increased FGF2/FGFR1-signaling through downregulation of specific microRNAs has been identified as a major upstream contributor to the elevated *FGF2* and *FGFR1* expression in PAH (63, 146). On the other hand, both FGFR2 IIIb ligands, FGF7 and FGF10, are known facilitators of regeneration (146, 190) and appear to improve survival in another pathology featuring vascular remodeling and pulmonary

hypertension: FGF7 attenuated pulmonary hypertension in the rat hyperoxia model of bronchopulmonary dysplasia (BPD) (157), while expression of *FGF10* was found to be decreased in infants suffering from BPD (64, 191).

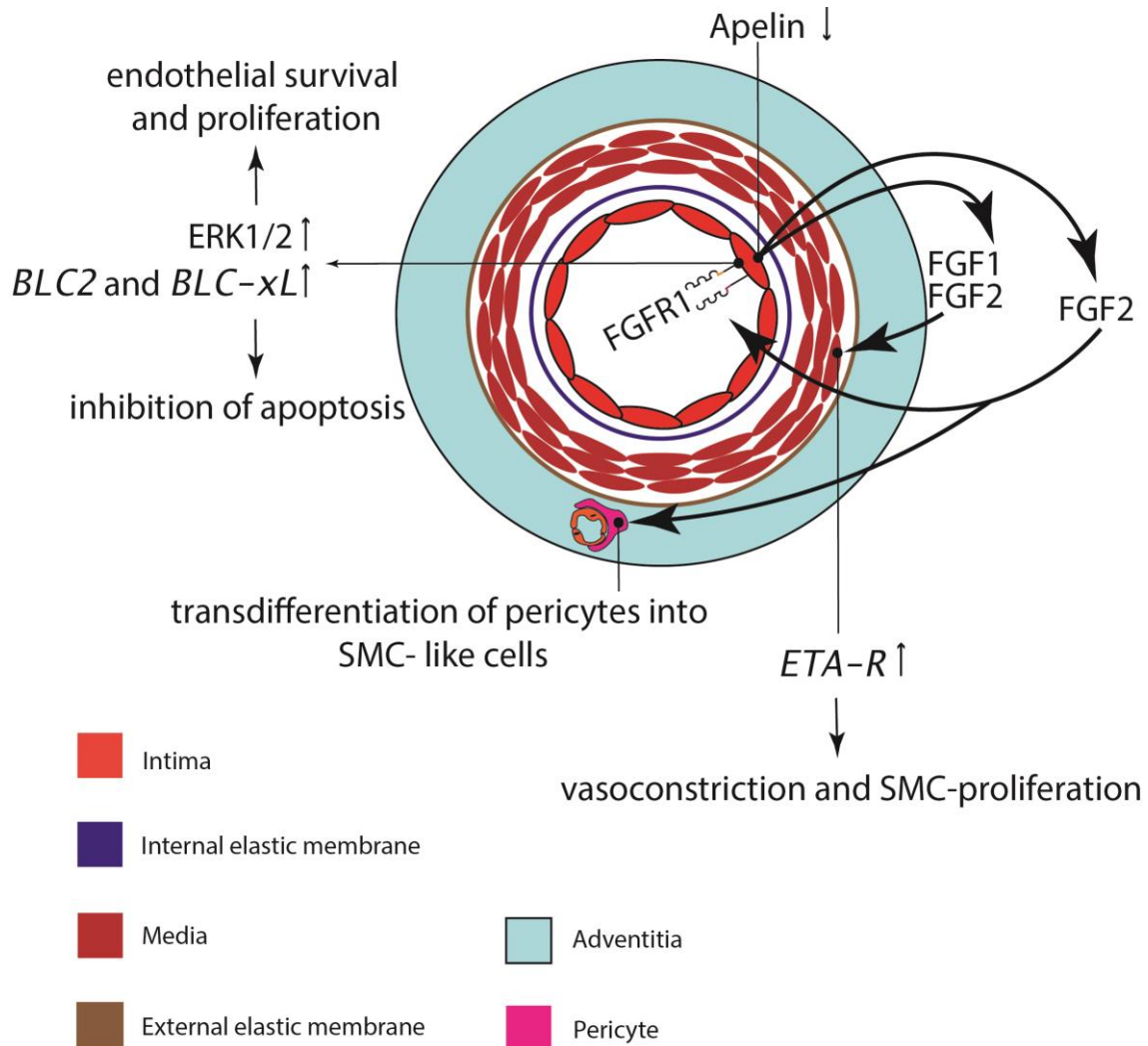


Fig. 25 Synopsis of the involvement of the prototypic FGFs in pulmonary vascular remodeling in the context of PH – As mentioned before (compare 1.2.3), decreased *Apelin*-expression in endothelial cells has been identified as an upstream factor of increased fibroblast growth factor 2 (*FGF2*) and fibroblast growth factor receptor 1 (*FGFR1*) expression (63). Elevated endothelial *FGF2* acts on the endothelium via *FGFR1* through an autocrine loop, activates the downstream *ERK1/2* pathway (compare 1.4) and increases *BLC2* and *BLC-xL* expression (146, 150). Endothelial *FGF1* and *FGF2* act on PASM and stimulate Endothelin-1 (ET-1)-*ETA-R* signaling (189). Paracrine, endothelial *FGF2* might facilitate the potential transdifferentiation of pericytes into SMC-like cells (151). Figure modified from El Agha, Seeger et al. 2017 (146)

4.3 Fibroblast-growth factors in IPF

In the context of IPF, FGFs and their receptors have been subject to a multitude of studies (146), which unfolded dual and even conflicting roles: MacKenzie et al. found FGF1 to be increased at the protein level in lungs of IPF patients, compared to lungs of non-IPF patients (192). Hereby, FGF1 and FGFR1/2/3/4 were particularly prevalent in sites of both, ongoing fibrosis (e.g. fibroblastic foci) and in regions of dense, matured fibrosis - suggesting that FGF1 signaling might actively contribute to lung remodeling in IPF (192). Intriguingly, earlier studies depicted FGF1 primarily as an anti-fibrogenic factor, reverting TGF- β 1 mediated epithelial-to-mesenchymal transition and inhibiting ACTA2 expression in human lung fibroblasts (153, 193). However, as the anti-fibrogenic FGFR1/2 b-isoforms were found to be decreased in IPF lungs, while FGFR1/2/3 c-isoforms were increased, MacKenzie et al. reasoned, that profibrogenic FGF1/FGFR c-isoform signaling likely predominates in human IPF lungs (192). Furthermore, they deduced a dual role for FGF1, in which FGF1 indeed exerts antifibrogenic effects such as reduced collagen expression and increased apoptosis, but also mediates fibroblast invasion and migration (192). In contrast, FGF2 displays solely opposing characteristics likely by facilitating the profibrotic TGF- β 1 dependent differentiation of myofibroblasts, and is believed to be one of the initial instigators of aberrant remodeling in IPF (Fig.26) (146, 194, 107).

As mentioned in the introductory chapters (compare 1.4.2.), FGF7 and FGF10 promote antifibrotic effects (146). FGF7 encourages regenerative processes through proliferation of AEC2 (162) and protected against several forms of pulmonary injury in rodents (156, 155). Similar results were observed for the overexpression of *Fgf10* (158), so both FGF7 as well as FGF10 proofed beneficial against bleomycin-induced lung fibrosis in mice (158, 195). It can be concluded, that both entail protective qualities and regenerative potential in regards to the pulmonary epithelium. Particularly interesting is an observation by Farkas et al., in which FGF10 was found to be increased during the resolution phase of BMP-4-antagonist “Gremlin” mediated fibrosis in rat lungs (196). One might deduct from this, that increased levels of FGF10 potentially embody an endogenous response to injury and an attempt of regeneration - to some extent possibly functioning through reduced TGF- β expression (158, 196). Furthermore, McQualter et al. suggested that epithelial injury causes resident stromal cells to release FGF10 as a way to promote re-epithelialization, and depicted TGF- β as a key factor counteracting this “epithelial-supportive” response (Fig.26) (197). The main objective of this dissertation

was to determine whether a similar upregulation of FGF10 (and FGF7) could be observed in lungs IPF- and IPAH patients, and if so, whether these alterations are of beneficial or detrimental nature.

4.4 Interpretation of the expression patterns

FGF7, FGF10 and FGFR2 were found to be expressed almost exclusively in the remodeled vasculature of IPAH lungs, while FGFR1 was only mildly detected. The signal for FGF7 and FGF10 was particularly intense in hypertrophied endothelium and thickened media, but less intense in the neointima. This does not automatically imply, that FGF7 and FGF10 are synthesized and released at the location of the signal, however, given their paracrine nature and previous findings in which FGF10-positive cells later emerged as vascular smooth muscle cells (28), it can be considered a reasonable assumption. FGFR2 was found in all layers of the vasculature and to a lesser extent in the adventitia. Overall, there was a statistically significant increase in expression of FGF10 and FGFR2, as well as an upwards trend for FGF7 in lungs of IPAH patients compared to lungs of human donors - FGFR1 expression remained virtually unchanged. Additionally, it has been revealed that FGF10 expression levels inversely correlated with the mPAP measurements of the respective IPAH patients (a similarly directed trend was found for FGF7). The fact that overall FGF7/10-FGFR2 signaling is increased in IPAH lungs, but decreases relatively as the mPAP increases, could be interpreted as the “capitulation” of an already ineffective regeneration attempt during the later stages of IPAH (64).

FGF7, FGF10 and FGFR2 were upregulated significantly in IPF lungs compared to donors and were highly expressed in mature, dense fibrotic regions as well as remodeled vessels. In contrast, fibrotic foci, which are regarded as the sites of early and ongoing fibrotic response (64, 182), featured distinctively less immunoreactivity. This makes an involvement of FGF7/10-FGFR2 signaling in the initial fibrotic process less likely. Interestingly, a follow up investigation revealed, that FGF7 expression in the whole section leans towards a positive correlation with TLC, while FGF10 and FGFR2 expression lean towards negative correlations (64), which would indicate an increase in FGF10-FGFR2-signaling during later stages of IPF. One potential deduction could be, that although FGFR2 signaling through FGF10 increases with disease severity, it is not the initial trigger nor a driving factor behind early pulmonary remodeling in the context of IPF, which would be in line with previous findings generally depicting FGF7/10-

FGFR2 signaling as antifibrotic and regenerative (compare 4.2 and 4.3). In this scenario, a role as an ineffective antifibrotic mediator or a failed attempt at regeneration seems plausible. However, it might also function as a profibrotic mediator of remodeling during later stages, as potentially reflected by the aforementioned differences in expression between fibroblastic foci and mature fibrotic regions, as well as by the overall increased expression of FGF10/FGFR2 during the final stages of IPF. The results, and in particular the mentioned correlations, leave room for several possible interpretations and would benefit from the inclusion of a larger number of patients. Ultimately, however, they highlight the importance of further research in this field.

4.5 Lipofibroblasts in the context of IPF

As partially elucidated in the introductory chapters (compare 1.4.2), well-regulated mesenchymal *Fgf10* expression is essential for embryonic lung development in rodents (169) and even defines a population of mesenchymal progenitors, shown to evolve into vascular smooth muscle cells and lipofibroblasts (28). In rats and mice, alveolar lipofibroblasts are found in proximity to AEC2 (198) and are likely situated within a stem cell niche (19, 174), from which they closely interact with AEC2 during embryonic development, but also postnatally: Expression of parathyroid hormone-related protein (PTHrP) by AEC2 triggers the PPAR γ pathway in lipofibroblasts, which in turn express ADRP and secrete Leptin (199). ADRP is required for the storage of neutral-lipids and transfer of surfactant components to AEC2, while leptin stimulates the surfactant synthesis in AEC2 (199–201). Intriguingly, PPAR γ signaling seems to be essential for keeping lipofibroblasts true to their phenotype, while disruption of the PTHrP pathway leads to decreased PPAR γ signaling and a consecutive transdifferentiation of lipofibroblasts to myofibroblasts (compare 1.3.2. and 1.5) (199). AEC2 injury due to hyperoxia, nicotine and volutrauma (among others) are seen as causes for such a disruption and facilitate the associated shift towards the myogenic phenotype (116, 199, 202–204). Rehan and Torday demonstrated for several of these injuries, that PPAR γ agonists counteract this detrimental shift and are even capable of a partial reversal (199). As previously mentioned (compare 1.3.2.), recurring injury of AEC2 is believed to be one of the initial triggers of the fibrotic response in IPF and activated myofibroblasts have been identified as key effector cells (Fig.25) (19, 205). With the use of lineage-tracing in the bleomycin-induced mouse model of pulmonary fibrosis, our group was able to demonstrate that pre-existing lipofibroblasts do in fact undergo a phenotypic shift during

fibrosis formation and contribute to the cohort of activated myofibroblasts (19). Given the reversibility of bleomycin-induced fibrosis in mice, we further revealed that a subset of activated myofibroblasts reverted back to a “lipofibroblast-like-phenotype” upon fibrosis resolution (19). In order to analyze whether these observations in mice are of significance in the human context, first and foremost the presence of lipofibroblasts in the human lung had to be confirmed. Previous findings from other workgroups negated their occurrence in the human lung (24), while others saw them as fairly common (25). This doctoral dissertation presents evidence for lipofibroblasts in the form lipid-containing cells adjacent to AECII (Fig.23/24) in both donor- and IPF samples. In a follow up investigation these cells stained negative for the hematopoietic cell marker CD45 and are most likely resident cells (19). The opposing findings from other workgroups might be partially explained by their use of staining protocols involving strong organic solvents and by unique weak points of transmission electron microscopy with regard to the detection of certain neutral lipid compositions (206). In this study, comparative quantification of said lipid-containing cells under the light microscope unfortunately turned out as prone to error. Overlapping cells and no visible cell boundaries hindered accurate quantification of LipidTOX+ cells. However, we were able to later on demonstrate that the expression of genes correlating with lipogenic differentiation (ADRP, PPAR γ , C/EBP α) was decreased significantly in IPF patients compared to donors, while myofibroblast markers ACTA2 and COL1A1 were increased (19). This implies reduced lipofibroblast differentiation and increased myofibroblast differentiation in human IPF lungs. It is particularly fascinating, that these changes seem to be mediated by increased TGF- β activity, while PPAR γ agonists are able to attenuate these effects and reinforce the lipogenic phenotype (19). In fact, extrinsic stimulation of PPAR γ signaling seems to stabilize the lipogenic program and likely inhibits TGF β 1-mediated lipofibroblast-to-myofibroblast differentiation during fibrosis formation (19). Thus, PPAR γ agonists might potentially embody a new approach in the treatment of IPF, as demonstrated for rosiglitazone in vitro and in vivo (19, 207). Interestingly, *FGF10* was also found to be upregulated significantly at the mRNA-level in IPF patients (19), which is in harmony with the findings of this study at the protein level (compare 3.4). FGF10 has previously demonstrated the ability to activate PPAR γ signaling in the context of white adipose tissue formation (208, 209, 19) and its upregulation in IPF could be interpreted as an attempt to oppose the myogenic shift. Earlier findings by our group support this idea, as they demonstrated that *Fgf10* expression identifies lipofibroblast

progenitors during lung development and that FGF signaling is important for lipofibroblast formation (26). However, current treatment options for IPF heavily rely on the inhibition of tyrosine kinase receptors, which might inhibit potentially beneficial effects of FGF10 signaling with regard to the stabilization of the lipogenic phenotype. Following the promising results with PPAR γ agonist rosiglitazone, our workgroup proceeded to investigate the effects of another, prominent antidiabetic drug - metformin. Kheirollahi et al. hereby unveiled, that metformin supports myo- to lipofibroblast transdifferentiation in cultured human fibroblasts as well as in the bleomycin-mouse model (22). This antifibrotic effect is likely mediated through upregulation of *BMP2*, *PPAR γ* and the inhibition of profibrotic TGF β 1 signaling, which depicts metformin as a potential therapeutic option in the treatment of patients with IPF (22, 210).

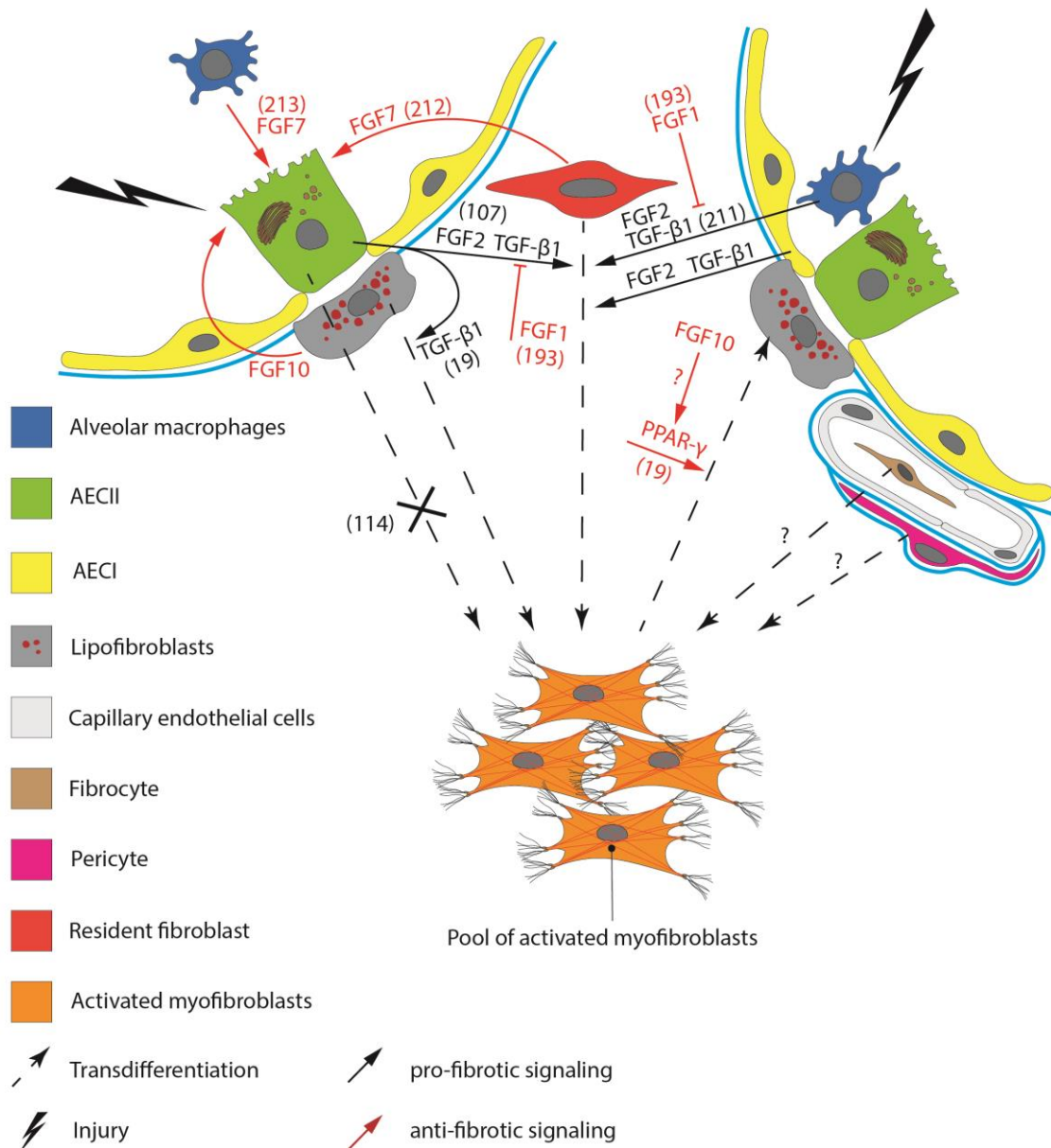


Fig. 26 Synopsis of the proposed involvement of FGFs in parenchymal remodeling in the context IPF – activated myofibroblasts are the primary executing cells of parenchymal remodeling and form a pool, to which other cell types contribute through transdifferentiation. During the pathogenesis of IPF, injury to the alveolar epithelium causes AEC and alveolar macrophages to release pro-fibrotic TGF- β 1 and FGF2, which in turn facilitate the transdifferentiation of resident fibroblasts into activated myofibroblasts (107, 194, 211). Additionally, lipofibroblast, too, contribute to the pool of activated myofibroblasts in a TGF- β 1 dependent manner, with stimulated PPAR γ -signaling favoring the reverse process (19). Pericytes and circulating fibrocytes are seen as additional contributors, epithelial-to-mesenchymal transdifferentiation of AEC on the other hand, has likely been ruled out (114). FGF1 is regarded as anti-fibrotic and inhibits the TGF- β 1 dependent accumulation of activated myofibroblasts (192, 193, 153). FGF7 and FGF10, produced in the mesenchyme (160, 212) and by alveolar macrophages in an experimental setting (213), seem to protect the pulmonary epithelium via FGFR2b. Upregulated endogenous FGFR2b signaling therefore might embody an intrinsic regenerative response (compare 4.4). Illustration developed upon aforementioned sources and adapted from El Agha, Seeger et al. 2017 (146)

4.6 Methodological challenges and limitations

Immunohistochemistry was chosen, as it not only enables a quantitative analyzation of the expression, but also visualizes the distribution and context of the signal. The intact tissue of a section allows for disease specific features to become identifiable, so that the immunoreactivity within specific regions can be visually assessed and compared to other regions or control tissue. Another distinct advantage is the longevity of the immunohistochemical chromogens, which is particularly relevant to this study, as it allows for prolonged quantification and frequent re-assessment over an extended period of time – without significant color fade.

Common sources of error, characteristic for but not limited to IHC, comprise “epitope masking” and “unspecific staining”. Epitope masking is a phenomenon common to certain fixing agents, which facilitate methylene-bridges (“cross links”) between the targeted epitope and amino groups of surrounding proteins (214, 215). As direct consequence, the antibody then is unable to reach the epitope and the affected region shows less or no visible immunoreactivity. These cross-links are partially susceptible to heat and protease activity, which allows them to be re-opened through “heat induced antigen retrieval” or “protease induced epitope retrieval” (216), both techniques were applied in this study. However, a certain loss of available epitopes is inevitable and to be expected. Depending on the extend, this potentially influences the validity of any immunohistochemical staining (214, 215).

Unwanted non-specific background noise is another phenomenon, which threatens the applicability of a particular staining and the validity of the results obtained. By choosing an indirect method of detection, two antibodies are of concern - the (unlabeled) primary antibody and a (biotinylated) secondary antibody – both of which are potential victims of misguided attraction and unspecific binding. Endogenous Fc receptors are thought to be the leading cause of unwanted background signal, as they are capable of attracting the Fc region of commonly used IgG antibodies during the staining process (217–219). Furthermore, non-immunological attraction due to increased hydrophobicity and electrostatics is believed to be a byproduct of formalin fixation and another major cause of background signal (219, 220). Contemporary countermeasures rely on blocking the unspecific bindings sites with normal serum and protein buffers, and although all these measures were applied in this study, their necessity and efficacy is debatable (219). The streptavidin-enzyme-complex, which binds the biotinylated secondary antibody is one further element prone to interference. Competing, endogenous

biotin-like molecules can falsely bind the enzyme-complex and cause unspecific background noise. This adverse effect might even be amplified through the use antigen retrieval methods (221), but was controlled through afore-mentioned blocking steps. Other factors potentially interfering with the signal and its intensity, namely temperature and incubation time, were meticulously standardized in this study. Ultimately, antibody specificity was verified by performing the complete staining procedure with only the primary or secondary antibody at a time (negative control). Staining of human kidney tissue with its known expression pattern served as the positive control. A key methodological limitation of immunohistochemistry, however, is that although the signal (FGF7 and FGF10) can be located in certain regions, this does not necessarily indicate that they are released on site. This implies the need for further confirmation, preferentially on the DNA level.

For the second half of this study, immunofluorescence (IF) was the method of choice. This technique stands out through high levels of sensitivity, specificity and resolution, especially when labeling multiple targets at the same time (222). Oil Red O and fluorescent Nile Red are two common dyes used for the staining of lipid droplets, with the distinct disadvantage of requiring strong organic solvents in their respective staining protocols (223). The protocol for the fluorescent LipidTOX, in contrast, relies on aqueous solutions and therefore is less likely to accidentally remove any proportion of the targeted lipid content. For the detection of SPC, indirect IF was chosen. This variant is comprised of an unconjugated primary antibody, which is directed against the selected target, while a fluorophore-conjugated secondary antibody is used for the detection of the primary antibody. Main advantages over direct IF are the further increased sensitivity and amplification of the signal (224). Disadvantages of IF in the context of this study are related to the reduced structural integrity of the frozen tissue sections and corresponding loss of information regarding their morphology. This makes analyzation of the structures surrounding the fluorescent signal more so challenging (225). Additionally, cellular dimensions and distribution patterns could only be estimated, which made quantification of the targeted lipofibroblasts not feasible. Indirect IF, in general, is prone to unwanted attraction towards endogenous immunoglobulin, causing unspecific background fluorescence (224). In a similar manner as with IHC, common precautions comprised blocking steps with normal serum of the species in which the secondary antibody was raised.

5 Summary

Fibroblast growth factors (FGFs) are a family of evolutionary related polypeptides, involved in a multitude of developmental and regenerative pathways in vertebrates. The human FGF family includes 22 members, which are categorized into intracrine, endocrine and paracrine FGFs, the latter of which primarily act through cell surface receptor tyrosine kinases (FGFRs) (133). While they serve as essential growth and differentiation factors during embryogenesis (165) and are crucial for maintaining homeostasis in the adult organism, aberrant FGF-signaling is also deeply enrooted within a wide number of pathologies (133, 226, 227). Loss-of-function mutations, decreased levels, but also excessive expression seem to be associated with certain hereditary, paraneoplastic and metabolic conditions, underlining the importance of well-regulated FGF-signaling.

Idiopathic pulmonary arterial hypertension (IPAH) and idiopathic pulmonary fibrosis (IPF) are hyperproliferative, nonmalignant pulmonary diseases, which both feature dysregulated and excessive cell proliferation in their pathogenesis. Although separate entities, they seem linked through their pathomechanisms, in which inflammatory and proliferative stimuli, in part mediated through various cytokines and growth factors, promote detrimental alterations of the pulmonary parenchyma and vasculature (93, 97). If left untreated, these alterations ultimately lead to impaired gas exchange, loss of cross-sectional area and increased pressure within the pulmonary circulation (34, 35, 94, 95). Despite readily available treatment regimens and growing insight into the pathophysiology, both conditions are still associated with a significantly reduced life expectancy (228, 229).

The involvement of fibroblast growth factors in IPF and IPAH is ambiguous and somewhat conflicting. In animal models, heightened levels of the prototypical FGFs, FGF1 and FGF2, were associated mostly with baneful effects in the form of proliferating pulmonary smooth-muscle cells, vasoconstriction and the profibrotic accumulation of myofibroblasts (107, 146, 150, 194). In contrast, increased expression of FGF7 and FGF10 protected against the development of pulmonary hypertension in rats and mitigated bleomycin-induced lung fibrosis in mice (157, 158, 195). Furthermore, FGF7 has been shown to promote the proliferation of AEC2 (162) and even prevented pulmonary injury in animals (155, 156), suggesting an overall protective effect on the alveolar epithelium. The author therefore hypothesized, that the expression of FGF7, FGF10 and FGFR2 would be altered in the course of IPF/ IPAH and aimed to further investigate, whether these alterations contribute to disease progression or rather represent

an intrinsic attempt at regeneration and restoring homeostasis.

Applying the techniques of immunohistochemistry, human lung tissue samples from patients with IPF and IPAH were analyzed for the expression patterns of FGF7, FGF10, FGFR1 and FGFR2, which then were compared to patterns found in healthy donor tissue. Our results demonstrate a marked increase in the overall expression of FGF7, FGF10 and FGFR2 in both, IPAH and IPF lungs, compared to donors. An in-depth analysis of the signal distribution revealed signal maxima confined to the remodeled parenchyma and vasculature. In IPF lungs, areas of mature fibrosis consistently featured strong immunoreactivity, while sites of early fibrosis (“fibroblastic foci”) displayed only light, occasional signal. Considering all the data presented in this study, we deduce that FGF7/FGF10-FGFR2 signaling is altered in the context of pulmonary remodeling, but is likely not the instigator. Follow-up observations indicated that FGF10 expression correlates with disease severity in IPF, which is compatible with our perception of the FGF10-FGFR2 signaling pathway as an “ineffective antifibrotic mediator” (64). Additional research regarding the significance of this pathway and potential benefits of its extrinsic stimulation in the context of pulmonary remodeling is duly needed. Especially, as current treatment options for IPF are primarily based on the inhibition of receptor tyrosine kinases and likely also inhibit FGFR2 signaling, mitigating any potentially antifibrotic effects of the FGF7/FGF10-FGFR2 signaling pathway.

During the second half of this study, focus has been turned to the alveolar lipofibroblast. There has been general consensus about the existence of these cells in rodents, where they maintain a close relationship with AEC2, storing and trafficking neutral-lipids for surfactant synthesis and protecting the lung against oxidant injury (16). At distinct phases during embryonic lung development in mice, FGF10-positive progenitor cells give rise to myofibroblasts and lipofibroblasts, the latter having demonstrated the tendency to later undergo a phenotypic shift into myofibroblasts in response to injurious stimuli (116, 28). Myofibroblasts are generally regarded as the main effector cells of pulmonary remodeling in IPF and our group has identified lipofibroblast-to-myofibroblast transdifferentiation as one source of activated myofibroblasts in the bleomycin mouse-model of fibrosis (19). In order to determine whether a similar phenotypic shift could be involved in the pathogenesis of IPF, we aimed to confirm the presence of alveolar lipofibroblasts in the human lung, where their existence has been controversial (24). Through utilization of the fluorescent neutral lipid stain “LipidTOX” on human lung tissue, we were able to gather strong evidence for neutral-lipid containing

cells in close proximity to AEC2 – in both, donor and IPF lungs. Subsequent investigations by our group confirmed that these cells are resident and likely lipofibroblasts. Considering the data presented by this study and reports of decreased lipofibroblast- and increased myofibroblast-markers in IPF lungs, the transdifferentiation of lipofibroblasts to myofibroblasts appears to be an underlying principle in the human condition as well (19). Our group proposed that this transdifferentiation is likely facilitated by TGF- β 1, while PPAR γ seems to stabilize and reinforce the lipogenic phenotype, which can be considered a significant advance towards a deeper understanding of the molecular principles of IPF. PPAR γ agonists and even metformin might therefore embody a way to counteract this detrimental shift during fibrosis formation or even later on (19, 22). In conclusion, alveolar lipofibroblasts have not only been identified as progenitors of the primary effector cells of remodeling in IPF, they also represent a novel pharmacological target, which might ultimately lead to new options in the treatment of patients with IPF.

5.1 Zusammenfassung

Fibroblasten-Wachstumsfaktoren (FGFs) bilden eine Familie evolutionär verwandter Polypeptide, die an einer Vielzahl von Entwicklungs- und Reparaturprozessen in Säugetieren beteiligt sind. Die FGF-Familie umfasst 22 Mitglieder, welche in intrakrine, endokrine und parakrine FGFs kategorisiert werden können, wobei letztere primär über membranständige Rezeptor-Tyrosinkinasen (FGFRs) agieren (133). FGFs fungieren als essentielle Wachstums- und Differenzierungsfaktoren während der Embryogenese (165) und sind entscheidend an der Aufrechterhaltung der Homöostase im erwachsenen Organismus beteiligt. Störungen in den entsprechenden Signalwegen führen zu einer Reihe umschriebener Pathologien (133, 226, 227). Sowohl Funktionsverlustmutationen als auch die verminderte oder übermäßige Expression von FGFs konnten mit einer Reihe von syndromalen, paraneoplastischen und metabolischen Erkrankungen in Verbindung gebracht werden, was die Bedeutung intakter und regulierter FGF-Signalwege unterstreicht.

Die idiopathische pulmonale arterielle Hypertonie (IPAH) und die idiopathische Lungenfibrose (IPF) sind hyperproliferative, nichtmaligne Lungenerkrankungen, deren Pathogenesen von einer fehlregulierten und exzessiven Zellproliferation geprägt sind. Obwohl es sich um separate Krankheitsbilder handelt, teilen sie gemeinsame Pathomechanismen, bei denen eine Vielzahl verschiedener Zytokine und

Wachstumsfaktoren entzündliche und proliferative Reize vermitteln, welche letztlich zu strukturellen Veränderungen des Lungenparenchyms und der Gefäße führen (93, 97). Unbehandelt haben diese Veränderungen den gestörten Gasaustausch, eine Verringerung des Gesamtquerschnitts der Lungengefäße und eine Druckerhöhung im Lungenkreislauf zur Folge (34, 35, 94, 95). Trotz etablierter Therapieschemata und eines zunehmenden Verständnisses der zugrundeliegenden Mechanismen sind beide Erkrankungen immer noch mit einer deutlich reduzierten Lebenserwartung verbunden (228, 229).

Die Rolle der Fibroblasten-Wachstumsfaktoren in der Pathogenese der IPF und IPAH ist nicht eindeutig und von Widersprüchen geprägt. In Tiermodellen waren erhöhte Spiegel der prototypischen FGFs, FGF1 und FGF2, mit verheerenden Wirkungen in Form von proliferierenden glatten Lungenmuskelzellen, Vasokonstriktion und der profibrotischen Akkumulation von Myofibroblasten verbunden (107, 146, 150, 194). Im Gegensatz dazu schützte die gesteigerte Expression von FGF7 und FGF10 in Ratten vor der Entwicklung einer pulmonalen Hypertonie und milderte die Bleomycin-induzierte Lungenfibrose bei Mäusen (157, 158, 195). Darüber hinaus förderte FGF7 die Proliferation von AEC2 (162) und milderte chemisch-toxische Lungenverletzungen bei Tieren (155, 156), was insgesamt eine schützende Wirkung auf das Alveolarepithel impliziert. Der Autor formulierte daher die Hypothese, dass sich die Expression von FGF7, FGF10 und FGFR2 im Rahmen der IPF/IPAH verändern würde und erhoffte weitere Erkenntnisse darüber zu erlangen, ob diese Veränderungen zur Krankheitsprogression beitragen oder aber einen intrinsischen Versuch der Regeneration bzw. Wiedererlangung der Homöostase darstellen.

Unter Anwendung der Techniken der Immunhistochemie wurden menschliche Lungengewebe von Patienten mit IPF und IPAH auf die Expressionsmuster von FGF7, FGF10, FGFR1 und FGFR2 analysiert, die dann mit Mustern aus gesundem Spendergewebe verglichen wurden. Unsere Ergebnisse zeigen einen deutlichen Anstieg der Gesamtexpression von FGF7, FGF10 und FGFR2 sowohl in IPAH- als auch in IPF-Lungen im Vergleich zu Spenderlungen. Die eingehende Analyse der Signalverteilung ergab eine räumliche Beschränkung der Signalmaxima auf das strukturell veränderte Parenchym und die dortigen Gefäße. In IPF-Lungen zeigten die Bereiche mit ausgereifter Fibrose durchweg eine starke Immunreaktivität, während Stellen mit beginnender und aktiver Fibrosierung („Fibroblasten-Foci“) nur ein leichtes, gelegentliches Signal aufwiesen. Unter Berücksichtigung aller in dieser Studie präsentierten Daten folgern wir, dass die FGF7/FGF10-FGFR2-Signalgebung im Kontext des pulmonalen Remodelings

maßgeblich beeinflusst wird, was aber wahrscheinlich nicht Auslöser dieser strukturellen Umbauprozesse ist. Folgebeobachtungen unserer Arbeitsgruppe zeigten, dass die FGF10-Expression im Falle der IPF mit der Schwere der Erkrankung korreliert, was mit unserer Wahrnehmung des FGF10-FGFR2-Signalwegs als einen „ineffektiven antifibrotischen Mediator“ vereinbar ist (64). Weiterführende Forschung bezüglich der Bedeutung dieses Signalwegs im Kontext des Lungenremodellings ist hier erforderlich. Insbesondere da die derzeitigen Therapieoptionen der IPF hauptsächlich auf der Hemmung von Rezeptor-Tyrosinkinasen basieren und somit ebenfalls die Signalübertragung via FGFR2 hemmen. Etwaige, potenziell antifibrotische Wirkungen des FGF7/FGF10-FGFR2-Signalwegs kommen somit nicht zur Geltung.

In der zweiten Hälfte dieser Studie wurde der Fokus auf die alveolären Lipofibroblasten gerichtet. Es besteht allgemeiner Konsens über die Existenz dieser Zellen in Nagetieren, wo sie eine enge Beziehung zu AEC2 unterhalten, neutrale Lipide für die Surfactant-Synthese speichern und transportieren, sowie die Lunge vor oxidativen Schäden schützen (16). In umschriebenen Phasen der embryonalen Lungenentwicklung bei Mäusen entstehen aus FGF10-positiven Vorläuferzellen Myofibroblasten und Lipofibroblasten, wobei letztere die Fähigkeit gezeigt haben als Reaktion auf schädigende Reize eine phänotypische Verschiebung zu Myofibroblasten zu durchlaufen (116, 28). Myofibroblasten gelten im Allgemeinen als die wichtigsten Effektorzellen des pulmonalen Remodelings im Rahmen der IPF. Interessanterweise gelang es unserer Arbeitsgruppe, die Transdifferenzierung von Lipofibroblasten zu Myofibroblasten als eine bedeutende Quelle für aktivierte Myofibroblasten im Bleomycin-Mausmodell der Fibrose zu identifizieren (19). Um zu überprüfen, ob eine ähnliche phänotypische Verschiebung an der Pathogenese von IPF beteiligt sein könnte, musste jedoch zunächst das Vorhandensein von alveolären Lipofibroblasten in der menschlichen Lunge bestätigt werden, denn deren dortige Existenz galt lange Zeit als umstritten (24). Durch die Verwendung des fluoreszierenden Lipidfarbstoffs „LipidTOX“ gelang es deutliche Indizien für neutrallipidhaltige Zellen in unmittelbarer Nähe zu AEC2 zu sammeln – sowohl in Spender- als auch in IPF-Lungen. Nachfolgende Untersuchungen unserer Gruppe bestätigten, dass es sich bei diesen Zellen mit großer Wahrscheinlichkeit um ortsansässige Lipofibroblasten handelt. Betrachtet man die in dieser Studie präsentierten Indizien, sowie Berichte über verminderte Lipofibroblasten- und erhöhte Myofibroblasten-Marker in IPF-Lungen, so erscheint die Transdifferenzierung von Lipofibroblasten zu Myofibroblasten als ein plausibler Mechanismus in der Pathogenese

der IPF (19). Unsere Gruppe konnte hierbei zeigen, dass dieser Vorgang mit großer Wahrscheinlichkeit durch TGF- β 1 vermittelt wird, während PPAR γ den umgekehrten Prozess in Richtung des lipogenen Phänotyps begünstigt. Dies ist ein relevanter Fortschritt in Richtung eines tieferen Verständnisses der IPF, denn theoretisch wären sowohl PPAR γ -Agonisten als auch Metformin somit in der Lage, der Verschiebung in Richtung des myogenen Phänotyps mittels Stabilisierung des lipogenen Phänotyps entgegenzuwirken (19, 22). Zusammenfassend lässt sich sagen, dass alveoläre Lipofibroblasten nicht nur als Vorläufer der primären Effektorzellen des Remodelings identifiziert werden konnten, sondern diese auch ein neues pharmakologisches Ziel darstellen, das letztendlich zu neuen Optionen in der Behandlung von Patienten mit IPF führen könnte.

6 Literature

1. Klinker R, Pape H-C, Kurtz A, Silbernagl S, Baumann R, Brenner B et al., editors. Physiologie. 6., vollst. überarb. Aufl. Stuttgart: Thieme; 2010.
2. Hick C, Hartmann J, editors. Intensivkurs Physiologie. 5., vollst. überarb. und aktualisierte Aufl. München: Elsevier Urban & Fischer; 2006. (Vorklinik).
3. Schünke M, Schulte E, Schumacher U, Voll M, Wesker K, editors. PROMETHEUS LernAtlas der Anatomie: Innere Organe. 2., überarbeitete und erweiterte Auflage. Stuttgart, New York, Stuttgart: Thieme; 2009.
4. Drake RL, Vogl AW, editors. Gray's Atlas der Anatomie: Deutsche Bearbeitung von Lars Bräuer. 3. Auflage. München: Urban & Fischer in Elsevier; 2021.
5. Kovacs G, Berghold A, Scheidl S, Olschewski H. Pulmonary arterial pressure during rest and exercise in healthy subjects: a systematic review. *Eur Respir J* 2009; 34(4):888–94.
6. Sommer N, Dietrich A, Schermuly RT, Ghofrani HA, Gudermann T, Schulz R et al. Regulation of hypoxic pulmonary vasoconstriction: basic mechanisms. *Eur Respir J* 2008; 32(6):1639–51.
7. Oliveira RKF, Ferreira EVM, Ramos RP, Messina CMS, Kapins CEB, Silva CMC et al. Usefulness of pulmonary capillary wedge pressure as a correlate of left ventricular filling pressures in pulmonary arterial hypertension. *J Heart Lung Transplant* 2014; 33(2):157–62.
8. Mason RJ. Biology of alveolar type II cells. *Respirology* 2006; 11 Suppl:S12-5.
9. Lüllmann-Rauch R. Taschenlehrbuch Histologie: 10 Tabellen. 2., komplett überarb. Aufl. Stuttgart: Thieme; 2006.
10. Phelps DS, Floros J. Localization of pulmonary surfactant proteins using immunohistochemistry and tissue in situ hybridization. *Exp Lung Res* 1991; 17(6):985–95.
11. Zacharias WJ, Frank DB, Zepp JA, Morley MP, Alkhaleel FA, Kong J et al. Regeneration of the lung alveolus by an evolutionarily conserved epithelial progenitor. *Nature* 2018; 555(7695):251–5.

12. Lee DF, Salguero FJ, Grainger D, Francis RJ, MacLellan-Gibson K, Chambers MA. Isolation and characterisation of alveolar type II pneumocytes from adult bovine lung. *Scientific Reports* 2018; 8(1):11927.
13. White ES. Lung extracellular matrix and fibroblast function. *Ann Am Thorac Soc* 2015; 12 Suppl 1(Suppl 1):S30-3.
14. Chua F, Laurent GJ. FIBROBLASTS. In: Laurent GJ, Shapiro SD, editors. *Encyclopedia of Respiratory Medicine*. Oxford: Academic Press; 2006. p. 213–9
Available from: URL:
<https://www.sciencedirect.com/science/article/pii/B0123708796001563>.
15. Epa AP, Thatcher TH, Pollock SJ, Wahl LA, Lyda E, Kottmann RM et al. Normal Human Lung Epithelial Cells Inhibit Transforming Growth Factor- β Induced Myofibroblast Differentiation via Prostaglandin E2. *PLoS One* 2015; 10(8):e0135266.
16. Rehan VK, Torday JS. The lung alveolar lipofibroblast: an evolutionary strategy against neonatal hyperoxic lung injury. *Antioxid Redox Signal* 2014; 21(13):1893–904.
17. Liu X, Rowan SC, Liang J, Yao C, Huang G, Deng N et al. Definition and Signatures of Lung Fibroblast Populations in Development and Fibrosis in Mice and Men. *bioRxiv* 2020:2020.07.15.203141.
18. Hinz B, Phan SH, Thannickal VJ, Galli A, Bochaton-Piallat M-L, Gabbiani G. The myofibroblast: one function, multiple origins. *Am J Pathol* 2007; 170(6):1807–16.
19. El Agha E, Moiseenko A, Kheirollahi V, Langhe S de, Crnkovic S, Kwapiszewska G et al. Two-Way Conversion between Lipogenic and Myogenic Fibroblastic Phenotypes Marks the Progression and Resolution of Lung Fibrosis. *Cell Stem Cell* 2017; 20(2):261-273.e3.
20. Scotton CJ, Chambers RC. Molecular targets in pulmonary fibrosis: the myofibroblast in focus. *Chest* 2007; 132(4):1311–21.
21. Gross TJ, Hunninghake GW. Idiopathic pulmonary fibrosis. *N Engl J Med* 2001; 345(7):517–25.
22. Kheirollahi V, Wasnick RM, Biasin V, Vazquez-Armendariz AI, Chu X, Moiseenko A et al. Metformin induces lipogenic differentiation in myofibroblasts to reverse lung fibrosis. *Nat Commun* 2019; 10(1):2987.

23. McGowan SE. The lipofibroblast: more than a lipid-storage depot. *Am J Physiol Lung Cell Mol Physiol* 2019; 316(5):L869-L871.
24. Tahedl D, Wirkes A, Tschanz SA, Ochs M, Mühlfeld C. How common is the lipid body-containing interstitial cell in the mammalian lung? *Am J Physiol Lung Cell Mol Physiol* 2014; 307(5):L386-94.
25. Rehan VK, Sugano S, Wang Y, Santos J, Romero S, Dasgupta C et al. Evidence for the presence of lipofibroblasts in human lung. *Exp Lung Res* 2006; 32(8):379–93.
26. Al Alam D, El Agha E, Sakurai R, Kheirollahi V, Moiseenko A, Danopoulos S et al. Evidence for the involvement of fibroblast growth factor 10 in lipofibroblast formation during embryonic lung development. *Development* 2015; 142(23):4139–50.
27. Simon DM, Mariani TJ. Role of PPARs and Retinoid X Receptors in the Regulation of Lung Maturation and Development. *PPAR Res* 2007; 2007:91240.
28. El Agha E, Herold S, Al Alam D, Quantius J, MacKenzie B, Carraro G et al. Fgf10-positive cells represent a progenitor cell population during lung development and postnatally. *Development* 2014; 141(2):296–306.
29. Simonneau G, Montani D, Celermajer DS, Denton CP, Gatzoulis MA, Krowka M et al. Haemodynamic definitions and updated clinical classification of pulmonary hypertension. *European Respiratory Journal* 2019; 53(1):1801913.
30. Sommer N, Ghofrani HA, Pak O, Bonnet S, Provencher S, Sitbon O et al. Current and future treatments of pulmonary arterial hypertension. *Br J Pharmacol* 2021; 178(1):6–30.
31. Butrous G. Pulmonary hypertension: From an orphan disease to a global epidemic. *Glob Cardiol Sci Pract* 2020; 2020(1):e202005.
32. Hoeper MM, Humbert M, Souza R, Idrees M, Kawut SM, Sliwa-Hahnle K et al. A global view of pulmonary hypertension. *Lancet Respir Med* 2016; 4(4):306–22.
33. Hoeper MM, Huscher D, Pittrow D. Incidence and prevalence of pulmonary arterial hypertension in Germany. *Int J Cardiol* 2016; 203:612–3.
34. Schermuly RT, Ghofrani HA, Wilkins MR, Grimminger F. Mechanisms of disease: pulmonary arterial hypertension. *Nat Rev Cardiol* 2011; 8(8):443–55.

35. Tuder RM, Abman SH, Braun T, Capron F, Stevens T, Thistlethwaite PA et al. Development and pathology of pulmonary hypertension. *J Am Coll Cardiol* 2009; 54(1 Suppl):S3-S9.
36. Tuder RM. Pulmonary vascular remodeling in pulmonary hypertension. *Cell Tissue Res* 2017; 367(3):643–9.
37. Stacher E, Graham BB, Hunt JM, Gandjeva A, Groshong SD, McLaughlin VV et al. Modern age pathology of pulmonary arterial hypertension. *Am J Respir Crit Care Med* 2012; 186(3):261–72.
38. Nicod LP. The endothelium and genetics in pulmonary arterial hypertension. *Swiss Med Wkly* 2007; 137(31-32):437–42.
39. Rabinovitch M. Pathobiology of pulmonary hypertension. *Annu Rev Pathol* 2007; 2:369–99.
40. Crnkovic S, Marsh LM, El Agha E, Voswinckel R, Ghanim B, Klepetko W et al. Resident cell lineages are preserved in pulmonary vascular remodeling. *J Pathol* 2018; 244(4):485–98.
41. Arribas SM, Hillier C, González C, McGrory S, Dominiczak AF, McGrath JC. Cellular aspects of vascular remodeling in hypertension revealed by confocal microscopy. *Hypertension* 1997; 30(6):1455–64.
42. Das M, Dempsey EC, Reeves JT, Stenmark KR. Selective expansion of fibroblast subpopulations from pulmonary artery adventitia in response to hypoxia. *Am J Physiol Lung Cell Mol Physiol* 2002; 282(5):L976-86.
43. Welsh DJ, Peacock AJ, MacLean M, Harnett M. Chronic hypoxia induces constitutive p38 mitogen-activated protein kinase activity that correlates with enhanced cellular proliferation in fibroblasts from rat pulmonary but not systemic arteries. *Am J Respir Crit Care Med* 2001; 164(2):282–9.
44. Morrell NW, Adnot S, Archer SL, Dupuis J, Lloyd Jones P, MacLean MR et al. Cellular and molecular basis of pulmonary arterial hypertension. *J Am Coll Cardiol* 2009; 54(1 Suppl):S20-S31.
45. Zhu P, Huang L, Ge X, Yan F, Wu R, Ao Q. Transdifferentiation of pulmonary arteriolar endothelial cells into smooth muscle-like cells regulated by myocardin

- involved in hypoxia-induced pulmonary vascular remodelling. *Int J Exp Pathol* 2006; 87(6):463–74.
46. Frid MG, Brunetti JA, Burke DL, Carpenter TC, Davie NJ, Reeves JT et al. Hypoxia-induced pulmonary vascular remodeling requires recruitment of circulating mesenchymal precursors of a monocyte/macrophage lineage. *Am J Pathol* 2006; 168(2):659–69.
47. Tuder RM, Archer SL, Dorfmueller P, Erzurum SC, Guignabert C, Michelakis E et al. Relevant issues in the pathology and pathobiology of pulmonary hypertension. *J Am Coll Cardiol* 2013; 62(25 Suppl):D4-12.
48. Stenmark KR, Nozik-Grayck E, Gerasimovskaya E, Anwar A, Li M, Riddle S et al. The adventitia: Essential role in pulmonary vascular remodeling. *Compr Physiol* 2011; 1(1):141–61.
49. Christman BW, McPherson CD, Newman JH, King GA, Bernard GR, Groves BM et al. An imbalance between the excretion of thromboxane and prostacyclin metabolites in pulmonary hypertension. *N Engl J Med* 1992; 327(2):70–5.
50. Ghofrani HA, Osterloh IH, Grimminger F. Sildenafil: from angina to erectile dysfunction to pulmonary hypertension and beyond. *Nat Rev Drug Discov* 2006; 5(8):689–702.
51. Launay J-M, Hervé P, Peoc'h K, Tournois C, Callebert J, Nebigil CG et al. Function of the serotonin 5-hydroxytryptamine 2B receptor in pulmonary hypertension. *Nature Medicine* 2002; 8(10):1129–35.
52. Gurtner HP. Chronic pulmonary hypertension of vascular origin, plexogenic pulmonary arteriopathy and the appetite depressant aminorex: addenda to an epidemic. *Swiss Med Wkly* 1985; 115(23):782-9contd.
53. Eddahibi S, Guignabert C, Barlier-Mur A-M, Dewachter L, Fadel E, Darteville P et al. Cross talk between endothelial and smooth muscle cells in pulmonary hypertension: critical role for serotonin-induced smooth muscle hyperplasia. *Circulation* 2006; 113(15):1857–64.
54. Ito T, Ikeda U, Shimpo M, Yamamoto K, Shimada K. Serotonin increases interleukin-6 synthesis in human vascular smooth muscle cells. *Circulation* 2000; 102(20):2522–7.

55. Moudgil R, Michelakis ED, Archer SL. The role of k⁺ channels in determining pulmonary vascular tone, oxygen sensing, cell proliferation, and apoptosis: implications in hypoxic pulmonary vasoconstriction and pulmonary arterial hypertension. *Microcirculation* 2006; 13(8):615–32.
56. Selimovic N, Bergh C-H, Andersson B, Sakiniene E, Carlsten H, Rundqvist B. Growth factors and interleukin-6 across the lung circulation in pulmonary hypertension. *Eur Respir J* 2009; 34(3):662–8.
57. Tsutsumi T, Nagaoka T, Yoshida T, Wang L, Kuriyama S, Suzuki Y et al. Nintedanib ameliorates experimental pulmonary arterial hypertension via inhibition of endothelial mesenchymal transition and smooth muscle cell proliferation. *PLoS One* 2019; 14(7):e0214697.
58. Quinn TP, Schlueter M, Soifer SJ, Gutierrez JA. Cyclic mechanical stretch induces VEGF and FGF-2 expression in pulmonary vascular smooth muscle cells. *Am J Physiol Lung Cell Mol Physiol* 2002; 282(5):L897-903.
59. Wollin L, Wex E, Pautsch A, Schnapp G, Hostettler KE, Stowasser S et al. Mode of action of nintedanib in the treatment of idiopathic pulmonary fibrosis. *Eur Respir J* 2015; 45(5):1434–45.
60. Ranchoux B, Antigny F, Rucker-Martin C, Hautefort A, Péchoux C, Bogaard HJ et al. Endothelial-to-mesenchymal transition in pulmonary hypertension. *Circulation* 2015; 131(11):1006–18.
61. Soubrier F, Chung WK, Machado R, Grünig E, Aldred M, Geraci M et al. Genetics and genomics of pulmonary arterial hypertension. *J Am Coll Cardiol* 2013; 62(25 Suppl):D13-21.
62. Kurakula K, Smolders, Valérie F E D, Tura-Ceide O, Jukema JW, Quax PHA, Goumans M-J. Endothelial Dysfunction in Pulmonary Hypertension: Cause or Consequence? *Biomedicines* 2021; 9(1).
63. Kim J, Kang Y, Kojima Y, Lighthouse JK, Hu X, Aldred MA et al. An endothelial apelin-FGF link mediated by miR-424 and miR-503 is disrupted in pulmonary arterial hypertension. *Nature Medicine* 2013; 19(1):74–82.
64. El Agha E, Schwind F, Ruppert C, Günther A, Bellusci S, Schermuly RT et al. Is the fibroblast growth factor signaling pathway a victim of receptor tyrosine kinase

inhibition in pulmonary parenchymal and vascular remodeling? *Am J Physiol Lung Cell Mol Physiol* 2018; 315(2):L248-L252.

65. Izikki M, Guignabert C, Fadel E, Humbert M, Tu L, Zadigue P et al. Endothelial-derived FGF2 contributes to the progression of pulmonary hypertension in humans and rodents. *J Clin Invest* 2009; 119(3):512–23.

66. Hansmann G, Wagner RA, Schellong S, Perez, Vinicio A de Jesus, Urashima T, Wang L et al. Pulmonary arterial hypertension is linked to insulin resistance and reversed by peroxisome proliferator-activated receptor-gamma activation. *Circulation* 2007; 115(10):1275–84.

67. Ameshima S, Golpon H, Cool CD, Chan D, Vandivier RW, Gardai SJ et al. Peroxisome proliferator-activated receptor gamma (PPARgamma) expression is decreased in pulmonary hypertension and affects endothelial cell growth. *Circ Res* 2003; 92(10):1162–9.

68. Hansmann G, de Jesus Perez, Vinicio A, Alastalo T-P, Alvira CM, Guignabert C, Bekker JM et al. An antiproliferative BMP-2/PPARgamma/apoE axis in human and murine SMCs and its role in pulmonary hypertension. *J Clin Invest* 2008; 118(5):1846–57.

69. Li M, Li Z, Sun X, Yang L, Fang P, Liu Y et al. Heme oxygenase-1/p21WAF1 mediates peroxisome proliferator-activated receptor-gamma signaling inhibition of proliferation of rat pulmonary artery smooth muscle cells. *FEBS J* 2010; 277(6):1543–50.

70. Martin-Nizard F, Furman C, Delerive P, Kandoussi A, Fruchart JC, Staels B et al. Peroxisome proliferator-activated receptor activators inhibit oxidized low-density lipoprotein-induced endothelin-1 secretion in endothelial cells. *J Cardiovasc Pharmacol* 2002; 40(6):822–31.

71. Herold G. *Innere Medizin 2019: Eine vorlesungsorientierte Darstellung : unter Berücksichtigung des Gegenstandskataloges für die Ärztliche Prüfung : mit ICD 10-Schlüssel im Text und Stichwortverzeichnis*. Köln: Herold Gerd; 2018.

72. Fisher MR, Forfia PR, Chamera E, Houston-Harris T, Champion HC, Girgis RE et al. Accuracy of Doppler echocardiography in the hemodynamic assessment of pulmonary hypertension. *Am J Respir Crit Care Med* 2009; 179(7):615–21.

73. Huang W-C, Hsu C-H, Sung S-H, Ho W-J, Chu C-Y, Chang C-P et al. 2018 TSOC guideline focused update on diagnosis and treatment of pulmonary arterial hypertension. *J Formos Med Assoc* 2019; 118(12):1584–609.
74. Hoeper MM, Kramer T, Pan Z, Eichstaedt CA, Spiesshoefer J, Benjamin N et al. Mortality in pulmonary arterial hypertension: prediction by the 2015 European pulmonary hypertension guidelines risk stratification model. *Eur Respir J* 2017; 50(2).
75. Galiè N, Humbert M, Vachiery J-L, Gibbs S, Lang I, Torbicki A et al. 2015 ESC/ERS Guidelines for the diagnosis and treatment of pulmonary hypertension: The Joint Task Force for the Diagnosis and Treatment of Pulmonary Hypertension of the European Society of Cardiology (ESC) and the European Respiratory Society (ERS): Endorsed by: Association for European Paediatric and Congenital Cardiology (AEPC), International Society for Heart and Lung Transplantation (ISHLT). *Eur Heart J* 2016; 37(1):67–119.
76. Hoeper MM, Ghofrani H-A, Grünig E, Klose H, Olschewski H, Rosenkranz S. Pulmonary Hypertension. *Dtsch Arztebl Int* 2017; 114(5):73–84.
77. Barratt SL, Creamer A, Hayton C, Chaudhuri N. Idiopathic Pulmonary Fibrosis (IPF): An Overview. *J Clin Med* 2018; 7(8).
78. Hopkins RB, Burke N, Fell C, Dion G, Kolb M. Epidemiology and survival of idiopathic pulmonary fibrosis from national data in Canada. *Eur Respir J* 2016; 48(1):187–95.
79. Hutchinson J, Fogarty A, Hubbard R, McKeever T. Global incidence and mortality of idiopathic pulmonary fibrosis: a systematic review. *Eur Respir J* 2015; 46(3):795–806.
80. Behr J, Günther A, Bonella F, Dinkel J, Fink L, Geiser T et al. S2K Guideline for Diagnosis of Idiopathic Pulmonary Fibrosis. *Respiration* 2021; 100(3):238–71.
81. Doubková M, Švancara J, Svoboda M, Šterclová M, Bartoš V, Plačková M et al. EMPIRE Registry, Czech Part: Impact of demographics, pulmonary function and HRCT on survival and clinical course in idiopathic pulmonary fibrosis. *Clin Respir J* 2018; 12(4):1526–35.
82. Cottin V, Hirani NA, Hotchkin DL, Nambiar AM, Ogura T, Otaola M et al. Presentation, diagnosis and clinical course of the spectrum of progressive-fibrosing interstitial lung diseases. *Eur Respir Rev* 2018; 27(150).

83. Swensen SJ, Aughenbaugh GL, Myers JL. Diffuse lung disease: diagnostic accuracy of CT in patients undergoing surgical biopsy of the lung. *Radiology* 1997; 205(1):229–34.
84. Collard HR, Tino G, Noble PW, Shreve MA, Michaels M, Carlson B et al. Patient experiences with pulmonary fibrosis. *Respir Med* 2007; 101(6):1350–4.
85. Zibrak JD, Price D. Interstitial lung disease: raising the index of suspicion in primary care. *NPJ Prim Care Respir Med* 2014; 24:14054.
86. Kolb M, Collard HR. Staging of idiopathic pulmonary fibrosis: past, present and future. *Eur Respir Rev* 2014; 23(132):220–4.
87. Behr J, Kreuter M, Hoepfer MM, Wirtz H, Klotsche J, Koschel D et al. Management of patients with idiopathic pulmonary fibrosis in clinical practice: the INSIGHTS-IPF registry. *Eur Respir J* 2015; 46(1):186–96.
88. Taskar VS, Coultas DB. Is idiopathic pulmonary fibrosis an environmental disease? *Proc Am Thorac Soc* 2006; 3(4):293–8.
89. Noth I, Zhang Y, Ma S-F, Flores C, Barber M, Huang Y et al. Genetic variants associated with idiopathic pulmonary fibrosis susceptibility and mortality: a genome-wide association study. *Lancet Respir Med* 2013; 1(4):309–17.
90. Wolters PJ, Collard HR, Jones KD. Pathogenesis of idiopathic pulmonary fibrosis. *Annu Rev Pathol* 2014; 9:157–79.
91. Raghu G, Collard HR, Egan JJ, Martinez FJ, Behr J, Brown KK et al. An official ATS/ERS/JRS/ALAT statement: idiopathic pulmonary fibrosis: evidence-based guidelines for diagnosis and management. *Am J Respir Crit Care Med* 2011; 183(6):788–824.
92. Richeldi L, Collard HR, Jones MG. Idiopathic pulmonary fibrosis. *Lancet* 2017; 389(10082):1941–52.
93. Seeger W, Adir Y, Barberà JA, Champion H, Coghlan JG, Cottin V et al. Pulmonary hypertension in chronic lung diseases. *J Am Coll Cardiol* 2013; 62(25 Suppl):D109-16.
94. Shorr AF, Wainright JL, Cors CS, Lettieri CJ, Nathan SD. Pulmonary hypertension in patients with pulmonary fibrosis awaiting lung transplant. *Eur Respir J* 2007; 30(4):715–21.

95. Hoepfer MM, Behr J, Held M, Grunig E, Vizza CD, Vonk-Noordegraaf A et al. Pulmonary Hypertension in Patients with Chronic Fibrosing Idiopathic Interstitial Pneumonias. *PLoS One* 2015; 10(12):e0141911.
96. Sherner J, Collen J, King CS, Nathan SD. Pulmonary hypertension in idiopathic pulmonary fibrosis: epidemiology, diagnosis and therapeutic implications. *Current Respiratory Care Reports* 2012; 1(4):233–42.
97. Corte TJ, Wort SJ, Wells AU. Pulmonary hypertension in idiopathic pulmonary fibrosis: a review. *Sarcoidosis Vasc Diffuse Lung Dis* 2009; 26(1):7–19.
98. Sgalla G, Iovene B, Calvello M, Ori M, Varone F, Richeldi L. Idiopathic pulmonary fibrosis: pathogenesis and management. *Respir Res* 2018; 19(1):32.
99. Raghu G, Anstrom KJ, King TE, JR, Lasky JA, Martinez FJ. Prednisone, azathioprine, and N-acetylcysteine for pulmonary fibrosis. *N Engl J Med* 2012; 366(21):1968–77.
100. Seibold MA, Wise AL, Speer MC, Steele MP, Brown KK, Loyd JE et al. A common MUC5B promoter polymorphism and pulmonary fibrosis. *N Engl J Med* 2011; 364(16):1503–12.
101. Allen RJ, Porte J, Braybrooke R, Flores C, Fingerlin TE, Oldham JM et al. Genetic variants associated with susceptibility to idiopathic pulmonary fibrosis in people of European ancestry: a genome-wide association study. *Lancet Respir Med* 2017; 5(11):869–80.
102. Mathai SK, Newton CA, Schwartz DA, Garcia CK. Pulmonary fibrosis in the era of stratified medicine. *Thorax* 2016; 71(12):1154–60.
103. Issa J-P. Aging and epigenetic drift: a vicious cycle. *J Clin Invest* 2014; 124(1):24–9.
104. Liu F, Killian JK, Yang M, Walker RL, Hong JA, Zhang M et al. Epigenomic alterations and gene expression profiles in respiratory epithelia exposed to cigarette smoke condensate. *Oncogene* 2010; 29(25):3650–64.
105. Huang W-T, Akhter H, Jiang C, MacEwen M, Ding Q, Antony V et al. Plasminogen activator inhibitor 1, fibroblast apoptosis resistance, and aging-related susceptibility to lung fibrosis. *Exp Gerontol* 2015; 61:62–75.

106. Grimminger F, Günther A, Vancheri C. The role of tyrosine kinases in the pathogenesis of idiopathic pulmonary fibrosis. *Eur Respir J* 2015; 45(5):1426–33.
107. Xiao L, Du Y, Shen Y, He Y, Zhao H, Li Z. TGF-beta 1 induced fibroblast proliferation is mediated by the FGF-2/ERK pathway. *Front Biosci (Landmark Ed)* 2012; 17:2667–74.
108. Yu Z, Wang D, Zhou Z, He S, Chen A, Wang J. Mutant soluble ectodomain of fibroblast growth factor receptor-2 IIIc attenuates bleomycin-induced pulmonary fibrosis in mice. *Biol Pharm Bull* 2012; 35(5):731–6.
109. Correll KA, Edeen KE, Zemans RL, Redente EF, Mikels-Vigdal A, Mason RJ. TGF beta inhibits expression of SP-A, SP-B, SP-C, but not SP-D in human alveolar type II cells. *Biochem Biophys Res Commun* 2018; 499(4):843–8.
110. Hoepfer MM, Barst RJ, Bourge RC, Feldman J, Frost AE, Galié N et al. Imatinib mesylate as add-on therapy for pulmonary arterial hypertension: results of the randomized IMPRES study. *Circulation* 2013; 127(10):1128–38.
111. Hostettler KE, Zhong J, Papakonstantinou E, Karakiulakis G, Tamm M, Seidel P et al. Anti-fibrotic effects of nintedanib in lung fibroblasts derived from patients with idiopathic pulmonary fibrosis. *Respir Res* 2014; 15(1):157.
112. Desmoulière A, Chaponnier C, Gabbiani G. Tissue repair, contraction, and the myofibroblast. *Wound Repair Regen* 2005; 13(1):7–12.
113. Maharaj SS, Baroke E, Gauldie J, Kolb MRJ. Fibrocytes in chronic lung disease--facts and controversies. *Pulm Pharmacol Ther* 2012; 25(4):263–7.
114. Rock JR, Barkauskas CE, Cronic MJ, Xue Y, Harris JR, Liang J et al. Multiple stromal populations contribute to pulmonary fibrosis without evidence for epithelial to mesenchymal transition. *Proc Natl Acad Sci U S A* 2011; 108(52):E1475-83.
115. Hecker L, Jagirdar R, Jin T, Thannickal VJ. Reversible differentiation of myofibroblasts by MyoD. *Exp Cell Res* 2011; 317(13):1914–21.
116. Rehan V, Torday J. Hyperoxia augments pulmonary lipofibroblast-to-myofibroblast transdifferentiation. *Cell Biochem Biophys* 2003; 38(3):239–50.
117. Behr J, Günther A, Bonella F, Geißler K, Koschel D, Kreuter M et al. German Guideline for Idiopathic Pulmonary Fibrosis - Update on Pharmacological Therapies 2017. *Pneumologie* 2017; 71(7):460–74.

118. Raghu G, Rochweg B, Zhang Y, Garcia CAC, Azuma A, Behr J et al. An Official ATS/ERS/JRS/ALAT Clinical Practice Guideline: Treatment of Idiopathic Pulmonary Fibrosis. An Update of the 2011 Clinical Practice Guideline. *Am J Respir Crit Care Med* 2015; 192(2):e3-19.
119. Daniels CE, Lasky JA, Limper AH, Mieras K, Gabor E, Schroeder DR. Imatinib treatment for idiopathic pulmonary fibrosis: Randomized placebo-controlled trial results. *Am J Respir Crit Care Med* 2010; 181(6):604–10.
120. Wollin L, Maillet I, Quesniaux V, Holweg A, Ryffel B. Antifibrotic and anti-inflammatory activity of the tyrosine kinase inhibitor nintedanib in experimental models of lung fibrosis. *J Pharmacol Exp Ther* 2014; 349(2):209–20.
121. Richeldi L, Du Bois RM, Raghu G, Azuma A, Brown KK, Costabel U et al. Efficacy and safety of nintedanib in idiopathic pulmonary fibrosis. *N Engl J Med* 2014; 370(22):2071–82.
122. Bonella F, Kreuter M, Hagemeyer L, Neurohr C, Keller C, Kohlhaeufel MJ et al. Insights from the German Compassionate Use Program of Nintedanib for the Treatment of Idiopathic Pulmonary Fibrosis. *Respiration* 2016; 92(2):98–106.
123. Nakazato H, Oku H, Yamane S, Tsuruta Y, Suzuki R. A novel anti-fibrotic agent pirfenidone suppresses tumor necrosis factor- α at the translational level. *Eur J Pharmacol* 2002; 446(1-3):177–85.
124. Iyer SN, Gurujeyalakshmi G, Giri SN. Effects of pirfenidone on transforming growth factor- β gene expression at the transcriptional level in bleomycin hamster model of lung fibrosis. *J Pharmacol Exp Ther* 1999; 291(1):367–73.
125. Gurujeyalakshmi G, Hollinger MA, Giri SN. Pirfenidone inhibits PDGF isoforms in bleomycin hamster model of lung fibrosis at the translational level. *Am J Physiol* 1999; 276(2):L311-8.
126. Iyer SN, Gurujeyalakshmi G, Giri SN. Effects of pirfenidone on procollagen gene expression at the transcriptional level in bleomycin hamster model of lung fibrosis. *J Pharmacol Exp Ther* 1999; 289(1):211–8.
127. Kobayashi T, Liu X, Wen F-Q, Kohyama T, Shen L, Wang XQ et al. Smad3 mediates TGF- β 1-induced collagen gel contraction by human lung fibroblasts. *Biochem Biophys Res Commun* 2006; 339(1):290–5.

128. Jin J, Togo S, Kadoya K, Tulafu M, Namba Y, Iwai M et al. Pirfenidone attenuates lung fibrotic fibroblast responses to transforming growth factor- β 1. *Respir Res* 2019; 20(1):119.
129. Oltmanns U, Kahn N, Palmowski K, Träger A, Wenz H, Heussel CP et al. Pirfenidone in idiopathic pulmonary fibrosis: real-life experience from a German tertiary referral center for interstitial lung diseases. *Respiration* 2014; 88(3):199–207.
130. Lancaster LH, Andrade JA de, Zibrak JD, Padilla ML, Albera C, Nathan SD et al. Pirfenidone safety and adverse event management in idiopathic pulmonary fibrosis. *Eur Respir Rev* 2017; 26(146).
131. Müller A-K, Meyer M, Werner S. The roles of receptor tyrosine kinases and their ligands in the wound repair process. *Semin Cell Dev Biol* 2012; 23(9):963–70.
132. Min H, Danilenko DM, Scully SA, Bolon B, Ring BD, Tarpley JE et al. Fgf-10 is required for both limb and lung development and exhibits striking functional similarity to *Drosophila* branchless. *Genes Dev* 1998; 12(20):3156–61.
133. Itoh N, Ornitz DM. Fibroblast growth factors: from molecular evolution to roles in development, metabolism and disease. *J Biochem* 2011; 149(2):121–30.
134. Itoh N, Ornitz DM. Evolution of the Fgf and Fgfr gene families. *Trends Genet* 2004; 20(11):563–9.
135. Goldfarb M, Schoorlemmer J, Williams A, Diwakar S, Wang Q, Huang X et al. Fibroblast growth factor homologous factors control neuronal excitability through modulation of voltage-gated sodium channels. *Neuron* 2007; 55(3):449–63.
136. Ornitz DM, Itoh N. The Fibroblast Growth Factor signaling pathway. *Wiley Interdiscip Rev Dev Biol* 2015; 4(3):215–66.
137. Zhang X, Ibrahimi OA, Olsen SK, Umemori H, Mohammadi M, Ornitz DM. Receptor specificity of the fibroblast growth factor family. The complete mammalian FGF family. *J Biol Chem* 2006; 281(23):15694–700.
138. Turner N, Grose R. Fibroblast growth factor signalling: from development to cancer. *Nat Rev Cancer* 2010; 10(2):116–29.
139. Beenken A, Mohammadi M. The FGF family: biology, pathophysiology and therapy. *Nat Rev Drug Discov* 2009; 8(3):235–53.

140. Dailey L, Ambrosetti D, Mansukhani A, Basilico C. Mechanisms underlying differential responses to FGF signaling. *Cytokine Growth Factor Rev* 2005; 16(2):233–47.
141. Xie Y, Su N, Yang J, Tan Q, Huang S, Jin M et al. FGF/FGFR signaling in health and disease. *Signal Transduct Target Ther* 2020; 5(1):181.
142. Thisse B, Thisse C. Functions and regulations of fibroblast growth factor signaling during embryonic development. *Dev Biol* 2005; 287(2):390–402.
143. Lin X. Functions of heparan sulfate proteoglycans in cell signaling during development. *Development* 2004; 131(24):6009–21.
144. Touat M, Ileana E, Postel-Vinay S, André F, Soria J-C. Targeting FGFR Signaling in Cancer. *Clin Cancer Res* 2015; 21(12):2684–94.
145. Su N, Jin M, Chen L. Role of FGF/FGFR signaling in skeletal development and homeostasis: learning from mouse models. *Bone Research* 2014; 2(1):14003.
146. El Agha E, Seeger W, Bellusci S. Therapeutic and pathological roles of fibroblast growth factors in pulmonary diseases. *Dev Dyn* 2017; 246(4):235–44.
147. Fon Tacer K, Bookout AL, Ding X, Kurosu H, John GB, Wang L et al. Research resource: Comprehensive expression atlas of the fibroblast growth factor system in adult mouse. *Mol Endocrinol* 2010; 24(10):2050–64.
148. Powers CJ, McLeskey SW, Wellstein A. Fibroblast growth factors, their receptors and signaling. *Endocr Relat Cancer* 2000; 7(3):165–97.
149. Ju W, Zhihong Y, Zhiyou Z, Qin H, Dingding W, Li S et al. Inhibition of α -SMA by the ectodomain of FGFR2c attenuates lung fibrosis. *Mol Med* 2012; 18(1):992–1002.
150. Tu L, Dewachter L, Gore B, Fadel E, Darteville P, Simonneau G et al. Autocrine fibroblast growth factor-2 signaling contributes to altered endothelial phenotype in pulmonary hypertension. *Am J Respir Cell Mol Biol* 2011; 45(2):311–22.
151. Ricard N, Tu L, Le Hiress M, Huertas A, Phan C, Thuillet R et al. Increased pericyte coverage mediated by endothelial-derived fibroblast growth factor-2 and interleukin-6 is a source of smooth muscle-like cells in pulmonary hypertension. *Circulation* 2014; 129(15):1586–97.

152. Izikki M, Mercier O, Lecerf F, Guin LL, Hoang E, Dorfmüller P et al. The beneficial effect of suramin on monocrotaline-induced pulmonary hypertension in rats. *PLoS One* 2013; 8(10):e77073.
153. Ramos C, Becerril C, Montaña M, García-De-Alba C, Ramírez R, Checa M et al. FGF-1 reverts epithelial-mesenchymal transition induced by TGF- β 1 through MAPK/ERK kinase pathway. *Am J Physiol Lung Cell Mol Physiol* 2010; 299(2):L222-31.
154. Joannes A, Brayer S, Besnard V, Marchal-Sommé J, Jaillet M, Mordant P et al. FGF9 and FGF18 in idiopathic pulmonary fibrosis promote survival and migration and inhibit myofibroblast differentiation of human lung fibroblasts in vitro. *Am J Physiol Lung Cell Mol Physiol* 2016; 310(7):L615-29.
155. Yi ES, Williams ST, Lee H, Malicki DM, Chin EM, Yin S et al. Keratinocyte growth factor ameliorates radiation- and bleomycin-induced lung injury and mortality. *Am J Pathol* 1996; 149(6):1963–70.
156. Yano T, Deterding RR, Simonet WS, Shannon JM, Mason RJ. Keratinocyte growth factor reduces lung damage due to acid instillation in rats. *Am J Respir Cell Mol Biol* 1996; 15(4):433–42.
157. Frank L. Protective effect of keratinocyte growth factor against lung abnormalities associated with hyperoxia in prematurely born rats. *Biol Neonate* 2003; 83(4):263–72.
158. Gupte VV, Ramasamy SK, Reddy R, Lee J, Weinreb PH, Violette SM et al. Overexpression of fibroblast growth factor-10 during both inflammatory and fibrotic phases attenuates bleomycin-induced pulmonary fibrosis in mice. *Am J Respir Crit Care Med* 2009; 180(5):424–36.
159. Shimbori C, El Agha E. Good Things Come in 2s: Type 2 Alveolar Epithelial Cells and Fibroblast Growth Factor Receptor 2. *Am J Respir Cell Mol Biol* 2020; 62(5):543–5.
160. Finch PW, Rubin JS, Miki T, Ron D, Aaronson SA. Human KGF is FGF-related with properties of a paracrine effector of epithelial cell growth. *Science* 1989; 245(4919):752–5.
161. Werner S, Peters KG, Longaker MT, Fuller-Pace F, Banda MJ, Williams LT. Large induction of keratinocyte growth factor expression in the dermis during wound healing. *Proc Natl Acad Sci U S A* 1992; 89(15):6896–900.

162. Ulich TR, Yi ES, Longmuir K, Yin S, Biltz R, Morris CF et al. Keratinocyte growth factor is a growth factor for type II pneumocytes in vivo. *J Clin Invest* 1994; 93(3):1298–306.
163. Guo L, Degenstein L, Fuchs E. Keratinocyte growth factor is required for hair development but not for wound healing. *Genes Dev* 1996; 10(2):165–75.
164. Qiao J, Uzzo R, Obara-Ishihara T, Degenstein L, Fuchs E, Herzlinger D. FGF-7 modulates ureteric bud growth and nephron number in the developing kidney. *Development* 1999; 126(3):547–54.
165. El Agha E, Al Alam D, Carraro G, MacKenzie B, Goth K, Langhe SP de et al. Characterization of a novel fibroblast growth factor 10 (Fgf10) knock-in mouse line to target mesenchymal progenitors during embryonic development. *PLoS One* 2012; 7(6):e38452.
166. Yamasaki M, Miyake A, Tagashira S, Itoh N. Structure and expression of the rat mRNA encoding a novel member of the fibroblast growth factor family. *J Biol Chem* 1996; 271(27):15918–21.
167. Ohuchi H, Hori Y, Yamasaki M, Harada H, Sekine K, Kato S et al. FGF10 acts as a major ligand for FGF receptor 2 IIIb in mouse multi-organ development. *Biochem Biophys Res Commun* 2000; 277(3):643–9.
168. Sekine K, Ohuchi H, Fujiwara M, Yamasaki M, Yoshizawa T, Sato T et al. Fgf10 is essential for limb and lung formation. *Nat Genet* 1999; 21(1):138–41.
169. Ramasamy SK, Mailleux AA, Gupte VV, Mata F, Sala FG, Veltmaat JM et al. Fgf10 dosage is critical for the amplification of epithelial cell progenitors and for the formation of multiple mesenchymal lineages during lung development. *Dev Biol* 2007; 307(2):237–47.
170. Hokuto I, Perl A-KT, Whitsett JA. Prenatal, but not postnatal, inhibition of fibroblast growth factor receptor signaling causes emphysema. *J Biol Chem* 2003; 278(1):415–21.
171. Klar J, Blomstrand P, Brunmark C, Badhai J, Håkansson HF, Brange CS et al. Fibroblast growth factor 10 haploinsufficiency causes chronic obstructive pulmonary disease. *J Med Genet* 2011; 48(10):705–9.

172. Mailloux AA, Kelly R, Veltmaat JM, Langhe SP de, Zaffran S, Thiery JP et al. Fgf10 expression identifies parabronchial smooth muscle cell progenitors and is required for their entry into the smooth muscle cell lineage. *Development* 2005; 132(9):2157–66.
173. Igarashi M, Finch PW, Aaronson SA. Characterization of Recombinant Human Fibroblast Growth Factor (FGF)-10 Reveals Functional Similarities with Keratinocyte Growth Factor (FGF-7)*. *J Biol Chem* 1998; 273(21):13230–5. Available from: URL: <https://www.sciencedirect.com/science/article/pii/S002192581957939X>.
174. Barkauskas CE, Cronce MJ, Rackley CR, Bowie EJ, Keene DR, Stripp BR et al. Type 2 alveolar cells are stem cells in adult lung. *J Clin Invest* 2013; 123(7):3025–36.
175. DakoCytomation GmbH. Handbuch immunchemische Färbemethoden. 3. Aufl. Hamburg; 2003.
176. Vector Laboratories, Inc. Data Sheet VECTASTAIN® Universal Quick HRP Kit, Peroxidase:
https://vectorlabs.com/productpdf/download/file/id/1178/name/VECTASTAIN%25C2%25AE_Universal_Quick_HRP_Kit%252C_Peroxidase_%2528Concentrate%2529.pdf/.
177. Vector Laboratories, Inc. Data Sheet Vector® VIP Substrate Kit, Peroxidase (HRP):
https://vectorlabs.com/productpdf/download/file/id/1235/name/Vector%25C2%25AE_VIP_Substrate_Kit%252C_Peroxidase_%2528HRP%2529.pdf/.
178. Kosanovic D, Luitel H, Dahal BK, Cornitescu T, Janssen W, Danser AJ et al. Chymase: a multifunctional player in pulmonary hypertension associated with lung fibrosis. *European Respiratory Journal* 2015; 46(4):1084.
179. Yi ES, Kim H, Ahn H, Strother J, Morris T, Masliah E et al. Distribution of obstructive intimal lesions and their cellular phenotypes in chronic pulmonary hypertension. A morphometric and immunohistochemical study. *Am J Respir Crit Care Med* 2000; 162(4 Pt 1):1577–86.
180. Katzenstein A-LA, Mukhopadhyay S, Myers JL. Diagnosis of usual interstitial pneumonia and distinction from other fibrosing interstitial lung diseases. *Hum Pathol* 2008; 39(9):1275–94.

181. King TE, JR, Pardo A, Selman M. Idiopathic pulmonary fibrosis. *Lancet* 2011; 378(9807):1949–61.
182. Yamaguchi M, Hirai S, Tanaka Y, Sumi T, Miyajima M, Mishina T et al. Fibroblastic foci, covered with alveolar epithelia exhibiting epithelial-mesenchymal transition, destroy alveolar septa by disrupting blood flow in idiopathic pulmonary fibrosis. *Lab Invest* 2017; 97(3):232–42.
183. Parra ER, Kairalla RA, de Carvalho, Carlos Roberto Ribeiro, Capelozzi VL. Abnormal deposition of collagen/elastic vascular fibres and prognostic significance in idiopathic interstitial pneumonias. *Thorax* 2007; 62(5):428–37.
184. Calabrese F, Kipar A, Lunardi F, Balestro E, Perissinotto E, Rossi E et al. Herpes virus infection is associated with vascular remodeling and pulmonary hypertension in idiopathic pulmonary fibrosis. *PLoS One* 2013; 8(2):e55715.
185. Ebina M, Shimizukawa M, Shibata N, Kimura Y, Suzuki T, Endo M et al. Heterogeneous increase in CD34-positive alveolar capillaries in idiopathic pulmonary fibrosis. *Am J Respir Crit Care Med* 2004; 169(11):1203–8.
186. Patel NM, Kawut SM, Jelic S, Arcasoy SM, Lederer DJ, Borczuk AC. Pulmonary arteriole gene expression signature in idiopathic pulmonary fibrosis. *Eur Respir J* 2013; 41(6):1324–30.
187. Patel NM, Lederer DJ, Borczuk AC, Kawut SM. Pulmonary hypertension in idiopathic pulmonary fibrosis. *Chest* 2007; 132(3):998–1006.
188. Lefèvre G, Babchia N, Calipel A, Mouriaux F, Faussat A-M, Mrzyk S et al. Activation of the FGF2/FGFR1 autocrine loop for cell proliferation and survival in uveal melanoma cells. *Invest Ophthalmol Vis Sci* 2009; 50(3):1047–57.
189. Li P, Oparil S, Sun J-Z, Thompson JA, Chen Y-F. Fibroblast growth factor mediates hypoxia-induced endothelin-- a receptor expression in lung artery smooth muscle cells. *J Appl Physiol (1985)* 2003; 95(2):643-51; discussion 863.
190. El Agha E, Kosanovic D, Schermuly RT, Bellusci S. Role of fibroblast growth factors in organ regeneration and repair. *Semin Cell Dev Biol* 2016; 53:76–84.
Available from: URL:
<https://www.sciencedirect.com/science/article/pii/S1084952115002062>.

191. Benjamin JT, Smith RJ, Halloran BA, Day TJ, Kelly DR, Prince LS. FGF-10 is decreased in bronchopulmonary dysplasia and suppressed by Toll-like receptor activation. *Am J Physiol Lung Cell Mol Physiol* 2007; 292(2):L550-8.
192. MacKenzie B, Korfei M, Henneke I, Sibinska Z, Tian X, Hezel S et al. Increased FGF1-FGFRc expression in idiopathic pulmonary fibrosis. *Respir Res* 2015; 16(1):83.
193. Ramos C, Montaña M, Becerril C, Cisneros-Lira J, Barrera L, Ruíz V et al. Acidic fibroblast growth factor decreases α -smooth muscle actin expression and induces apoptosis in human normal lung fibroblasts. *Am J Physiol Lung Cell Mol Physiol* 2006; 291(5):L871-L879.
194. Khalil N, Xu YD, O'Connor R, Duronio V. Proliferation of pulmonary interstitial fibroblasts is mediated by transforming growth factor-beta1-induced release of extracellular fibroblast growth factor-2 and phosphorylation of p38 MAPK and JNK. *J Biol Chem* 2005; 280(52):43000–9.
195. Aguilar S, Scotton CJ, McNulty K, Nye E, Stamp G, Laurent G et al. Bone marrow stem cells expressing keratinocyte growth factor via an inducible lentivirus protects against bleomycin-induced pulmonary fibrosis. *PLoS One* 2009; 4(11):e8013.
196. Farkas L, Farkas D, Gauldie J, Warburton D, Shi W, Kolb M. Transient overexpression of Gremlin results in epithelial activation and reversible fibrosis in rat lungs. *Am J Respir Cell Mol Biol* 2011; 44(6):870–8.
197. McQualter JL, McCarty RC, van der Velden J, O'Donoghue RJJ, Asselin-Labat M-L, Bozinovski S et al. TGF- β signaling in stromal cells acts upstream of FGF-10 to regulate epithelial stem cell growth in the adult lung. *Stem Cell Res* 2013; 11(3):1222–33.
198. O'Hare KH, Sheridan MN. Electron microscopic observations on the morphogenesis of the albino rat lung, with special reference to pulmonary epithelial cells. *Am J Anat* 1970; 127(2):181–205.
199. Rehan VK, Torday JS. PPAR γ Signaling Mediates the Evolution, Development, Homeostasis, and Repair of the Lung. *PPAR Res* 2012; 2012:289867.
200. Torday JS, Sun H, Wang L, Torres E, Sunday ME, Rubin LP. Leptin mediates the parathyroid hormone-related protein paracrine stimulation of fetal lung maturation. *Am J Physiol Lung Cell Mol Physiol* 2002; 282(3):L405-10.

201. Torday JS, Rehan VK. Stretch-stimulated surfactant synthesis is coordinated by the paracrine actions of PTHrP and leptin. *Am J Physiol Lung Cell Mol Physiol* 2002; 283(1):L130-5.
202. Krebs M, Sakurai R, Torday JS, Rehan VK. Evidence for in vivo nicotine-induced alveolar interstitial fibroblast-to-myofibroblast transdifferentiation. *Exp Lung Res* 2010; 36(7):390–8.
203. Rehan VK, Wang Y, Sugano S, Romero S, Chen X, Santos J et al. Mechanism of nicotine-induced pulmonary fibroblast transdifferentiation. *Am J Physiol Lung Cell Mol Physiol* 2005; 289(4):L667-76.
204. Rehan VK, Fong J, Lee R, Sakurai R, Wang Z-M, Dahl MJ et al. Mechanism of reduced lung injury by high-frequency nasal ventilation in a preterm lamb model of neonatal chronic lung disease. *Pediatr Res* 2011; 70(5):462–6.
205. Thannickal VJ, Toews GB, White ES, Lynch JP3, Martinez FJ. Mechanisms of pulmonary fibrosis. *Annu Rev Med* 2004; 55:395–417.
206. Ahlbrecht K, McGowan SE. In search of the elusive lipofibroblast in human lungs. *Am J Physiol Lung Cell Mol Physiol* 2014; 307(8):L605-8.
207. Genovese T, Cuzzocrea S, Di Paola R, Mazzon E, Mastruzzo C, Catalano P et al. Effect of rosiglitazone and 15-deoxy-Delta12,14-prostaglandin J2 on bleomycin-induced lung injury. *Eur Respir J* 2005; 25(2):225–34.
208. Asaki T, Konishi M, Miyake A, Kato S, Tomizawa M, Itoh N. Roles of fibroblast growth factor 10 (Fgf10) in adipogenesis in vivo. *Mol Cell Endocrinol* 2004; 218(1-2):119–28.
209. Sakaue H, Konishi M, Ogawa W, Asaki T, Mori T, Yamasaki M et al. Requirement of fibroblast growth factor 10 in development of white adipose tissue. *Genes Dev* 2002; 16(8):908–12.
210. Rangarajan S, Bone NB, Zmijewska AA, Jiang S, Park DW, Bernard K et al. Metformin reverses established lung fibrosis in a bleomycin model. *Nature Medicine* 2018; 24(8):1121–7.
211. Khalil N, Greenberg AH. The role of TGF-beta in pulmonary fibrosis. *Ciba Found Symp* 1991; 157:194-207; discussion 207-11.

212. Rubin JS, Bottaro DP, Chedid M, Miki T, Ron D, Cunha GR et al. Keratinocyte growth factor as a cytokine that mediates mesenchymal-epithelial interaction. *EXS* 1995; 74:191–214.
213. Sakamoto S, Yazawa T, Baba Y, Sato H, Kanegae Y, Hirai T et al. Keratinocyte growth factor gene transduction ameliorates pulmonary fibrosis induced by bleomycin in mice. *Am J Respir Cell Mol Biol* 2011; 45(3):489–97.
214. Scalia CR, Boi G, Bolognesi MM, Riva L, Manzoni M, DeSmedt L et al. Antigen Masking During Fixation and Embedding, Dissected. *J Histochem Cytochem* 2017; 65(1):5–20.
215. Boenisch T. Effect of heat-induced antigen retrieval following inconsistent formalin fixation. *Appl Immunohistochem Mol Morphol* 2005; 13(3):283–6.
216. Russell Myers. Technical Brief of Heat Induced Epitope Retrieval.
217. Bussolati G, Leonardo E. Technical pitfalls potentially affecting diagnoses in immunohistochemistry. *J Clin Pathol* 2008; 61(11):1184–92.
218. Daneshtalab N, Doré JJE, Smeda JS. Troubleshooting tissue specificity and antibody selection: Procedures in immunohistochemical studies. *J Pharmacol Toxicol Methods* 2010; 61(2):127–35.
219. Buchwalow I, Samoilova V, Boecker W, Tiemann M. Non-specific binding of antibodies in immunohistochemistry: fallacies and facts. *Scientific Reports* 2011; 1(1):28.
220. Kim SH, Shin YK, Lee KM, Lee JS, Yun JH, Lee SM. An improved protocol of biotinylated tyramine-based immunohistochemistry minimizing nonspecific background staining. *J Histochem Cytochem* 2003; 51(1):129–32.
221. Kim SH, Jung KC, Shin YK, Lee KM, Park YS, La Choi Y et al. The enhanced reactivity of endogenous biotin-like molecules by antigen retrieval procedures and signal amplification with tyramine. *Histochem J* 2002; 34(3-4):97–103.
222. Tan WCC, Nerurkar SN, Cai HY, Ng HHM, Wu D, Wee YTF et al. Overview of multiplex immunohistochemistry/immunofluorescence techniques in the era of cancer immunotherapy. *Cancer Commun (Lond)* 2020; 40(4):135–53.
223. Majka SM, Miller HL, Helm KM, Acosta AS, Childs CR, Kong R et al. Chapter Fifteen - Analysis and Isolation of Adipocytes by Flow Cytometry. In: Macdougald OA,

editor. *Methods in Enzymology : Methods of Adipose Tissue Biology, Part A*. Academic Press; 2014. p. 281–96 [cited 2021 Nov 9]. Available from: URL: <https://www.sciencedirect.com/science/article/pii/B978012411619100015X>.

224. Molecular Probes School of Fluorescence. Immunolabeling: Labeled antibodies allow you to target almost any cellular target in a fixed and permeabilized cell [cited 2021 Nov 8]. Available from: URL: <https://www.thermofisher.com/de/de/home/life-science/cell-analysis/cell-analysis-learning-center/molecular-probes-school-of-fluorescence/imaging-basics/labeling-your-samples/immunolabeling.html>.

225. Bourgeois MA, Oaks JL. Chapter 12 - Laboratory Diagnosis of Viral Infections. In: Sellon DC, Long MT, editors. *Equine Infectious Diseases (Second Edition)*. St. Louis: W.B. Saunders; 2014. 132-140.e2 Available from: URL: <https://www.sciencedirect.com/science/article/pii/B9781455708918000129>.

226. Lin Y, Wang F. FGF signalling in prostate development, tissue homeostasis and tumorigenesis. *Biosci Rep* 2010; 30(5):285–91.

227. Yang J, Meyer M, Müller A-K, Böhm F, Grose R, Dauwalder T et al. Fibroblast growth factor receptors 1 and 2 in keratinocytes control the epidermal barrier and cutaneous homeostasis. *J Cell Biol* 2010; 188(6):935–52.

228. Ley B, Collard HR, King TE, JR. Clinical course and prediction of survival in idiopathic pulmonary fibrosis. *Am J Respir Crit Care Med* 2011; 183(4):431–40.

229. Nickel N, Golpon H, Greer M, Knudsen L, Olsson K, Westerkamp V et al. The prognostic impact of follow-up assessments in patients with idiopathic pulmonary arterial hypertension. *Eur Respir J* 2012; 39(3):589–96.

7 Appendix

7.1 Abbreviations

5-HT(2B)	5-Hydroxytryptamine receptor 2B / serotonin receptor 2B
NT-proBNP	N-terminal prohormone of brain natriuretic peptide
6-MWT	Six-minute walk test
α -SMA	Alpha-smooth-muscle actin
AB	Acid-Box
ACTA2	Actin alpha 2
ADRP	Adipose differentiation related protein
AECI	Alveolar epithelial cells type I
AECII	Alveolar epithelial cells type II
AEP	Alveolar epithelial progenitor
APLN	Apelin
BCL2	“B-cell lymphoma 2”
BCL-xL	“B-cell lymphoma-extra large”
BMPR2	Bone morphogenic type 2 receptor
BMPs	Bone morphogenetic proteins
BPD	Bronchopulmonary dysplasia
BSA	Bovine Serum Albumin
C/EBP α	CCAAT/Enhancer-binding Protein α
Ca	Calcium
c-Abl	Abelson murine leukemia viral oncogene homolog 1
CD45	Receptor-Typ Tyrosin-Proteinphosphatase C
cGMP	Cyclic guanosine monophosphate

CH ₃ CO ₂ H	Acetic acid
CH ₃ OH	Methanol
CO	cardiac output
CO ₂	carbon dioxide
COL1A1	Collagen type I alpha 1
COPD	Chronic obstructive pulmonary disease
CTEPH	chronic thromboembolic pulmonary hypertension
DAB	3,3'-diaminodbenzidine
DAPI	4',6-Diamidin-2-phenylindol
DL	Diffusing capacity
DLCO	Diffusing capacity for carbon monoxide
DNA	Deoxyribonucleic acid
EC	Endothelial-cell
ECM	Extracellular matrix
EMT	Epithelial-mesenchymal transition
EndMT	Endothelial-mesenchymal transition
ERAs	Endothelin receptor antagonists
ESC/ERS	European Society of Cardiology/European Respiratory Society
ETA/B	Endothelin-A/B-Rezeptor
eurIPFreg	European IPF registry
Fc receptor	Fragment crystallizable receptor
FGF	Fibroblast growth factor
FGFR	Fibroblast growth factor receptor
FRS2	Fibroblast growth factor receptor substrate 2
FVC	Forced vital capacity

GAP	Gender-Age-Physiology
H&E	Hematoxylin + Eosin
H ₂ O ₂	Hydrogen peroxide
HPV	Hypoxic pulmonary vasoconstriction
HRCT	High-resolution computed tomography
HRP	Horseradish peroxidase
HSGP	Heparan sulfate proteoglycan
IF	Immunofluorescence
Ig	Immunoglobulin-like domain
IHC	Immunohistochemistry
IIPs	Idiopathic interstitial pneumonias
IL-6	Interleukin-6
ILD	Interstitial lung disease
IP receptor	Prostacyclin-receptor
IPAH	Idiopathic pulmonary arterial hypertension
KCL	Potassium chloride
KGF	Keratinocyte Growth Factor
KH ₂ PO ₄	Potassium dihydrogen phosphate
LFB	Lipofibroblast
LSAB	Labeled Streptavidin–Biotin
LVEDP	Left ventricular end-diastolic pressure
LVEF	Left ventricular ejection fraction
MAPK/ERK	mitogen-activated protein kinase/extracellular signal-regulated kinase
microRNA	Micro ribonucleic acid
mPAP	Mean pulmonary arterial pressure

MUC5AC	Mucin 5AC gene
MYF	Myofibroblast
Na ₂ HPO ₄	Disodiumhydrogenphosphate
NO	Nitric oxide
O ₂	Oxygen
P	Phosphoryl group
PaCO ₂	Partial pressure of carbon dioxide
PAH	Pulmonary arterial hypertension
PASMC	Pulmonary Artery Smooth Muscle Cells
PBS	Phosphate buffered saline
PCH	Pulmonary capillary hemangiomatosis
PCWP	Pulmonary capillary wedge pressure
PDE5	Phosphodiesterase-5
PDGF	Platelet-derived growth factor
PDGFR α/β	Platelet-derived growth factor receptor A/Beta
PH	Pulmonary hypertension
PLC γ	PLC gamma pathway
PPAR- γ	Peroxisome proliferator-activated receptor gamma
PTHrP	Parathyroid hormone-related protein
PTHrP	Parathyroid hormone-related protein-signaling
PVOD	Pulmonary veno-occlusive disease
PVR	pulmonary vascular resistance
RA	Right atrial size
RAF	RAF serine/threonine-protein kinase
RAP	Right atrial pressure

RAS	Ras small G-Proteins
RHC	right heart catheterization
SE	Standard error
SEM	Standard error of the mean
sGC	Soluble guanylate cyclase
sPAP	Systolic pulmonary artery pressure
SPC	Surfactant protein C
STAT	Signal transducer and activator of transcription
TBS	Tris-buffered saline
TBS-T	Tris-buffered saline with Tween
TGF- β 1	transforming growth factor- β 1
TK	Intracellular tyrosine kinase domain
TLC	Total lung capacity
TM	Transmembrane domain
TNF- α	Tumor necrosis factor
TRV	Tricuspid regurgitation velocity
TRV	Tricuspid regurgitation velocity
TTE	transthoracic echocardiography
UIP	Usual interstitial pneumonia
UPR	Unfolded protein response
VEGF	Vascular Endothelial Growth Factor
vWF	Von-Willebrand-Faktor
WSPH	World Symposium on Pulmonary Hypertension

7.2 List of figures

Fig.1	Pathophysiological mechanisms of vascular remodeling in PAH	11
Fig.2	FGFs gene families, cofactors and mode of action	19
Fig.3	Schematic illustration of the FGF-FGFR structure	21
Fig.4	Loss of function of <i>Fgf10</i> in mice leading to lung and limb agenesis	23
Fig.5	Laboratory equipment	31
Fig.6	Desktop workstation featuring motorized microscope with digital interface	35
Fig.7	Semi-automated workflow	35
Fig.8	A lung tissue section from an IPF patient stained for FGF10	36
Fig.9	Expression of FGF receptors and ligands in serial sections	39
Fig.10	Remodeled pulmonary artery in IPAH	40
Fig.11	Histopathological features of IPF in serial sections	41
Fig.12	Histological sections of donor- and IPF-tissue stained for FGF7	42
Fig.13	FGF7 immunostaining of donor-tissue compared to IPAH-tissue sample	42
Fig.14	FGF10 immunostaining donor lung tissue compared to an IPF sample	43
Fig.15	FGF10 immunostaining of donor lung tissue compared to plexiform lesion	43
Fig.16	FGFR2 immunostaining of donor lung tissue compared to advanced IPF	44
Fig.17	FGFR2 immunostaining of donor lung tissue compared to IPAH lung tissue	44
Fig.18	FGFR1 immunostaining of donor lung tissue compared to IPF lung tissue	45
Fig.19	FGFR1 immunostaining of a donor lung tissue compared to IPAH sample	45

Fig.20	Expression of FGF receptors and ligands in serial sections	46
Fig.21	Conclusion of the expression patterns for all four targets	47
Fig.22	Expression levels in FR versus FF; mPAP correlation data	48
Fig.23	Fluorescent LipidTOX-, DAPI- and SPC-staining of frozen lung tissue	49
Fig.24	Multiple clusters of neutral-lipid droplets in IPF lung tissue	50
Fig.25	Synopsis of the involvement of the prototypic FGFs in PH	52
Fig.26	Synopsis of the proposed involvement of FGFs in IPF	58

7.3 List of tables

Table 1	Updated classification of pulmonary hypertension	6
Table 2	Classification of Interstitial lung disease	14
Table 3	Selected targets and their corresponding primary antibodies	31
Table 4	Primary antibodies utilized in the α -SMA/ vWF double staining	34
Table 5	Primary antibody utilized in the neutral lipid/pro SP-C double staining	38

8 Publication index

El Agha E, Moiseenko A, Kheirollahi V, Langhe S de, Crnkovic S, Kwapiszewska G et al. Two-Way Conversion between Lipogenic and Myogenic Fibroblastic Phenotypes Marks the Progression and Resolution of Lung Fibrosis. *Cell Stem Cell* 2017; 20(2):261-273.e3

El Agha E, Schwind F, Ruppert C, Günther A, Bellusci S, Schermuly RT et al. Is the fibroblast growth factor signaling pathway a victim of receptor tyrosine kinase inhibition in pulmonary parenchymal and vascular remodeling? *Am J Physiol Lung Cell Mol Physiol* 2018; 315(2):L248-L252.

9 Acknowledgements

I would like to take the opportunity to thank Prof. Dr. Ralph Schermuly for accepting me into his research group and granting me the privilege to work in the inspirational environment of the Excellence Cluster Cardio-Pulmonary System (ECCPS).

My deep gratitude goes out to my supervisors, Prof. Elie El Agha and Dr. Djuro Kosanovic, for their continuous support, despite my intermittent shift of priorities and my lengthened period of absence. Through their unparalleled dedication to the project and high level of patience, regardless of their many other demanding commitments, they empowered me to complete my thesis.

I would also like to thank Ewa Bienek and Stephanie Viehmann for training me in the methods of immunohistochemistry and immunofluorescence. Without hesitation, they both shared their extensive knowledge and helped me develop and improve my skillset in the laboratory.

My special thanks go to Dr. Alena Moiseenko and Dr. Vahid Kheirollahi for all those friendly conversations, the helpful advice and regular troubleshooting. Furthermore, I would like to thank Prof. Dr. Saverio Bellusci for the opportunity to work in his laboratory and for letting me benefit from the vast expertise in his workgroup.

Finally, I would like to thank my parents and my life partner, Dr. med. Lisa Hübner, for their infinite patience and unconditional support.

10 Declaration

Hiermit erkläre ich, dass ich die vorliegende Arbeit selbständig und ohne unzulässige Hilfe oder Benutzung anderer als der angegebenen Hilfsmittel angefertigt habe. Alle Textstellen, die wörtlich oder sinngemäß aus veröffentlichten oder nichtveröffentlichten Schriften entnommen sind, und alle Angaben, die auf mündlichen Auskünften beruhen, sind als solche kenntlich gemacht. Bei den von mir durchgeführten und in der Dissertation erwähnten Untersuchungen habe ich die Grundsätze guter wissenschaftlicher Praxis, wie sie in der „Satzung der Justus-Liebig-Universität Gießen zur Sicherung guter wissenschaftlicher Praxis“ niedergelegt sind, eingehalten sowie ethische, datenschutzrechtliche und tierschutzrechtliche Grundsätze befolgt. Ich versichere, dass Dritte von mir weder unmittelbar noch mittelbar geldwerte Leistungen für Arbeiten erhalten haben, die im Zusammenhang mit dem Inhalt der vorgelegten Dissertation stehen, oder habe diese nachstehend spezifiziert. Die vorgelegte Arbeit wurde weder im Inland noch im Ausland in gleicher oder ähnlicher Form einer anderen Prüfungsbehörde zum Zweck einer Promotion oder eines anderen Prüfungsverfahrens vorgelegt. Alles aus anderen Quellen und von anderen Personen übernommene Material, das in der Arbeit verwendet wurde oder auf das direkt Bezug genommen wird, wurde als solches kenntlich gemacht. Insbesondere wurden alle Personen genannt, die direkt und indirekt an der Entstehung der vorliegenden Arbeit beteiligt waren. Mit der Überprüfung meiner Arbeit durch eine Plagiatserkennungssoftware bzw. ein internetbasiertes Softwareprogramm erkläre ich mich einverstanden.

Ort/Datum

Felix Schwind

11 Curriculum Vitae